Synthèse et caractérisation thermodynamique d'hydrates de gaz contenant de l'hydrogène

Amir Abbas Karimi

HAL Id: pastel-00998311

https://pastel.archives-ouvertes.fr/pastel-00998311

Submitted on 1 Jun 2014

THÈSE

Pour obtenir le grade de

Docteur de l'École Polytechnique

Présentée et soutenue publiquement par

Amir A. KARIMI

Le 22 novembre 2013

**Synthèse et caractérisation thermodynamique
d'hydrates de gaz contenant de l'hydrogène**

----

*« Synthesis and thermodynamic characterisation
of gas hydrates containing hydrogen »*

Directeur de thèse : Didier DALMAZZONE

Jury :

Bertrand Chazallon	**Rapporteur**
Anthony Delahaye	**Rapporteur**
Danièle Clausse	**Examinateur**
Antonin Chapoy	**Examinateur**
Jean Philippe Torre	**Examinateur**
Didier Dalmazzone	**Examinateur**

To my parents…

Acknowledgements

First and foremost I would like to thank my supervisor Didier Dalmazzone. It has been an honour to be his Ph.D. student. He has taught me, both consciously and unconsciously, how good experimental thermodynamics is. I appreciate all his contributions of time and ideas to make my Ph.D. experience productive and stimulating. Thank you Didier, not only because of what you have taught me, but also because of your kindness and your patience through these past three years!

The joy and enthusiasm Didier has for his research was contagious and motivational for me, even during tough times in the Ph.D. pursuit. I am also thankful for the excellent example he has provided as a successful researcher and professor.

I would also like to thank the director of our laboratory Walter Fürst, for giving me the opportunity to realize my research at the best possible condition under his direction.

Collective and individual acknowledgements are conveyed to my thesis reading committee members. I am grateful to my thesis referees Dr. Antonin Chapoy and Dr. Antony Delahaye for accepting this role and reading the thesis manuscript with great care, interest and patience. It was an extreme honor for me to have them as well as other members of the jury, Dr. Danièle Clausse, Dr. Bertrand Chazallon and Dr. Jean Philippe Torre as my thesis board of examiners.

This thesis was funded by École Polytechnique de Paris, and I would like to thank both École Polytechnique and ENSTA for their generous support. Both schools have provided me a rich and fertile environment to study and explore new ideas. At École Polytechnique I would like to thank all the members of Graduate School (EDX) and the administration staff. At ENSTA, the members of the UCP (Unité de Chimie et Procédés) have contributed immensely to my personal and professional time. The group has been a source of friendships as well as good advice and collaboration. I am especially grateful to Alain Gaunand, Patrice Paricaud, Laurent Catoire, Henri Planche and I would like to specially thank Elise Provost and Johnny Deschamps for their help and technical support during my thesis.

I would like to acknowledge Oleksandr Doltko post-doc researcher who was here on the first year of my PhD. We worked together on H_2-TBPBH$_4$ system, and I very much appreciated his enthusiasm, willingness and support.

My time at ENSTA was made enjoyable in large part thanks to my many friends that became a part of my life. I am grateful for time spent with my friends, for making one of the most pleasant periods of my life, to Julien Glorian (Ju) my office mate and my French teacher at the same time! (vocabulary & pronunciation) Mickael Matrat (Mickey) again my French teacher focusing on grammar & writing, Aurélien Demenay (DéDé), Elodie Fazer, Kodjo Coudoro (The last king of Togo), Jean-Baptiste May-Carle (JB), Karl Chatelain (Karlito) and also to my Asian friends Zhewei Yu (JiJi), Ayako Fukumoto and Wei Lin.

I would like to express my gratitude to a group of my best friends outside UCP, starting with Behzad Nazer who has always been like a brother for me, the very old friend Mohsen Laali, fascinating Bora Erdamar (Boracim) who opened new horizons in my personal life and way of thinking, my very kind friend and former neighbour Robert Somogyi, very supportive Susan Memari for whom I wish all the best, and special thanks to Yassaman Sarabi a very compassionate and everlasting friend of mine.

I gratefully acknowledge the unforgettable support of Nastaran Manoucheri specially in the first days and months of my arrival to France. I would like to thank Dr. Amir Mohammadi at École des Mines de Paris and all the other Iranian friends of mine in France.

Last but not least, I would like to thank my family for all their love and encouragement. For my parents who raised me with love and supported me in all my pursuits. For my sister who has been my best friend all my life and I love her dearly and thank her for all her advice and support. For the presence of my aunt and his kind husband in Paris, for all their loving and encouraging support. Thank you.

TABLE OF CONTENTS

LIST OF ABBREVIATION AND SYMBOLS

Abbreviations

C	Molar concentration	$mol \cdot m^{-3}$
C_S	Heat capacity of sample	$J \cdot K^{-1} \cdot kg^{-1}$
C_R	Heat capacity of reference	$J \cdot K^{-1} \cdot kg^{-1}$
CNG	Compressed Natural Gas	
DOE	United states' Department Of Energy	
DSC	Differential Scanning Calorimeter	
G	Gas phase	
GC	Gas Chromatography	
H	Hydrate phase	
h	Molar enthalpy	$J \cdot mol^{-1}$
hyd	Hydrate structure	
Ih	Hexagonal ice	
K	Heat transfer coefficient	
L/ Liq.	Liquid phase	
LNG	Liquefied Natural Gas	
M	Molar mass	$kg \cdot mol^{-1}$
MOF	Metal Organic Framework	
n	Mole number	mol
P	Pressure	Pa
q	Molar heat flow	$J \cdot mol^{-1}$
R	Thermal Resistance	
S	Molar entropy	$J \cdot K^{-1} \cdot mol^{-1}$
T	Temperature	K
TBAB	Tetra-butyl-ammonium bromide	
TBABh	Tetra-butyl-ammonium brohydride	
TBACl	Tetra-butyl-ammonium chloride	
TBAF	Tetra-butyl-ammonium fluoride	
TBAOH	Tetra-butyl-ammonium hydroxide	
$TBPBH_4$	Tetra-butyl-phosphonium brohydride	
THF	Tetrahydrofuran	
TMA	Trimethylamine	

V	Vapour phase	
w_{is}	Isothermal work	$J \cdot mol^{-1}$
Z	Compressibility factor	

Greek Letters

γ	Thermal conductivity	$W \cdot K^{-1} m^{-1}$
μ_{jT}	Joule-Thompson coefficient	$K \cdot Pa^{-1}$
ρ	Density	$Kg \cdot m^{-3}$
φ	Heat flow rate	$J \cdot mol^{-1} \cdot s^{-1}$

Subscripts

0	Initial
A	Aqueous phase
eq	Equilibrium sate
F	Furnace
H	Hydrate phase
HC	Hydrocarbon
L	Liquid phase
R	Reference
S	Sample
V	Vapour
W	water

Constants

R	Universal gas constant	$8.134 \, J \cdot mol^{-1} \cdot K^{-1}$

LIST OF FIGURES:

LIST OF TABLES:

Contexte et Objectifs et L'étude

Dans la perspective de la transition vers de nouvelles sources énergétiques, l'hydrogène apparaît comme un vecteur d'énergie prometteur. L'hydrogène est doté d'excellentes propriétés physico-chimiques qui en font un combustible d'avenir : il constitue une énergie propre, renouvelable, avec un pouvoir calorifique trois fois supérieur à celui de l'essence. Mais les difficultés liées au stockage et au transport de l'hydrogène restent des obstacles majeurs au développement d'une économie de l'hydrogène comme vecteur énergétique.

Dans ce contexte, la présente étude concerne la synthèse et la caractérisation d'hydrates d'hydrogène du type clathrate et semi-clathrates par analyse calorimétrique différentielle sous haute pression (40 MPa) et en réacteur isochorique pour les mesures volumétriques.

Dans un premier temps, une famille particulière de semi-clathrates qui se forment à partir d'eau et de gaz en présence de sels d'ammonium (TBAOH) ou de phosphonium quaternaires (TBPBH$_4$) a été étudiée. Nous présentons dans cette partie une étude du comportement des systèmes TBAOH-H$_2$-H$_2$O, TBPBH$_4$ -H$_2$ -H$_2$O etTBPBH$_4$ - N$_2$ -H$_2$O, leurs diagrammes de phases isobares (x, T) et une étude volumétrique de la quantité de gaz stocké.

Dans un deuxième temps, le concept de Tuning a été développé dans un mélange de H$_2$-C$_3$H$_8$ afin d'étudier son impact sur la stabilité de l'hydrate d'hydrogène. Enfin, la séparation de l'hydrogène dans un mélange équimolaire de CO$_2$-H$_2$ par cristallisation d'hydrate a été étudiée et l'analyse des compostions initiale et finale du mélange de gaz réalisée.

Mots clé: Hydrates de H$_2$, hydrates semi-clathrates, équilibre de phase, analyse calorimétrique différentielle, mesure volumétrique

Introduction

The limited supply of fossil fuels and the environmental issues they provoke make shifting towards clean and renewable energy sources inevitable. In this perspective, hydrogen as a clean energy career is attracting more and more attention. Hydrogen is a clean fuel which its combustion does not produce any pollutant or any greenhouse gas. Moreover, its energetic density is around three times higher than those of conventional fuels [1]. In spite of its favourable chemical properties, storage and transport of hydrogen has always been a challenge for industry. In this regard, different technologies were proposed from hydrogen compression and liquefaction, to hydrogen adsorption in carbon nanotubes and metal organic frameworks.

Any proposed method for industrial storage of hydrogen must cover two criteria: Firstly, the mass density of the stored hydrogen must meet the economic/industrial requirements and secondly the energy consumption of the storage method itself must not exceed the energy content of stored hydrogen. Respecting these two criteria, clathrate hydrates have been studied as a potential storage medium for hydrogen.

Clathrate hydrates are inclusion compounds made up of water and a guest molecule. They are formed by insertion of gas molecules into cavities formed by water molecules arranged in polyhedral patterns, under low temperatures and relatively high gas pressures. Hydrate dissociation and formation conditions depend principally on the nature of the crystalline structure, size of the guest molecule, gas pressure and the molecular interaction between guest molecules and hydrate structure. In order to reduce the severe hydrate formation conditions, usually some additives are added. These additives are usually organic salts or constituents of natural gas.

This work comprises synthesis and characterization of hydrogen hydrates of different structures in presence of water soluble additives and gas promoters. At the first step, the phase equilibria of semi-clathrate systems made in presence of an ammonium quaternary salt (TBAOH) and a phosphonium quaternary salt ($TBPBH_4$) were investigated. Using a differential scanning calorimeter (DSC) the equilibrium dissociation temperatures of these semi-calthrates were measured under different hydrogen pressures. Their phase diagrams were established and the effect of hydrogen pressure upon their stability was studied. Moreover, using an isochoric high pressure reactor the quantity of hydrogen stored in these semi-clathrates was investigated.

In the second part, effect of a promoter gas such as propane on the stability of hydrogen hydrate was investigated. These investigations were preceded by independent measurements of pure propane hydrate which were followed on the hydrogen + propane mixture of 1 mol%, 3 mol %, 5 mol% and 10 mol% of propane. The effect of the composition and total gas pressure was investigated using DSC.

The last system studied was the clathrate hydrates formed in the CO_2-H_2 gas mixture. The phase equilibrium of the system was studied and compared with the literature data of pure CO_2 hydrate and pure H_2 hydrate. The tendency of both components in occupying hydrate cavities was investigated by analyzing the initial (before hydrate formation) and final (after hydrate formation) gas composition.

The first chapter of this dissertation is a bibliographic review of hydrogen's industrial applications and storage technologies. The second chapter describes the experimental techniques that were used

during the thesis. In the third and fourth chapters, the results obtained in the presence of saline and gas additives are presented and discussed, respectively.

Chapter One:

Introduction on hydrogen storage

This chapter comprises the physical and chemical properties of hydrogen as an energy source as well as different hydrogen production methods in industry and its application in different industrial sectors.

Respecting the main objective of this research on hydrogen storage, common known hydrogen storage methods are presented and are described here and finally, clathrates hydrates are introduced as a potential for gas storage. This chapter terminates by a literature review on the history of hydrates, their properties, structure, formation / dissociation conditions are given.

1.1. Introduction

Hydrogen as an environmentally clean and efficient energy carrier is attracting more and more attention worldwide. Study of fuel evolution history demonstrates a general trend in the increase of hydrogen content of fossil fuels from coal to petroleum oil and then to natural gas. This trend of increase of hydrogen content may finally reach the consumption of pure hydrogen; therefore it is not far from imagination if hydrogen is called the fuel of the future.

At ambient conditions, hydrogen is a colourless and odourless nontoxic gas. It has the lowest density among all the elements and after helium it has the lowest melting and boiling temperatures. Hydrogen has a high diffusion coefficient and a high heat capacity. Due to its single valence electron, it is a highly reactive and flammable gas, producing a great amount of energy which is at least three times more than the average value of liquid hydrocarbons [Table 1].

Table 1 - Comparison of heating values and CO_2 emission of common fuels and H_2 [1]

Fuel	Heating value (kJ/g)	Chemical Formula	kg[CO_2] / L
Propane	50.4	C_3H_8	1.55
Ethanol	29.7	C_2H_5OH	1.55
Gasoline	46.5	C_7H_{16}	2.39
Diesel	45.8	$C_{12}H_{26}$	2.63
Biodiesel	39.6	$C_{18}H_{32}O_2$	2.27
Methane	55.8	CH_4	0.35
Oil	47.9	$C_{14}H_{30}$	2.39
Wood	14.9	-	1.07
Coal	30.2	-	2.27
Hydrogen	141.9	H_2	0

Hydrogen is considered as a clean energy source because its combustion does not produce pollutant reaction. Its combustion in internal combustion engines produces low pollution and even no pollution in fuel cell engines. The combustion of hydrogen with oxygen produces water as its only product:

$$H_{2(g)} + \frac{1}{2}O_{2(g)} \rightarrow H_2O_{(g)}$$ *Equation (1)*
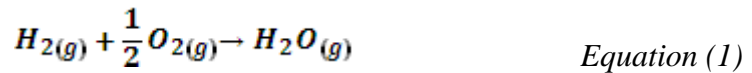
The enthalpy of this reaction is $\Delta_R H = -242$ MJ·kmol^{-1}. If the water condenses in this reaction, the enthalpy of condensation will be added to the total enthalpy of reaction making $\Delta_R H = -285$ MJ·kmol^{-1} and giving a heating value (the gross calorific value) of $H_o = 142$ MJ·kg^{-1} [2].

Due to the high temperature of hydrogen combustion some nitrogen molecules in the air may react with the oxygen molecules and produce nitrogen oxides (NO_X).

$$H_2 + O_2 + N_2 \rightarrow H_2O + N_2 + NO_X$$ *Equation (2)*
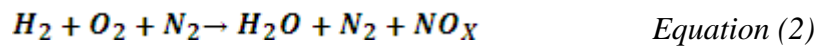
In addition to the nitrogen oxides, some traces of carbon oxides may also be produced originating from the oil used in the combustion chamber.

Source of hydrogen:

Although hydrogen is the most abundant element on the earth, only less than 1% of it exist in the form of molecular hydrogen gas (H_2) [3]. Hydrogen can form chemical compounds (hydrides) with most of the elements. Due to its ability to combine with carbon to make long chains, it plays an important role in organic life. The major source of hydrogen in nature is water in which hydrogen molecules are chemically bond to oxygen molecules and can be released either by electrolysis of water or thermal dissociation of H_2O molecules. But from about $5 \cdot 10^{10}$ kg of the hydrogen consumed each year worldwide, hydrogen is to a large extent produced from *steam reforming of natural gas* at high temperatures (973-1373K) [3]. This reaction can be summarized as:

$$CH_4 + H_2O \rightarrow CO + 3H_2$$ *Equation (3)*
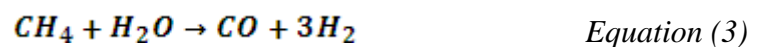
The product mixture is known as *synthesis gas*. Using the excess of water stream, through a reaction called *water shift reaction*, CO molecules convert into CO_2. This reaction is also the industrial process for production of carbon dioxide:

$$CO + H_2O \rightarrow CO_2 + H_2$$ *Equation (4)*

Production of hydrogen in this way bears a manufacture cost about three times higher than petroleum products [3]. Therefore, any proposed method for storage of hydrogen must avoid imposing considerable operational costs.

1.2. Chemical & physical properties

Producing, storing and consuming hydrogen is not possible without knowing its physical and chemical properties. In this part a summary of important properties of hydrogen related to its storage process is presented. A more detailed list of hydrogen's physical and chemical properties are gathered and presented in Table 3.

Thermodynamic equation of state:

Hydrogen as well as all the other pure substances can exist under vapour, liquid and solid phases. Like all the pure substances the thermodynamic state of hydrogen can be defined by knowing two independent intensive state variables. At ambient pressure hydrogen is in the gas form and obeys the *ideal gas* equation of state:

$$Pv = RT$$

Equation (5)

In which:

v [m^3·mol^{-1}]: molar volume

R = 8.31472 [J·mol^{-1}·K^{-1}]: Universal gas constant

T [K]: Kelvin

P[Pa] : gas pressure

This equation is applicable for most of the gases at low pressures and sufficiently high temperatures (*i.e.* above critical temperature). An improvement of this equation was introduced by *van der Waals*. By considering the intermolecular forces of the gas, *van der Waals* equation of state (equation 6) is qualitatively reasonable for low temperatures as well:

$$\left(p + \frac{a}{v^2}\right)(v - b) = RT$$

Equation (6)

In this equation '*a*' and '*b*' are the specific parameters of the pure component. For hydrogen these parameters are:

a = 0.025 [m^6·Pa·mol^{-2}]

b = 2.66·10^{-5} [m^3·mol^{-1}]

As already mentioned, neither the ideal gas equation nor the van der Waals equations are applicable at high pressure ranges. As an approach for accounting the effect of pressure on the

behaviour of real gases a dimensionless factor called the *compressibility factor* Z is introduced in the ideal equation of state:

$$Pv = ZRT$$

Equation (7)

For an ideal gas at ambient pressure the value of Z is defined 1 and therefore any deviation from this value is a measure of the deviation of the behaviour from the ideal gas state. The compressibility factor for different gases is determined experimentally and can be found in literature and reference handbooks [1, 2]. The value of the compressibility factor (Z) for hydrogen at high pressure and low temperatures can be found in the diagram presented in Figure 1.
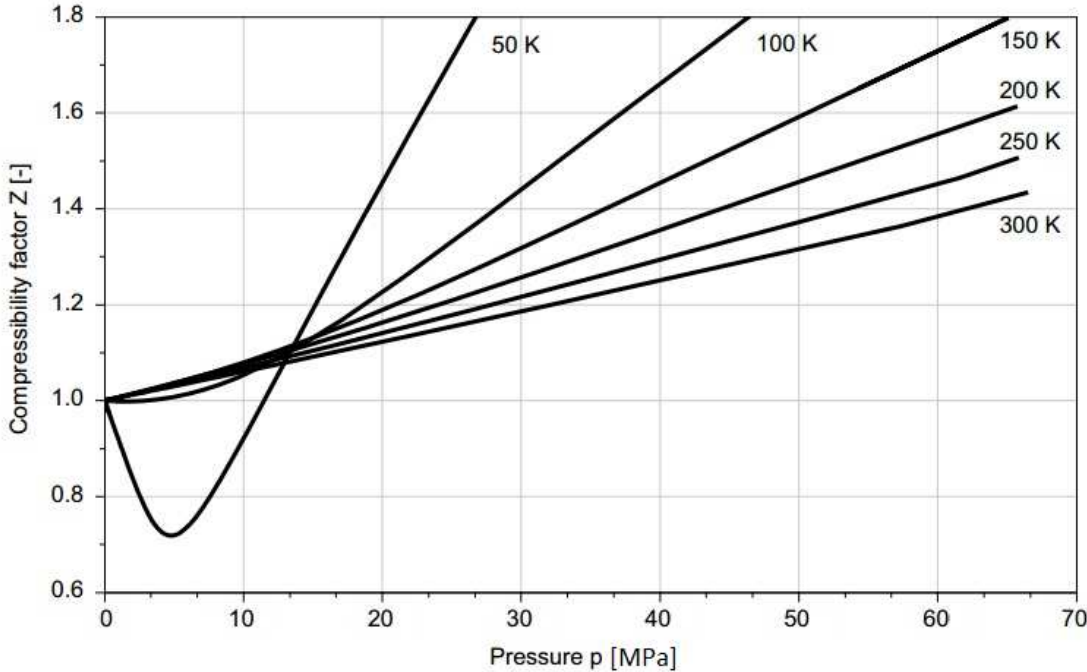
Figure 1 – Compressibility factor (Z) of hydrogen

In this figure for instance at 30 MPa and in a temperature range of 250-300K, the hydrogen compressibility factor has the value of 1.2. This means that at 30 MPa and this temperature range, without considering Z in the ideal gas equation, the calculation will show a false mass amount, 20% more than the reality.

Density:

As previously stated, hydrogen has the lowest atomic weight among all elements and therefore has a very low density both in gas and liquid state in comparison to other

substances. Table 2 presents the comparative data on vapour and liquid densities of hydrogen, methane, gasoline, water.

Table 2 - Comparative data on vapour and liquid densities of hydrogen, methane and gasoline

Substance	Vapour Density (kg·m^{-3}) 293 K – 0.1 MPa	Liquid Density (kg·m^{-3}) boiling point, 0.1 MPa
Hydrogen	0.08376	70.8
Methane	0.65	422.8
Gasoline	4.4	700
Water	-	958

As it can be seen, even at liquid state hydrogen is not very dense. In comparison with water in which one oxygen atom is chemically bonded with two hydrogen atoms, one cubic meter of water contains approximately 111 kg of hydrogen whereas one cubic meter of liquid hydrogen contains only 71 kg of hydrogen. This is an undesirable property specially in the case of storing hydrogen for the purpose of vehicle fuel; in this case the low density of hydrogen necessitates a relatively large volume of hydrogen for a short driving range.

Boiling point & expansion rate

At the atmospheric pressure, hydrogen liquefies at 20 K which is the second lowest boiling point among all elements after helium. This low boiling temperature causes some inconveniences for storing hydrogen in liquid form. On the other hand, for storing hydrogen in the form of compressed gas, another property that must be studied is the expansion ratio. *Expansion ratio* is the ratio of the volume of a gas/liquid in the storage condition, compared to the volume of that gas/liquid under atmospheric pressure. For liquid hydrogen expanding into atmosphere, the expanding ratio is 1:848 meaning that hydrogen in gas form under atmospheric conditions, occupies 848 times more space than hydrogen in liquid form. Although increasing gas pressure increases the expansion ratio (e.g. at 25 MPa the expansion ratio of hydrogen is 1:240) hydrogen gas can never reach the liquid hydrogen expansion ratio.

Leakage

Having high diffusivity and low density, hydrogen can diffuse easily through many materials and leak from different connections. Leakage of hydrogen is dangerous and its mixture with air produces a high potential risk of fire. However, due to their low molecular weight, and their high diffusivity the leaked streams rise and dilute very fast in the environment.

Table 3 - Hydrogen Properties [2]

	Property	Value & Unit
	Molar mass	2.016 kg kmol^{-1}
	Particular gas constant	4124 J kg^{-1} K^{-1}
	(Gravimetric) Calorific value H$_u$	120 MJ kg^{-1}= 33.33 kWh kg^{-1}
at triple point :	Temperature	13.8 K
	Pressure	0.007 MPa
	Density gaseous	0.125 kg m^{-3}
	Density liquid	77 kg m^{-3}
	Heat of fusion	58.5 kJ kg^{-1}
at boiling point (at 0,101 MPa), Liquid phase	Boiling temperature	20.3 K
	Heat of vaporization	445.4 kJ kg^{-1}
	Density	70.8 kg m^{-3}
	(Volumetric) Calorific value	8.5 MJ dm^{-3}
	Specific heat capacity C_p	9.8 kJ kg^{-1} K^{-1}
	Specific heat capacity C_v	5.8 kJ kg^{-1} K^{-1}
	Thermal conductivity	0.099 W m^{-1} K^{-1}
	Dynamic viscosity	11.9*10^{-6} N s m^{-2}
	Speed of sound	1089 m s^{-1}
at critical point:	Temperature	33.20 K
	Pressure	1.31 MPa
	Density	31.4 kg m^{-3}
at standard conditions: (0°C and 0,101 MPa)	Density	0.09 kg m^{-3}
	(Volumetric) Calorific value	0.01 MJ dm^{-3}
	Specific heat capacity C_p	14.32 kJ kg^{-1} K^{-1}
	Specific heat capacity C_v	10.17 kJ kg^{-1} K^{-1}
	Thermal conductivity	0.184 W m^{-1} K^{-1}
	Coefficient of diffusion	0.61 cm^2 s^{-1}
	Dynamic viscosity	8.9* 10-6 N s m^{-2}
	Speed of sound	1246 m s^{-1}

1.3. Industrial applications of hydrogen

Hydrogen has an important role in many industries, from chemical and refining plants to metallurgical, glass and electronic industry. Most of its applications are due to its high reactivity which has caused a rapid increase in its demand especially in petrochemical industry [4]. Generally speaking hydrogen's industrial application can be divided into 3 main categories:

1. As a *reactant* to reduce the heterogonous atoms such as nitrogen and sulphur or in petrochemical industry to saturate the unsaturated hydrocarbons.

2. As an oxygen scavenger in heating applications to prevent corrosion in the equipments.

3. As a fuel.

1.3.1. Hydrogen as a reactant

More than 50% of the worldwide production of hydrogen is devoted to ammonia production [4]. Ammonia is the main feedstock for the fertilizer industry and is produced by the reaction of hydrogen and nitrogen in a process called *Haber*.

In petrochemical industry, hydrogen is mostly used to produce refined hydrocarbons with bigger H/C ratios. Through a process called hydrocraking, hydrogen reacts catalytically with heavy hydrocarbons to finally produce smaller hydrocarbon molecules. In petrochemical plants, due to environmental regulations, pollutants such as sulphur must be removed in a stable chemical form. One common process is hydroprocessing of nitrogen and sulphur components using hydrogen in order to remove them in the form of H_2S and NH_3. These products are toxic and are subsequently converted into sulphur (through Claus process) and KNO_3 (nitrogen fixation)

Apart from these applications, hydrogen is the main feedstock for production of many petrochemicals such as methanol. Methanol is produced from the reaction of hydrogen and carbon dioxide over a mixture of catalysts at a relatively high pressure (5-10 MPa) and high temperature (~523 K) [4]. In additions, hydrogen streams are used to recover oxidized catalysts such as nickel to the active metal form.

1.3.2. Hydrogen as oxygen scavenger

In metallurgy industry, hydrogen mixed with nitrogen is used to trap oxygen molecules and remove it from the system. In this method hydrogen reacts with oxygen to form water. The same method is used in boiling water reactors to reduce the risk of corrosion [4].

1.3.3. Hydrogen as a fuel

Hydrogen in liquid form is mainly used as a propellant in the aerospace industry. Its mixture with liquid oxygen is known to have high energy content per mass which is a key factor for spatial projects.

Regarding its high energy content and its environmentally clean nature hydrogen seems to be an interesting fuel for automobiles; however the major concern for this purpose is its storage difficulties. A conventional automobile with a combustion engine, consumes around 46 L (0.03-0.04 m^3) of diesel weighing 43 kg for a distance of 500 km, while a hydrogen car with a fuel cell engine needs about 5 kg of hydrogen for the same distance to travel. The major problem is that 5 kg of hydrogen at ambient conditions occupies around 56000 L (56 m^3) of space. One possible solution is to use pressurized hydrogen gas but as previously stated, hydrogen gas is not dense and therefore to reach such energy content a large storage tank is required. For the case of a fuel cell engine at 70 MPa a high pressure tank of 260 L (0.26 m3) weighing 125 kg is needed for a driving distance of 500 km [2].

For this purpose, in January 2003 the US Department Of Energy (DOE) has established a Hydrogen Fuel Initiative to perform research, development and demonstration for developing hydrogen storage methods to replace gasoline engines with fuel cells by 2015.

1.4. Hydrogen storage methods

Storage is probably the main obstacle in the immediate use of hydrogen as a fuel. Traditional storage methods based on compression and liquefaction are efficient but their safety concerns and their energy consuming process are not negligible. On the other hand, innovative methods for storing hydrogen through entrapping gas molecules in porous materials or metal solids either do not have a favourable thermodynamic or do not have an acceptable gravimetric hydrogen content.

It must be reminded that efficiency of a hydrogen storage system is not only a problem of mass density of hydrogen, or fast kinetics and favourable thermodynamics but also a matter of energy consumption of the storage method itself. In fact, in each storage method the energy

needed to transform hydrogen from ambient condition to the storage condition, the energy required to keep hydrogen in the storage medium and finally the energy consumed for recovering hydrogen is of great importance.

In this section, the most common hydrogen storage methods are described regarding mass density of stored hydrogen, storage thermodynamic conditions and the energy consumption of the process. It is clear that the purpose of this dissertation is not to present all the hydrogen storage methods, but to gather the most common ones and then introducing clathrate hydrates as an alternative and innovative potential medium for hydrogen storage.

1.4.1. Gaseous storage (Compression)

Storage of hydrogen in gas form in the pressure vessels is known to be the simplest and the most traditional storage method. Compressed hydrogen is usually stored under pressures between 20 MPa to 35 MPa in special containers [5]. As hydrogen has a tendency to diffuse into materials and cause leakage, it is usually stored in vessels made up of austenitic stainless steel and aluminium alloys to overcome this inconvenience. Recently new carbon fiber-jacketed aluminium-alloy cylinders are made, which can bear pressures up to 70 MPa [6].

One of the major inconveniences of stainless steel vessels is their weight. While the gravimetric energy density of hydrogen stored in conventional steel containers under 20-30 MPa is calculated to be around 0.4 kWh·kg^{-1}, efforts have been made to reduce the weight of container to increase the gravimetric energy density of the system. New composite materials have been suggested to replace the steel containers to increase the gravimetric energy density of the system up to 1.833 kWh·kg^{-1}. The main characteristics of two types of gaseous hydrogen containers are compared in Table 4. As it can be seen in this table, reduction in the weight of hydrogen containers is in favour of gravimetric energy density and storage pressure. The important point in this table is that the cost of these containers varies from 40 €/kWh of stored hydrogen for conventional stainless steels containers to 150 €/kWh for new composite one.

Apart from the cost of the storage equipments such as vessels, valves, pipelines and safety systems, one must consider the cost of the compressing process of hydrogen. From thermodynamics the minimum work required for a reversible gas compression is the isothermal compression in which temperature remains constant during the process through cooling:

$$w_{is} = h_2 - h_1 + q_c \qquad \textit{Equation (8)}$$

For a reversible process, the heat exchanged for keeping the temperature constant (q_c) can be calculated:

$$q_c = T.\Delta s \qquad \textit{Equation (9)}$$

A simple thumb-calculation of the isothermal work of compressing hydrogen from 0.1 MPa to 10 MPa at 300K gives:

$$w_i = 4275 - 4227 + 2812 = 2860 \, \textbf{kJ} \cdot \textbf{kg} - \textbf{1}$$

Dividing this value by the hydrogen gravimetric calorific value (120 MJ kg^{-1}) shows that the isothermal compressing of hydrogen is about 2.3% of the gravimetric calorific value of hydrogen. Considering 50% efficiency for a normal compressor this energy increases to 5%.

Table 4 - Characteristics of commercial hydrogen storage containers [2]

Net volume [dm^3]	2.5	20	50	65	120
	Stainless steel containers			*Composite containers*	
Pressure (MPa)	20	20	30	35	70
Tank system weight [kg]	3.5	31.6	58	33	84
Tank system volume [dm^{-3}]	3.6	27	64.7	100	200
H$_2$ density at 25°c [kg m^{-3}]	14.5	14.5	20.6	23.3	39.3
H$_2$ content [kg]	0.4	3.22	11.43	1.52	4.65
Gravimetric H$_2$ content [kg H$_2$ kg^{-1}]	0.04	0.29	1.03	0.047	0.055
Volumetric H$_2$ content [kg H$_2$ dm^{-3}]	0.009	0.011	0.016	0.021	0.023
Gravimetric energy density [kWh kg^{-1}]	0.333	0.305	0.367	1.567	1.833
Volumetric energy density [kWh dm^{-3}]	0.300	0.367	0.533	0.700	0.767

It means that for compressing hydrogen pressure up to 10 MPa, 5% of the energy content must be spent for compression. This percentage reaches 15% if hydrogen is compressed up to

90 MPa. It must be insisted that the calculated work is the minimum work required to compress hydrogen while in practice, hydrogen is compressed through an adiabatic process.

When a fluid flows through a restriction, such as a valve or a vessel, without any considerable change in kinetic or potential energy, the primary result of the process is the pressure drop in the fluid. This is called a throttling process in which no shaft work is produced. If this process is done adiabatically *i.e.* in absence of heat exchange, the process occurs at constant enthalpy. What happens during an isenthalpic compression is the change in temperature. This behaviour can be predicted by employing the *Joule-Thompson Coefficient*:

$$\mu_{JT} = \left(\frac{\partial T}{\partial P}\right)_h$$

Equation (10)

A positive Joule-Thompson coefficient means that during an isenthalpic pressure drop, temperature will decrease, while a negative Joule-Thompson coefficient will result in temperature increase during an isenthalpic pressure drop. During the filling of a pressure vessel, hydrogen flows from a reservoir of a higher pressure in to an empty tank. In the relevant pressure range of hydrogen compression, hydrogen has a negative Joule-Thompson coefficient; therefore by filling the container, the gas temperature will increase. When the warmed-up hydrogen in the closed container cools down to the ambient temperature the pressure of the gas inside the vessel starts to decrease. This phenomenon will cause a loss of hydrogen pressure in the compressing and filling process compared to the expected stored hydrogen.

Although storing hydrogen in gas form is the simplest method, due to low hydrogen mass density and the potential safety risks it does not satisfy the requirements for all hydrogen storage applications.

1.4.2. Liquid storage (Liquefaction)

Difficulties in storing hydrogen in liquid form can be understood from its phase diagram [Figure 2]. As can be seen in this diagram, there is only a small region between the triple point (T=13.803 K, P=0.00704 MPa) [1] and the critical point (T=32.98K, P=1.325 MPa) [1] in which hydrogen can exist in liquid form. Hydrogen's boiling point at ambient pressure (0.1 MPa) is about 20.39 K which is the second lowest boiling point of any element after helium.
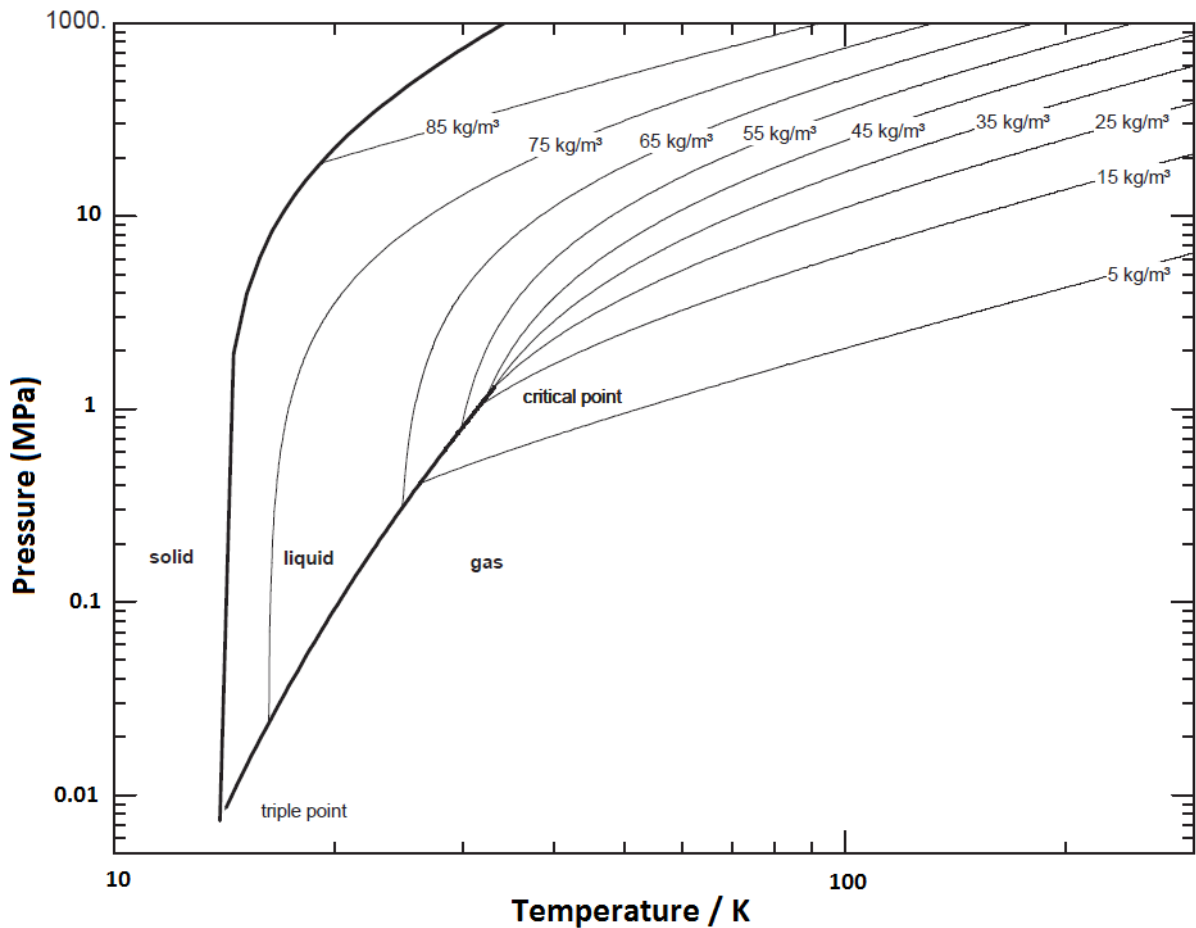
Figure 2 – Phase diagram of Hydrogen [2]

Theoretically hydrogen can be condensed and liquefied by using helium as a cooling medium but such a process is economically unviable. In an alternative process, hydrogen is expanded to 30 bar and then with the help of liquid nitrogen is cooled down to 80 K. The cooled down hydrogen then enters in a cycle of expansion turbines to cool down again to about 30 K. The last stage of cooling is through a Joule-Thompson valve, with a positive Joule-Thompson coefficient which cools down hydrogen from 30K to 20K [2].

The theoretical work needed for condensing hydrogen is 3.23 kW h/kg but in practice this work is five times more *i.e.* 15.2 kW h/kg [5]. The real efficiency of the process in industry is around 30% which implies that around 30% of the energy content of stored hydrogen must be consumed for its liquefaction.

Another inconvenience in storing hydrogen in liquid form is boil-off phenomenon. Despite insulation of storage tanks, due to the inevitable heat transfer from the surrounding environment, hydrogen will evaporate inside the storage tank which results in an increase of vessel's pressure. Consequently, when pressure reaches a safety threshold, hydrogen has to be

blown out to keep the tank pressure constant. This boil-off results in 1-2% loss of the mass of stored hydrogen per day [6].

Figure 3 compares the gravimetric energy density of pure hydrogen storage systems with gasoline and natural gas storage systems. As it can be seen in this diagram, gasoline and CNG, in spite of their lower gravimetric density, have a better overall gravimetric energy density and appear to be more long lasting energy sources especially because of their light and cheap storage systems.

Despite of high gravimetric H_2 content of 33.3 kg [H_2] kg^{-1} the economical and technical difficulties of hydrogen storage in liquid form makes usage of liquid hydrogen limited to applications such as spatial industry, where the high cost of liquefaction and its continuous loss during boil-off is affordable.
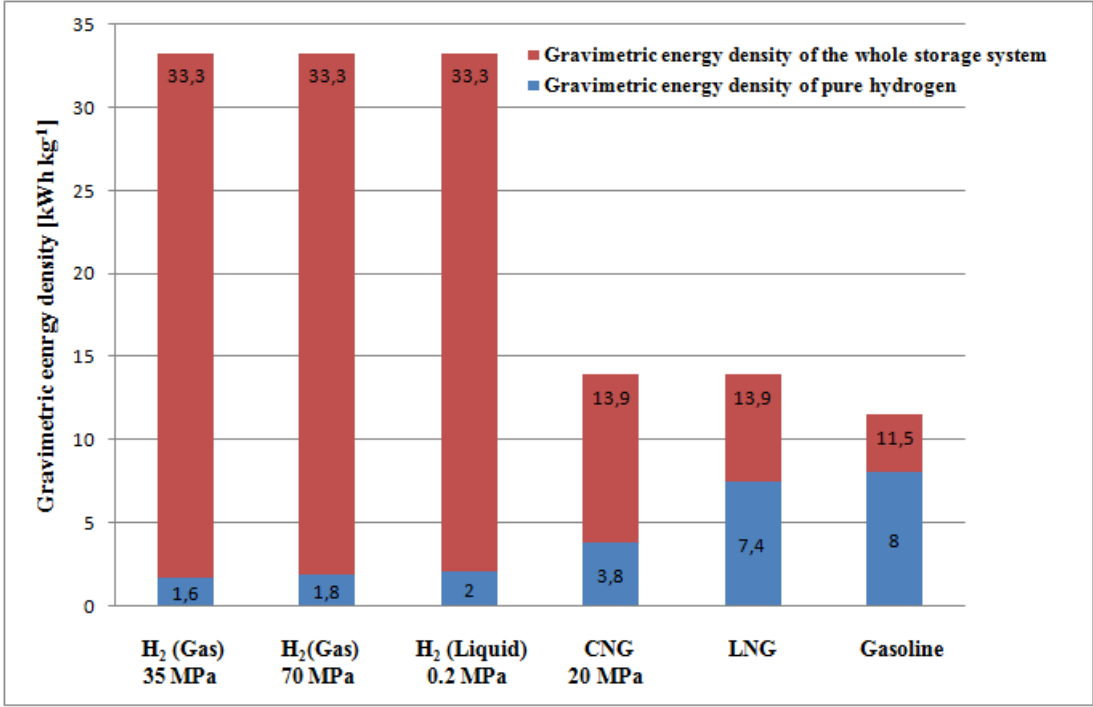
Figure 3 – Comparison of the gravimetric energy densities of pure stored hydrogen with other energy sources [2]

1.4.3 Physical adsorption of hydrogen in porous materials

As it was previously stated, pure storage of hydrogen in gas or liquid form demands severe operational conditions and relatively high costs. They also have several safety issues and cause serious disadvantages for mobile application.

One alternative solution is to trap hydrogen molecules through an interaction with other compounds by means of molecular or chemical bonds. Depending on the nature of interaction between hydrogen and the supporting medium this phenomenon can be called physisorption (physical adsorption) or chemisorptions (chemical adsorption).

In physical adsorption hydrogen is adsorbed in molecular form through *van der Waals* forces with the molecules on the surface of adsorbent. Physical adsorption is an exothermic process and because it occurs in molecular scale, without any dissociation of hydrogen molecule, the heat released from this process is not considerable. This is an advantage for physical adsorption compared to chemisorption methods, in which the excessive amount of heat produced results in the increase of the temperature of hydrogen storage tank. However because of the weak *van der Waals* interaction between hydrogen molecule and solid surface the amount of stored hydrogen is low.

Another advantage of physisorption is that it is a reversible process which means hydrogen can be easily adsorbed and desorbed several times without any loss. Moreover, desorption process demands generally no activation energy which makes adsorption/desorption kinetics favourable. This favourable fast and reversible kinetic is a key point in application of physisorption for mobile storage of hydrogen.

One key parameter in efficiency of physisorption is the Surface Specific Area (SSA) which controls hydrogen adsorption capacity of the adsorbent material [7]. The larger the specific surface area is, the more hydrogen molecules will be adsorbed on the adsorbent surface. In this sense, the most frequently used materials for hydrogen physisorption are activated carbons, carbon nano structures (*e.g.* carbon nanotube), fullerenes, zeolites and metal organic frame works (MOF) which are explained below:

Carbon materials

In the nature, carbon exists in two principal forms of diamond and graphite which none of them are porous. However, a porous nano-structural form of carbon exists which is made up of cyclohexane like carbon chains. This variety of carbons differs from each other by the way these carbon hexagons are arranged. These porous carbon materials are generally divided into two main groups: carbon nanotubes which are composed of long ordered chains of carbon hexagons and active carbons which have irregular structures.

Activated carbons with a high surface area (up to 3300 $m^2 \cdot g^{-1}$) are reported to have a storage capacity of about 6 wt% at 70 K and 4 MPa [7]. Reducing pressure to 2 MPa at the same temperature (77 K) gives a storage capacity of 5 wt% [8]. The same activated carbon at the same temperature and at ambient pressure is reported to have a storage capacity of 4.5 wt% [9]. Comparatively, carbon nanotubes at liquid nitrogen temperature (77 K) and 4 MPa were reported to adsorb up to 8 wt% of hydrogen [10].

Fullerenes

Contrary to carbon nanotubes and activated carbons, bulk fullerene C_{60} powder does not have a high surface area. Nevertheless the solid C_{60} is capable of hosting some hydrogen molecules. The hydrogen capacity of C_{60} is limited to 0.1-0.2 wt% of H_2 [11-13] while by increasing the pressure until 30 MPa it will reach the maximum capacity of 0.7 wt% [14].

Zeolites

Zeolites are crystalline compounds composed of aluminosilicate structure made between Si^{+4} and Al^{+3} ions with oxygen. Due to the ionic base of their structure and therefore presence of electrostatic forces inside these pores, zeolites can produce adsorption sites for hosting different molecules. Several investigations have been carried on the storage capacity of zeolites for storing hydrogen recently. The very early results show a small capacity of 0.1 wt% at ambient conditions [15] while another research at 77 K shows a storage capacity of up to 2.5 wt% at 1.5 MPa [16].

Metal-Organic Frame works (MOFs)

Among different materials for storing hydrogen by physisorption, Metal Organic Frame works (MOFs) have attracted the most attentions. MOFs are crystalline coordination polymers consisting of metal clusters connected together by organic linkers [Figure 4]. Combining different organic ligands and ion cluster make it possible to synthesize different MOFs with different structure modified properly for hydrogen storage.

This possibility of modifying the structure makes MOFs the most interesting storage materials among all the physical adsorption methods. Furthermore they have an extremely high surface area (10400 m^2/g for MOF-200 and MOF-210 [17]) which permits a high hydrogen adsorption for this group of materials.

The first investigation on the MOFs storage capacity for hydrogen storage shows an interesting value of 1 wt% at ambient temperature and 0.2 MPa for MOF-5 [18]. Although

this storage capacity is relatively low, it is still one of the best among all the physisorption mechanisms at ambient temperature. However, at lower temperatures (78 K) the storage capacity of the same MOFs rises to 4.5 wt% [18]. Recently a maximum storage capacity of 4.5-5.2 wt% was reported for MOF-5 at 5 MPa and 77 K [19-21].
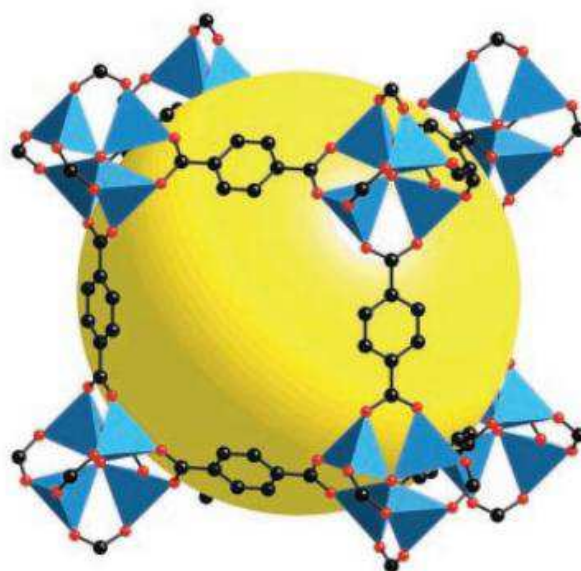
Figure 4 – Single crystal structure x-ray of MOF-5. Eight metal clusters each containing four ZnO4 tetrahedral nodes, make a enclosed large cavity for entrapping hydrogen molecules. Reprinted from [18].

After MOF-5 many other MOF structures were investigated for hydrogen storage showing storage capacity of 7.5 wt% at 77 K and 8 MPa [21]. This value is the highest storage capacity reported for any porous material storing hydrogen in molecular form.

1.4.4. Metal hydrides and complex hydrides (Chemisorption)

Apart from the physisorption in which hydrogen is adsorbed in molecular form by making *van der Waals* bonds, hydrogen can chemically react (chemisorption) with some solids forming covalent or ionic bonds. The most important materials for storage of hydrogen through chemisorption are metal hydrides. Metal hydrides are single phase compounds formed by chemical bonds between a host metal and hydrogen. Historically, chemistry of hydrides has been mostly developed for making rechargeable batteries however new research are being targeted on using hydrides as a storage medium for hydrogen.

Depending on the metal host, metal hydrides can be divided as:

Ionic or Saline hydrides: which contain binary hydride of alkali metals such as calcium, sodium, lithium, or barium. In these series of hydrides hydrogen is in the form of negative ion (H⁻) and makes a ionic bond with solid metals. The most common ionic hybrids are NaH and CaH_2. MgH_2 as the most studied hybrid of this group is not completely a real ionic hydride. In MgH_2 the chemical bond between hydrogen and metal is partly ionic and partly covalent, however due to the nature of Mg it is categorized in this group [2]. The main reason of attention to magnesium hydride is that between all the ionic hydrides MgH_2 shows a high hydrogen gravimetric capacity of 7.7 wt% with a good reversible behaviour [22]. However the main inconvenience of MgH_2 as well as the other metal hydrides is its slow and high endothermic desorption process which results in an increase in the temperature of the released hydrogen. For example, desorption of MgH_2 releases hydrogen at 573 K and with a hydrogen pressure of 0.1 MPa [23]. In additions, MgH_2 is highly reactive with air.

Metallic hydrides are compounds of hydrogen and transition metals including rare earth elements. Examples of these series of hydrides are, TiH_2 or ThH_2.

Complex hydrides in which hydrogen is directly bounded to the central atom through covalent bonds. The general chemical formula of complex hydrides is $A_xMe_yH_z$ where A is usually an element from the first group or the second group of the periodic table and Me is usually either boron or aluminium [2]. The most well studied complex hybrid is LiBH4 which has proved to have hydrogen gravimetric density of 18 wt% [24]. Table 5 presents a comparative hydrogen gravity density of some well described complex hydrides.

As it is shown in Table [5], despite of their high hydrogen content, dehydrogenation (decomposition) of these complex hydrides is highly endothermic and demands a lot of energy. On the other hand those hydrides that adsorb and desorb hydrogen at ambient temperature and pressure mainly consist of transition metals and therefore the gravimetric hydrogen content is dramatically reduced (less than 3wt%). For instance, $LaNi_5H_5$ with a volumetric density of 115 kg m⁻³ has a gravimetric hydrogen content of only 1.4 wt% [4].

To summarize hydrogen storage in hydrides, it must be emphasized that although metal hydrides and complex hydrides have the advantage of containing high hydrogen contents, the slow adsorption/desorption kinetics and heat release during their dehydrogenation process is a big obstacle in their usage as a commercial hydrogen storage medium. On the other hand those hydrides which possess a favourable adsorption/desorption kinetics have low gravimetric hydrogen contents.

Table 5 - Comparative hydrogen storage data of most common complex hydrides

Hydride	Molecular weight (g mol^{-1})	Decomposition temperature (K)	Hydrogen content (wt%)	Reference
LiBH$_4$	21.8	320	18.4	[24]
NaBH$_4$	37.8	450	10.6	[25]
KBH$_4$	53.8	584	7.4	[26]
Be(BH$_4$)$_2$	38.6		20.7	[2]
Mg(BH$_4$)$_2$	53.9	320	14.8	[27]
Ca(BH$_4$)$_2$	69.8	360	11.5	[28]
Al(BH$_4$)$_3$	71.4	~40	16.8	[29]

1.5. Clathrate hydrates

Clathrate hydrates are inclusion structures made up of water and small (typically gas) molecules. Under appropriate thermodynamic conditions, *i.e.* high pressure & low temperature, water molecules form an enclosed hydrogen bonded structure (cages) around small captured molecules. Due to their potential in future energy storage, they have been subject of many researches, particularly over the last 20 years. This work, investigates clathrate hydrates as an alternative solution for hydrogen storage. Due to the focus of this work on clathrate hydrates as a storage media, a more detailed description of these compounds seems inevitable. For this reason, the first part of this work is dedicated to general properties of inclusion compounds and their different structure. In the second part a brief history of hydrogen storage in clathrate hydrates is reviewed.

1.5.1. Introduction

Natural gas hydrates are subset of a larger group of compounds known as clathrate or inclusion compounds. A clathrate is a compound in which a molecule of one substance (typically gas) is enclosed in a structure built from molecules of another substance [31]. Natural gas hydrates are composed of an aqueous solution and gas molecules in which gas molecules (guests) are trapped in water cavities (host). These cavities are formed as a result of hydrogen bonds between water molecules. Typical hydrate former constituents of natural gas are methane, ethane, propane, and carbon dioxide [30].

Although hydrates have been probably encountered by many chemists during history, it was Sir Humphrey Davy who first reported the formation of hydrate of chlorine in 19th century

[30, 31]. Michael Faraday continued Davy's work, by studying the composition of chlorine hydrates, and in 1823 for the first time he measured the composition of hydrate. But it was not until 20th century that the industrial importance of gas hydrates was discovered. During the development of gas industry it was discovered that under relatively high pressure, pipelines and processing equipments plug because of the formation of an ice like substance, which conditions of formation was however different than ordinary ice.

1.5.2. Water and Ice (irregular) properties

For a better understanding of hydrates, one must first study water (and Ice) unusual properties caused by hydrogen bonding. Water molecules possess four valance electrons from lone pair orbital of two oxygen atoms. The shared electrons with the protons give the water molecule two positive charges (hydrogen atoms) and the lone pair electrons give the molecule two negative charges (oxygen atoms). The result is a molecule with four charges and a permanent electric dipole.

Hydrogen bond is caused by the attraction of the positive poles on one molecule to the negative poles on a neighbouring water molecule [Figure 5a]. Through this hydrogen bond, each water molecule is attached to four others, giving two and accepting two hydrogen bonds. This is shown in Figure 5b. The four surrounding molecules are arranged tetrahedrally around the central molecule. The energy required to break a hydrogen bond, lies between the molecular *van der Waals* bonds and chemical covalent bonds [30]. Hydrogen bonds inhibit the vaporization of liquid water, which results in an increase in boiling temperature of water, in comparison to similar molecular weight compounds such as methane. Other unusual properties of water caused by hydrogen bonds include the density maximum as a function of temperature, increase in specific heat by reduction of temperature, and increase in diffusion constant as the density increases [30].
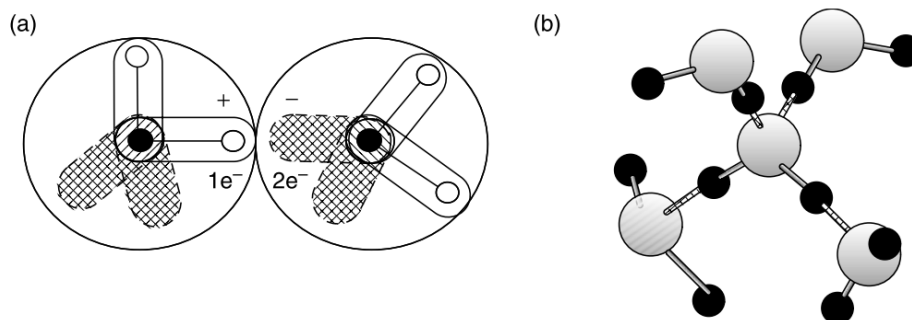
Figure 5 - Hydrogen bond in water molecule: a) between two molecules b) between four molecules [30]

The most common solid form of water is ice Ih, *i.e.* hexagonal ice [30]. In molecular structure of ice each water molecule (circles) is connected to four other water molecules through hydrogen bond forming tetrahedral angles. It is suggested [30] that these tetrahedral coordination, represents the most feasible way of packing of water molecules in order to fully develop hydrogen bonds. This package of water molecules hydrogen bonded together in a solid lattice is the ice crystal [Figure 6].

The formation of hydrates is also a result of the presence of hydrogen bonds between water molecules. The hydrogen bonds cause water molecules to align in regular orientation and in presence of certain hydrophobic molecules water molecules make a hydration shell around them. This behaviour is attributed to clathrate behaviour of water in which water molecules form into rather pentagonal structures (cage) compared to tetrahedral structures in pure water ice [30, 31].
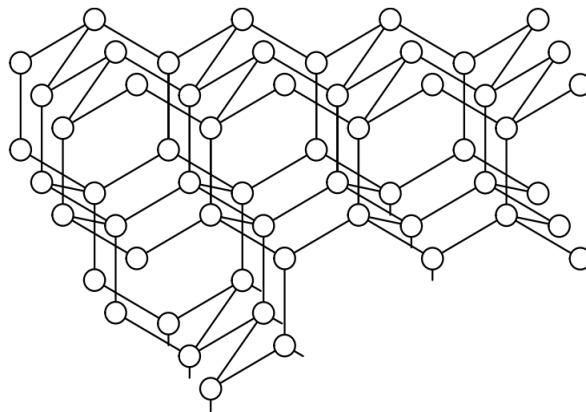
Figure 6 - Crystal structure of ice Ih [30]

In this structure, water molecules are called *host molecules* and other compounds, which stabilize this crystal structure (hydrate), are called *guest molecules*. This stabilization, results from *van der Waals* forces between molecules rather than electrostatic forces in hydrogen bonds. It must be emphasized that there is no bonding between guest molecules and host molecules of the cage, and the guest molecules can easily rotate inside cages. It is for this nature of hydrates that they are usually described as *solid solutions*.

1.5.3. Structures of different hydrate types

Hydrate structures include five different polyhedral structures as shown in Figure 7. The common nomenclature for these compounds is usually described in form of $n_i^{m_i}$, where n_i is

the number of edges in face type i and m_i is the number of faces with n_i edges. For example pentagonal dodecahedron, a cavity with 12 sides is called 5^{12}.
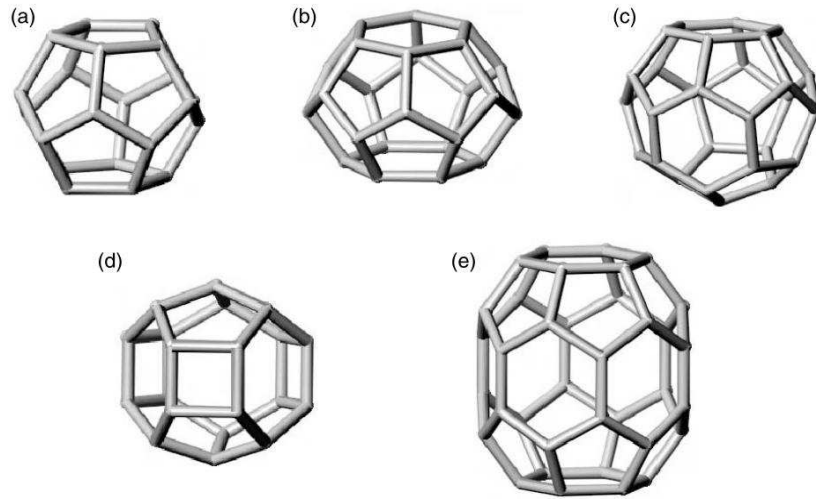
Figure 7 - Five different gas hydrate cavities rates: (a) pentagonal dodecahedron (5^{12}), (b) Tetrakaidecahedron ($5^{12}6^2$), (c) hexakaidecahedron ($5^{12}6^4$), (d) irregular dodecahedron ($4^35^66^3$), and (e) icosahedron ($5^{12}6^8$) [30]

A brief and summarized description of these cavities is given below:

a) **Pentagonal Dodecahedra (5^{12}):** It is the characteristic feature of the gas hydrates structure. Pentagonal dodecahedra ($H_{40}O_{20}$) with its 12 pentagonal faces (5^{12}), 20 vertices, and 30 edges shown in figures 3a is the smallest cavity in all known natural gas hydrate structures [30, 32]. This cavity is almost spherical with a radius of 3.91 Å in structures I and II respectively [30]. Unlike other polyhedral familiar to solid state, *e.g.* the tetrahedron, the pentagonal dodecahedron cannot fill space in any face-sharing periodic arrangement [32], that is different polyhedral structures such as 14-hedra 16-hedra are needed to provide the three-dimensional repeating patterns necessary to form a crystal structure.

b) **Tetrakaidecahedron ($5^{12}6^2$):** This cavity is formed by 2 facing hexagons and 12 connecting pentagons. Each hexagon has six pentagons attached to its edges, resulting in two cup shape hemispheres, each formed from a hexagon at the base with six pentagons at the hexagon sides. Figure 7b shows that this cavity is the most nonspherical cavity in sI or sII structures. With an average radius of 4.33 Å,

tetrakaidecahedron is large enough to contain molecules smaller the 6.0 Å in diameter [30].

c) **Hexakaidecahedron ($5^{12}6^4$):** It is a sixteen-sided polyhedron with twelve pentagonal faces and four hexagonal faces. Each hexagonal face is surrounded entirely by pentagonal faces. 16-hedron is the most spherical cavity of five types, and can contain molecules as large as 6.6 Å. Therefore, when larger components of natural gas such as propane or iso-butane form simple (single guest) hydrates, they stabilize this cavity alone [30, 31].

d) **Irregular dodecahedron ($4^35^66^3$) and the icosahedron ($5^{12}6^8$):** These two rare cavities are constructing parts of structure H of hydrates. Irregular dodecahedron has three square faces, six pentagonal faces and three hexagonal faces. Icosahedron is a twenty-sided polyhedron with twelve pentagonal faces and eight hexagonal faces.

Assembly of hydrate cavities together, forms different clathrate hydrate structures, sometimes known as hydrate types. Among different possible hydrate structures, three types are the most common clathrate hydrate structures: structure I (sI), structure II (sII) and structure H (sH). A brief description of each of these different structures is given:

I. Structure I (sI):

This is the simplest structure of hydrates, made up of 2 dodecahedron (5^{12}) and 6 tetrakaidecahedron ($5^{12}6^2$). There are only 46 water molecules inside the structure I lattice, and there are only 8 polyhedral patterns totally included within the cube. In the presence of a hydrate former (X), and in the case that this guest molecule occupies all the cages, the theoretical formula would be X.5 ¾ H_2O, but it should be taken into account that not all of the hydrate structures are stoichiometric, which means a stable hydrate can form without a guest molecule occupying all the cages [30,31]. Common guest molecules for this structure include CH_4, CO_2 and H_2S. A schematic view of this structure is given in Figure 8.
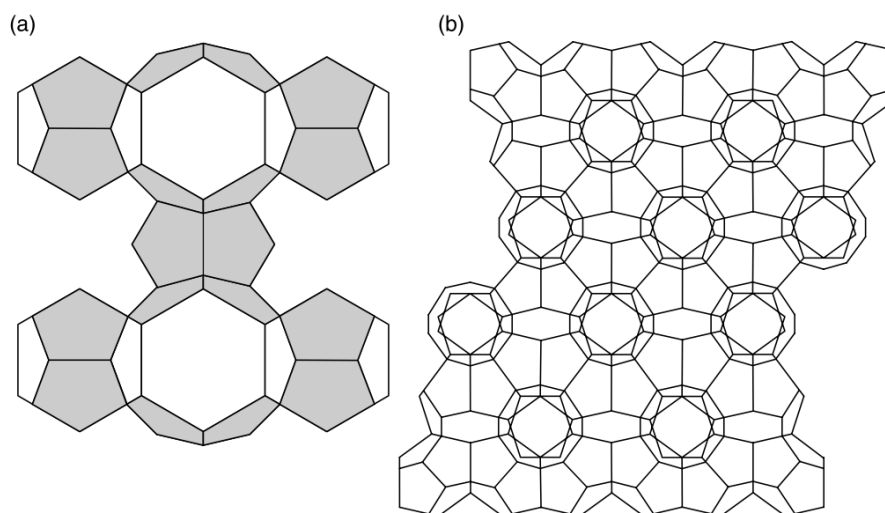
Figure 8 - View of structure I of hydrate clathrate. a) five 5^{12} polyhedral are connected by two $5^{12}6^2$ polyhedral b) two-dimensional view of sI [3]

II.   Structure II (sII) :

Type II lattice is made up of two type of cages: 16 dodecahedron (5^{12}) cavities and 8 hexakaidecahedron ($5^{12}6^4$) cavities, and consists of 136 water molecules. Again this type is not stoichiometric. If all of the cages are filled with guest molecules the theoretical composition would be X.5 2/3 H_2O and when only large cages are filled, the composition is X.17 H_2O. Common known guest molecules for this structure are nitrogen, propane and isobutane [30, 31]. A schematic diagram of this structure is shown in Figure 9.

III.   Structure H (sH):

This type is much less common that sI and sII structures. In contrast to two other types, sH is composed of three cages: 3 dodecahedron (5^{12}), 2 irregular dodecahedron ($4^35^66^3$) and 1 icosahedron ($5^{12}6^8$). Another important characteristic of sH hydrates is that, for formation of this type, two sizes of molecules are required (to stabilize the structure). Small molecules such as methane or hydrogen sulphide fill up small cages (5^{12} and $4^35^66^3$) and large molecules (> 7.3 Å) such as 2,2-dimethylbutane fill up $5^{12}6^8$ cavities [30, 31]. A schematic diagram of this structure is presented in Figure 10.
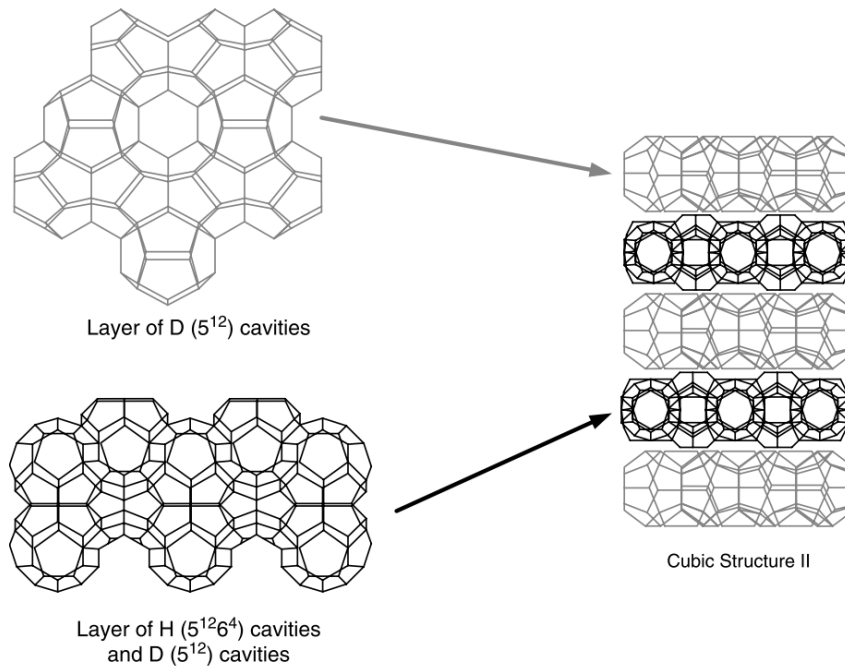
Figure 9 - Schematic of hydrate structure II [30]

Layer of D (5^{12}) cavities

Layer of H ($5^{12}6^4$) cavities
and D (5^{12}) cavities

Cubic Structure II
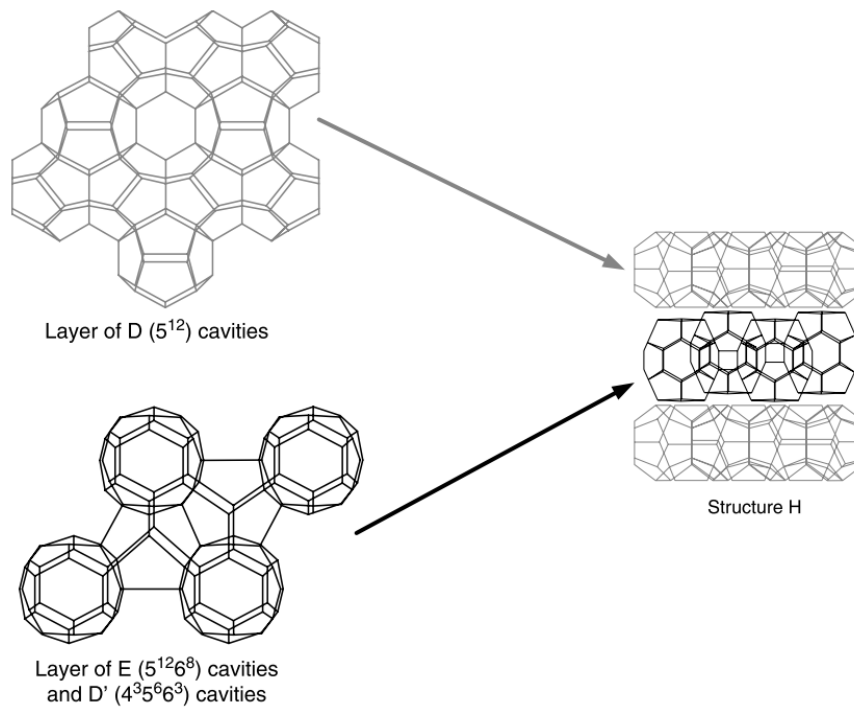
Figure 10 - Schematic presentation of hydrate structure H [30]

Layer of D (5^{12}) cavities

Layer of E ($5^{12}6^8$) cavities
and D' ($4^3 5^6 6^3$) cavities

Structure H

Table 6 summarizes the properties of different hydrate structures. It must be reminded that there are also some other structures known as *Jeffrey's structures* including structures III to VII which are not discussed here.

44

Table 6 - Geometry of hydrate cages

Hydrate Structure	sI		sII		sH		
Cavity	Small	Large	Small	Large	Small	Medium	Large
Description	5^{12}	$5^{12}6^2$	5^{12}	$5^{12}6^4$	5^{12}	$4^35^66^3$	$5^{12}6^8$
Number of cavities	2	6	16	8	3	2	1
Cavity radius (Å)	3.95	4.33	3.91	4.73	3.94	4.04	5.79
Vol. unit cell (m^3)	$1.728*10^{-27}$		$5.178*10^{-27}$				
Typical guests	CH_4, C_2H_6, H_2S, CO_2		$N_2, C_3H_8, i\text{-}C_4H_{10}$				

It must be noted that one key parameter which modifies hydrate structure is the size of the guest molecule. The relationship between the size of a molecule and the type of hydrate formed is given in Figure 11. According to this diagram, starting from the top, small molecules such as Ar, Kr and N_2 occupy small cavities of sII hydrate structure and larger molecules such as butane that occupy bigger cavities. Some of these molecules are small enough to occupy both small and large cavities of sII structure. In the lower region, methane, hydrogen sulphide and CO_2 are sI structure former. These molecules are small enough to fill both small and large cavities. After these two regions, there are larger molecules such as ethane and propane which fill larger cavities of sI and sII structures respectively [30, 31].

There are also other criteria for guest molecules. It is believed [30] that these molecules must be of one of the following groups: 1. Hydrophobic compounds 2. Water-soluble acid gases 3) water soluble polar compounds and 4. Water soluble ternary or quaternary alkylammonium salts. Moreover, guest molecule must not contain either a single strong hydrogen-bond group or a number of moderately strong hydrogen-bond groups [30].
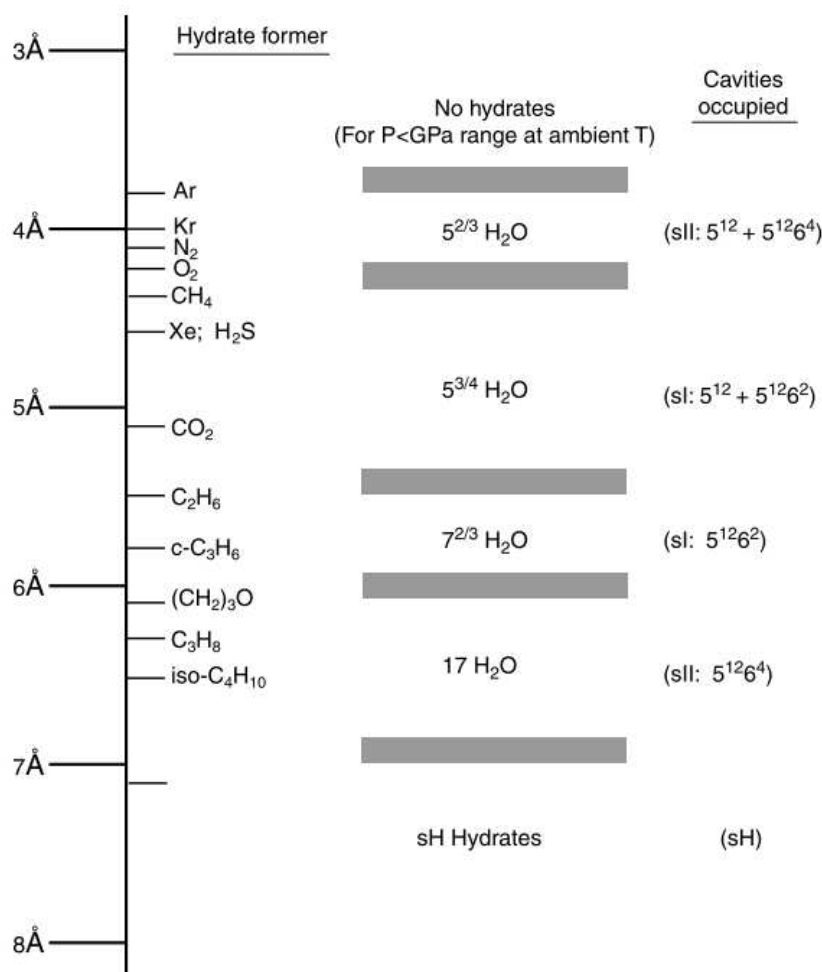
Figure 11 - Guest size relationship with hydrate type [30]

1.5.4. Hydrogen storage in inclusion compounds

1.5.5. Binary systems

Historically it was thought that hydrogen molecule was too small to stabilize clathrate hydrates [33, 34]. It was first *Udachin et al.* [35] who experimentally reported that binary system of hydrogen / helium with tetrahydrofuran (THF) and hexafluorophosphoric acid (HPF_6) forms sII clathrate. They reported that THF or HPF_6, occupy large cages ($5^{12}6^2$) of sII clathrate, while He or H_2 enter the small cages (5^{12}). According to their results, at 7 kbar (700 MPa) and 210 K, in the binary system of THF+H_2, filling degree of small cavities reaches 121% which shows that there is the possibility of double occupancy of small cavities with hydrogen. In the HPF_6 system, in the same range of temperature and pressure, the maximum filling reached 98.2%.

46

In 1999, Dyadin et al. [36] demonstrated formation of the first pure hydrogen hydrate (H_2+H_2O). Although they did not study hydrate structure by diffraction methods, they confirmed formation of classical hydrates of hydrogen, with $H_2:H_2O$ ratio of 1 to 6 ($H_2.6H_2O$) with ice II framework through the similarities in liquid water + hydrate + vapour equilibrium curves between H_2 system and that of other noble gases such as Xe, Ar, Kr gained through thermal analysis. They also reported the phase boundaries of pure H_2 hydrate, ice Ih, and ice II in H_2 pressure range of 1 to 4 kbar.

Following the investigations of Dyadin et al. [36], in 2002 Mao et al. [37] performed the first detailed study on $H_2 + H_2O$ system and synthesized the first pure hydrogen clathrate hydrate. Under pressure of about 220 MPa, and temperature of 300 K, in an anvil diamond cell, the new crystalline phase was grown between the distinct hydrogen and liquid water phase, which by further X-ray diffraction methods, was identified as a hydrate. Moreover, using Raman spectroscopic measurement, they proved the presence of hydrogen molecules in hydrate phase. According to their work in the sII unit cell 136 H_2O molecules form frameworks around 8 large ($5^{12}6^4$) and 16 small (5^{12}) cages, in which they attribute 2 H_2 to each 5^{12} cage and 4 H_2 to each $5^{12}6^4$ cage, as shown in Figure 12, and in this way the concluded a stoichiometric composition of $H_2.2H_2O$ ($32DH_2.32LH_2. 136H_2O$).

 In order to study storage conditions of H_2 in clathrate hydrates, Mao *et al.* [38] performed another series of experiments on $H_2 + H_2O$ binary system. In this way they synthesized a hydrogen clathrate hydrate with stoichiometric composition of $H_2. 2H_2O$ at 200-300 MPa and 240-249 K. In order to improve the storage conditions of H_2 in this clathrate, they explored a low temperature method through which they could preserve H_2 stored in the ambient pressure route.
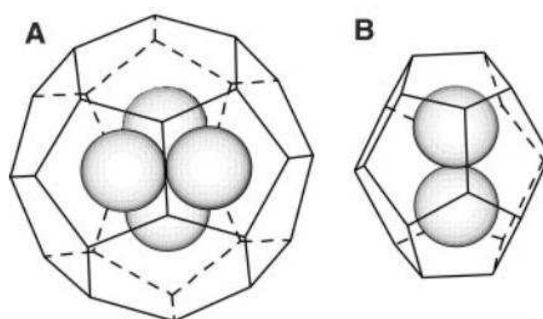
Figure 12 - The cage occupancy proposed by Mao al.[10] : A) 4 H₂ molecules occupy hexakaidecahedron
($5^{12}6^4$) cavities B) 2 H2 molecules occupy pentagonal (5^{12}) cavities

In their method, they proposed that hydrogen is retained and solidified by weak bonding to host molecules under moderate synthesis pressure and temperature. The solid is cooled down to low temperature (77 K) and the pressure is released to the ambient pressure. By this experiment they claimed that they have retained 50 $g \cdot L^{-1}$ hydrogen by volume, which is 5.3 wt%.

The results of Mao et al. [37, 38] were considered as important steps in hydrogen storage. The hydrogen content reported (5.3 wt%) was in line with the storage value targeted by DOE's 2010 goal (5.5 wt%). Moreover, simple hydrogen hydrate has several advantages as a hydrogen storage material. First of all, the storage material is pure water which is abundant and not expensive. Also, when hydrogen is released the only by-product is water which is again reusable and compatible with hydrogen fuel cells [34]. Secondly the formation and decomposition kinetics are rapid. Furthermore, as hydrogen is stored in molecular form, no chemical reaction is required for decomposition of hydrate and release of hydrogen.

After the works of Dyadin et al. [36] and Mao et al. [37, 38], Lokshin et al. [39] suggested a very fast method for hydrogen hydrate production from pure D_2 gas and ice Ih at 77-273 K, which is at least 100 times faster compared to conventional methods. (They used D_2O water/ice and D_2 gas for study instead of hydrogen, in order to minimize the background of collected diffraction patterns). In this experiment, instead of forming hydrate from H_2O/H_2 reaction, they produced hydrate from powdered ice Ih in presence of hydrogen gas. According to their results, at high pressures (1500- 2000 bar) hydrates forms in less than 5 minutes, and at moderate pressure (500 bar) hydrate forms in 30 minutes [39].

Following the work of Mao et al. [37,38] a controversy arose on the double occupancy of the small pentagonal cages by 2 hydrogen molecules, and the reproducibility of their results was questioned. It was first Lokshin et al. [40] who discussed the "unusually high guest/H_2O ratio of 0.45" proposed by Mao et al. [37, 38]. Through their neutron diffraction experiments they found out that the number of D_2 molecules (again deuterium was used in order to minimize the background of collected diffraction patterns) and their distribution in the clathrate structure depend on the temperature and pressure. They performed their measurements at two different thermal conditions. Firstly, at temperatures below 50 K and then at temperatures around 180 K. At temperatures below 50 K (ambient pressure) the large cage was found to be occupied by four D_2 molecules, whereas small cages were occupied by only one D_2 molecule [40]. As the temperature increases, cage occupancy decreases where at 180 K and 2 kbar, the

lowest occupancy of large cages is found to be 2 D_2 molecules which is probably a minimum value necessary for the stability of the framework structure. In contrary to Mao et al. findings [37,38], Lokshin et al. [40] demonstrated single cage occupancy of the small cavities by D_2 molecules at 163 K and atmospheric pressure. They also proposed a stoichiometric composition of $48H_2.136H_2O$ for hydrogen hydrate. This was also confirmed by Strobel et al. [34, 41]. Assuming single occupancy in small cavities, the maximum potential capacity of hydrogen hydrates storage systems reduces from 5 wt.% to 3.8 wt.% . Although this value is lower than DOE's goals, but it is still higher than the value in most metal hydrides considered as hydrogen storage materials [40].

1.5.6. Ternary systems

Extreme pressure and temperature conditions of hydrogen hydrates formation in additions to their low storage capacity led the efforts toward using promoters to enhance the stability of hydrogen hydrates. It was first shown by Udachin et al. [35] that in pressure of 3.5 kbar (210 K), a sII hydrate is formed with H_2 in the presence of tetrahydrofuran (THF) which correspond to the stoichiometric structure of $THF.3.64H_2.17H_2O$.

In 2004, Florusse et al. [42] showed that hydrogen clusters can be stabilized and stored at low pressures within the clathrate hydrate lattice by stabilizing the large water cages with THF as a second guest component. THF was selected as the second guest component because it is completely miscible in water and THF+water forms a sII hydrate alone. Through equilibrium studies on the ternary H_2+THF+H_2O system, they found that the presence of this second guest component stabilizes the clathrate at pressure of 5 MPa at 279.6 K, versus 300 MPa at 280 K for pure H_2 hydrogen [42]. Through diffraction and NMR measurements, they reported that all or most of the large cages are filled with THF leaving small cages for hydrogen molecules, and in this case, they reported the single occupancy of small molecules per small cage. In this situation, the storage capacity of clathrate is 1.0 wt%.

In 2005, Lee et al. [43] reported the double occupancy of the small cavities by hydrogen molecules at 12 MPa and 270 K. They also claimed that by tuning THF concentration (lowering below 1 mole % of THF) H_2 occupancy in hydrates was increased up to 4.03%. They reasoned that by lowering THF concentration below its eutectic concentration (1.0 mole %), both small and large cages can store H_2 molecules [43].

The results of Lee et al. [43] on double occupancy of small cages and accommodation of H_2 molecules in large cavities were studied later by other researchers [34-49]. Strobel et al. [44] studied the hydrogen storage capacity of THF-H_2 system, as a function of formation pressure and THF concentration. Contrary to reports of Lee et al. [43], Strobel et al. [44] reported no increase in hydrogen storage capacity upon decreasing THF concentration below its stoichiometric concentration (5.6 mol %). They also confirmed only single occupation of hydrogen in small cages and no hydrogen storage in large cavities. This means that, contrary to previous report [43] storage capacity does not change with THF concentrations. Over the range of experimental conditions, $13.8 < P < 60$ MPa, the maximum storage capacity of the sII THF-H_2 hydrate was found to be approximately 1.0 wt% [43].

In 2009, Sugahara et al. [46] provided new evidences of the presence of H_2 clusters in the large cages of sII by proposing a new method of hydrate preparation in which hydrogen storage capacity increases to 3.4 wt% (1 wt% lower than those of Lee et al. [43]). They confirmed variations in hydrogen storage capacity by THF concentration. In another study done by Sugahara et al. [47] in 2010, they confirmed that THF concentration in a range between stoichiometric concentration and eutectic concentration affects H_2 storage, and that H_2 molecules may occupy $5^{12}6^4$ cages.

1.5.7. Semi-clathrate hydrates

Although usage of promoters such as THF reduces considerably formation pressure of hydrates, and stabilizes them in near ambient pressure and temperature, these organic compounds also present a number of operational problems. The most important problem caused by these volatile compounds is contamination of hydrogen released from dissociated hydrate. This means that the practical application of this method demands further separation unit [50]. One solution, for avoiding these problems is the use of semi-clathrate compounds.

In addition to clathrate compounds, semi-clathrate are another type of inclusion compounds. This group includes both alkylamine hydrates and the quaternary ammonium salt hydrates [32]. Semi-clathrates have many common properties with true clathrate hydrates. Both of these structures are composed of hydrogen-bonded water lattice, but the main difference is that in true clathrate hydrates, guest molecules only occupy the cages, without any bonding with the composing lattice of clathrate, and they just help to stabilize the structure through van de Waals interactions. In contrast, in semi-clathrate, guest molecules occupy the cavities and also bond physically into the water framework. In the case of quaternary ammonium salt

semi-clathrate, the hydrophobic cation is encaged into a cavity, while the anion is bonded in the lattice network by substitution with a water molecule [33, 50, and 51].

Tetra-n-butyl ammonium bromide (TBAB)

In recent years, tetra-n-butyl ammonium bromide (TBAB) has become a subject of many researches as an additive for synthesizing semi-clathrate. According to Lipkowski et al. [52], TBAB constructs a polyhedron composed of four tetragonal faces. In this structure, the quaternary ammonium ion and bromine of TBAB are incorporated with the water molecules *i.e.* TBA^+ cations are disordered and are located at the centre of four cages (2 tetrakaidecahedra and 2 pentakaidecahedra) while all of the dodecahedral cages are empty [53].

Aladko *et al.* [54] were among the first who studied the TBAB clathrate hydrates. They reported the existence of crystals with various hydration numbers for pure TBAB: TBAB.24 H_2O, TBAB.26 H_2O, TBAB.32 H_2O, and TBAB.36 H_2O. In 2003, Shimada *et al.,* [55] for the first time announced that TBAB semi-clathrate can encage gas molecules. In their studies, they recognized two types of TBAB hydrates, type A and B with different hydration numbers and they observed gas bubbles released from both of them, which means both types are capable of storing gas. They proposed that an ideal unit cell of TBAB hydrate crystal consists of ten dodecahedrons, sixteen tetrakaidecahedrons and four pentakaidecahedrons, in which tetra-n-butyl ammonium is engaged in the centre of three tetrakaidecahedrons and one pentakaidecahedron with partially broken bonds, as it is shown in Figure 13. According to *Shimada et al.,* [55, 56], these are probably the dodecahedral cages which accommodate gas molecules.
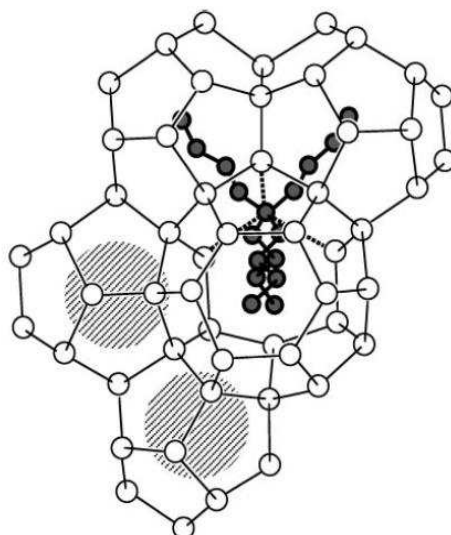
Figure 13 - Schematic structure of TBAB hydrate crystal [55]

While Shimada et al. [57] studied growth kinetics of TBAB clathrate, Oyama et al. [58], studied TBAB hydrates structures (type A and B) in more details. They measured different melting points for both types, and reported two different morphologies.

As it is shown in Figure 14, type A has columnar shape and type B has an undefined form composed of thin crystals [58]. Oyama et al. [58], measured eutectic point for type A, and reported that type B does not have any eutectic point. By measuring congruent melting points they calculated hydration numbers of 26 for type A and 38 for type B. By realizing DSC studies, they measured latent heat of these two types and reported that type B has a larger latent heat value; this is believed to be because of its larger hydration number.

In addition, they confirmed that it is more difficult to nucleate type B than type A. As a result, they proposed type A as more proper promoter in industrial applications. Hashimoto et al. [59], using Raman spectroscopic analysis, studied cage occupancy of H_2+TBAB+H_2O systems. They reported that phase behaviour of H_2+TBAB+H_2O system is the same as H_2+THF+H_2O system, and claimed that single hydrogen molecules occupy small cavities of TBAB semi-clathrate, while THF and TBAB occupy large cages of clathrate.
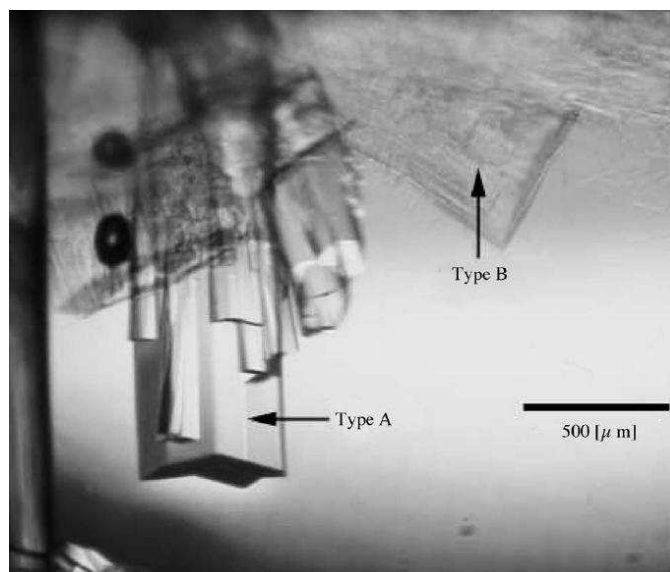
Figure 14 - TBAB semi-clathrate hydrate, type A and B [58]

As another approach for studying behaviour of semi-clathrate hydrates of quaternary ammonium compound (QAS), Chapoy et al. [60] determined the phase equilibria for H_2-TBAB-H_2O and H_2-TBAF-H_2O for temperature range of 280-310 K up to 25 MPa. According to their results, H_2-QAS clathrate, show considerable thermal and low-pressure stability in comparison with pure H_2 and THF hydrates. While pure H_2 hydrates required pressure up to 200 MPa, and H_2-THF hydrates are stabilized in pressures of 100 MPa at ambient temperature, H_2-QAS hydrates show a considerable stability in ambient condition, *i.e.* they have melting point if 302 K at ambient pressure [60]. They also suggested that single hydrogen molecules occupy small dodecahedral cages.

In another study, Shimada et al. [53], studied the structure of TBAB hydrate proposing tetra-n-butyl ammonium cations in the centre of two tetrakaidecahedra, two pentakaidecahedra while other surrounding dodecahedral cages are left empty (in contrary to their proposed structure in figure 9). In this structure, each butyl group is disordered over two possible sites with occupancy factor of 50%. A schema of this structure is presented in Figure 15. In this study, he reported storage capacity of H_2, 0.6 wt%.

Subsequent to their previous works, Hashimoto et al. [60] performed another series of experiments on cage occupancy of H_2 molecules; they confirmed that H_2 cage occupancy is independent of TBAB concentration and crystal type.

53
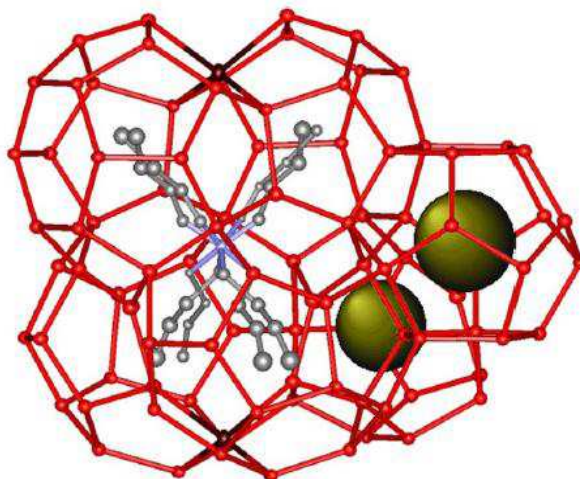
Figure 15 - The structure around the tetra-n-butylammonium cation, located at the centre of four cages [53]

Tetra-n-butyl ammonium fluoride (TBAF)

Another quaternary ammonium salt studied for synthesize of semi-clathrate hydrates was tetra-n-butyl ammonium fluoride (TBAF). Chapoy et al. [61] studied the phase equilibria of H_2+TBAF+H_2O system. They found that this semi-clathrate, like TBAB semi-clathrate, is stable at room temperature and ambient pressure. Moreover they reported single occupancy of small dodecahedron cavities by hydrogen molecules. They also claimed that QAS hydrates have much larger potential of H_2 storage than THF hydrates.

In 2008, Sakamoto et al. [62] made more detailed studies on TBAF semi-clathrate hydrates. They reported two structures for this semi-clathrate. A tetragonal structure with TBAF.32 H_2O stoichiometric composition and a rather more stable cubic structure of TBAF.28 H_2O composition. Their Raman spectra results show that the cage selectivity of H_2 for the H_2+TBAF semi-clathrate hydrate is independent of both the TBAF concentration in aqueous solutions, and the system pressure under experimental conditions. In this system, single H_2 molecules occupy small cages while the butyl group occupies other cages completely. Contrary to Chapoy et al. [61], Sakamato et al. [62] claim that H_2 storage capacity of TBAF does not exceed that of THF as the S-cage/other cages ratio per unit lattice in both TBAF structures is smaller than that of THF.

Tetra-n-butyl ammonium Borohydride (TBABh)

In the way to test capability of other tetra-alkyl ammonium salts with suitable anions, in 2009, Shin et al. [63] used Borohydride anion (BH_4^-) to form a semi-clathrate hydrate. In TBABh hydrate, BH_4^- plays the same role as Br^- in TBAB hydrate, *i.e.* it is substituted for an oxygen-

water position in the host lattice. One advantage of using borohydride salts such as $NaBH_4$ is that following a hydrolysis reaction they can generate hydrogen. It means the hydrolysable material can be used as a source of hydrogen from both dissociation of the semi-clathrate and hydrolysis of the salt.

In their PXRD analysis, Shin et al. [63], confirmed accommodation of hydrogen molecules in small dodecahedron cavities. The hydrogen storage capacity of hydrogen was measured volumetrically with and without considering hydrolysis reaction. Without hydrolysis reaction, about 0.5 wt% of hydrogen was physically stored in the TBABh hydrate. In presence of HCl (including hydrolysis hydrogen generation) a total of 1.35 wt% of hydrogen maybe released from the TBABh hydrate.

Moreover, through DSC studies, Shin et al. [36] reported that TBABh semi-clathrate is more stable than those of TBAB and TBAF.

Tetrabutylammonium chloride (TBACl) and Tetrabutyl Phosoponium bromide (TBPB)

In another study, Deschamps et al. [51], studied the thermal stability of $TBACl+H_2+H_2O$ and $TBPB+H_2+H_2O$ systems in the temperature range of 282-291 K. They reported a higher thermal stability for these two systems in comparison to that of THF and even TBAB but lower stability in comparison to TBAF system. Hydrogen stored value reported in this study was 0.12 wt% for TBACl system, and 0.14% wt% for TBPB system.

Trimethylamine (TMA)

One of the other additives adopted for forming semi-clathrate in mild conditions is trim ethylamine (TMA) which was studied by Ogata et al. [64]. The hexagonal unit cell of TMA hydrate is composed of three small 5^{12} cages, two medium $5^{12}6^2$ cages and two large $5^{12}6^3$ cages. In this semi-clathrate structure, two TMA molecules occupy medium cages and one large cage while the three small cages are left vacant. According to Ogata et al. [64], increasing of the pressure gradually increase hydrogen storage in small cavities until it reaches a plateau (here 80 MPa), *i.e.* even in higher pressure all the small cages are filled, and neither the medium nor the large cages will accommodate any hydrogen molecule. Moreover, no double cage occupancy of hydrogen molecules in small cavities was reported.

1.5.6. Conclusion

It can be seen that hydrogen storage in clathrate hydrates, has shifted from storage in pure binary hydrogen hydrates towards storage in semi-clathrate hydrates in order to address operational conditions for commercialization of storage process. This shift has been in expense of reduction in storage capacity. Table 7 shows a summary of this trend by providing hydrogen mass density and thermodynamic conditions of different systems during the time.

Table 7 - Summarized table of hydrogen clathrate data

System	Wt %	P (MPa)	T (K)	Reference
H_2+THF+H_2O		350	293	*35*
H_2+HPF$_6$+H_2O		700	293	*35*
H_2 +H_2O		220	300	*37*
H_2 +H_2O	5.3	250-600	249	*38*
H_2 +H_2O	3.77	220	200-270	*13*
H_2 +THF+H_2O	4	12	277.3	*43*
H_2 +THF+H_2O	1.05	60	270-278	*44*
H_2 +THF+H_2O	1.0	45	260-290	*46*
H_2 +MCH+H_2O	1.38	83-149	273-279	*45*
H_2 +THF+H_2O	3.44	60	255	*46*
H_2 +THF+H_2O	3.44	75	255	*47*
H_2 +Acetone+H_2O	3.6	70	255	*47*
H_2 +TBAB+H_2O	0.6	13.8	Ambient	*34*
H_2 +TBAB+H_2O	0.6	16	287	*61*
H_2 +TBABh+H_2O	0.5	70	253	*63*
H_2 +TBACl+H_2O	0.12	14.9	288.9	*51*
H_2 +TBPB+H_2O	0.14	12.1	285.0	*51*

Chapter two:

Experimental measurements

This chapter presents the experimental procedure, equipments and materials used in this work. Differential Scanning Calorimetry (DSC) and a high pressure isochoric cell are presented as the main experimental set-ups. Their application in hydrate studies is discussed and the experimental procedures used in this work are described. Apart from these two main equipments, gas chromatography and atomic absorption are presented for their application in the gas and liquid phase investigations, respectively. At the end the materials used during these experiments are presented in a table specifying their supplier and their purity.

2.1. Introduction

Any method for investigating the phase equilibrium and hydrogen storage capacity of gas hydrates must meet the following criteria:

1. It must hold pressures more than ~10 MPa
2. It must bear low temperatures until ~255 K
3. It must be equipped by an acquisition centre in order to monitor and save online the pressure and temperature data of the system
4. It must be equipped with a sampling system from either liquid phase or hydrate phase, to measure the storage capacity
5. For the case of a gas mixture of, a gas phase sampler is also needed

For meeting these criteria, two experimental set-ups are used in this work:

1. *Differential Scanning Calorimeter* (DSC) for investigating the dissociation point of hydrates under different gas pressures.

2. A high pressure isochoric reactor for investigating the equilibrium conditions of hydrate formation and the volumetric measurements of the quantity of the stored gas.

Although the *p-V-T* cell provides the required phase equilibrium with a high accuracy but unfortunately it is too much time consuming. For this reason, in this work DSC is used mainly for measuring phase equilibrium of hydrates systems as a relatively faster method. (For instance, measuring an equilibrium point by *p-V-T* measurements in the isochoric reactor, often take 4-5 days while the same data can be measured by DSC in 24 hours).

2.2. Differential Scanning Calorimeter (DSC)

Calorimetry is the technique of measuring heat or in other words the technique of measuring the heat exchange between two samples. This process of heat exchange creates a heat flow which results in a local temperature difference which can be used as a measure of the flowing heat. Since the invention of calorimetric measurements in 18th century a variety of calorimeters were constructed to measure heats and heat capacities in different fields of applications [65]. The apparatus that is used in our experiment is a Differential Scanning Calorimeter (DSC) which is an enhanced version of Differential Thermal Analysis (DTA).

This section is devoted to presentation of DSC, the mechanism of thermal analysis by DSC and their application in clathrate hydrates field are presented.

DSC is an apparatus in which the change of the difference in the heat flow rate to the sample and to a reference sample is analyzed while they are subjected to a temperature alteration [66]. As any other thermodynamic phenomenon which features a phase change, hydrate formation can be studied by thermal analysis methods [67].

In DSC, the sample temperature is not measured directly. The temperature signal is given by a thermometer which is located at the centre of the furnace, near the two vessels. Moreover, the sample is not at thermal equilibrium, since what is measured here is the heat flux exchanged between the sample and the furnace. In order to measure the equilibrium conditions of a given sample, the measured heat flux between the furnace and the two cells are compared analytically. Thus, physical transitions such as phase transitions as well as chemical transitions of the sample can be detected by observing the difference in the two measured heat flux [68].

In a DSC experiment, the reference and the sample are heated in a furnace, whose temperature is varied linearly with time. The difference in temperature between sample and the reference is zero initially. When there is a physical change in the sample, for example, a phase transition, the heat exchanged with the surrounding environment changes and the temperature difference is observed between the sample and the reference. The temperature difference vanishes at the end of the transition in an ideal DSC. Variation in temperature difference as a function of furnace temperature can provide information about physical or chemical change that occurs in the sample.

The metal used to construct the crucible should not react with the sample under the study or with the purge gas flushing DSC apparatus. The crucible material should also have high thermal conductivity and low heat capacity. Aluminium and stainless steel is most often used to construct the crucible but other materials such as gold, copper, sapphire and glass have been utilized depending on the specific experimental condition.

Mainly there are two designs of DSC:

1. Heat flux DSC with two modifications (disk-type and cylinder-type measuring system)

2. Power compensating DSC

2.2.1. Heat flux differential scanning calorimeters

In a heat flux DSC, the temperature difference between sample and reference sample is recorded as a direct measure of the difference in the heat flow rates to the sample and the reference sample. The heat flow rate difference is assigned by calorimetric calibration.

Two different models of this type of DSC are:

1. Disk type [Figure 16]
2. Cylinder type [Figure 17]

In the disk-type DSC, the crucibles with the specimens are positioned on a disk (made of metal, ceramics). The temperature difference ΔT_{SR} between the specimens is measured with temperature sensors integrated in the disk or contacting the disk surface.
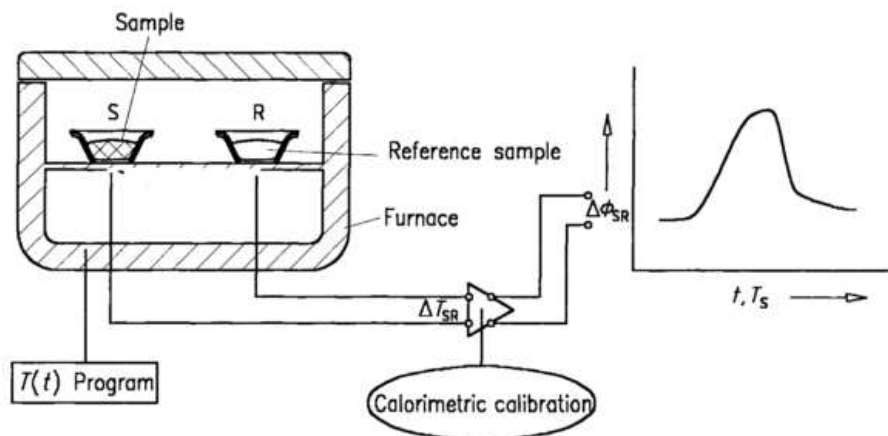
Figure 16 - Disk type DSC [66]

In a cylinder-type DSC, the furnace is provided with two (or more) cylindrical cavities. They take up hollow cylinders whose bottoms are closed (cells) and in which the specimens are placed directly or in suitable crucibles. Thermopiles or thermoelectrical sensors are arranged between the hollow cylinders and the furnace, which measure the temperature difference between hollow cylinder and furnace (integral measurement). A differential connection of the thermopiles furnishes the temperature difference between the two hollow cylinders, which is registered as the temperature difference ΔT_{SR} between sample and reference sample. Because of its geometry the sample cell is totally surrounded by the heat flow sensor. Thus cylinder DSC is generally more sensitive than disk DSC.
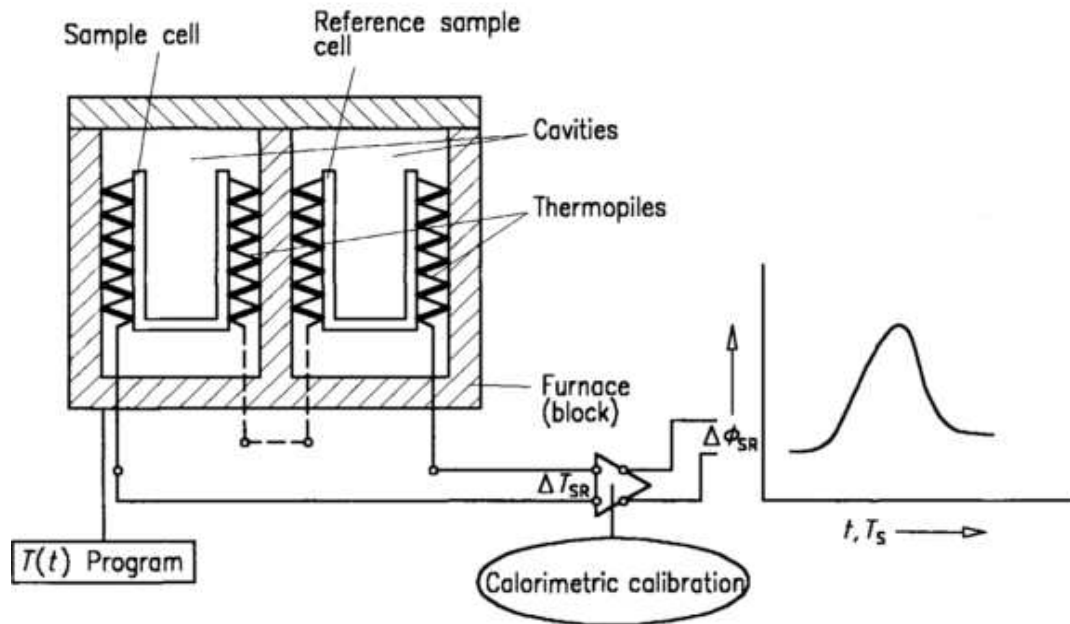
Figure 17 - Cylinder type DSC [66]

2.2.2. Power compensating differential scanning calorimeters

In a power compensating DSC, the specimens are arranged in two separate small furnaces in which each of them is provided with a heating unit and a temperature sensor [Figure 18]. During the measurement, the temperature difference between the two furnaces is maintained at a minimum with the aid of a controller that adapts the heating powers in a way that there is always a residual temperature difference between the two specimens (offset). When there is thermal symmetry in the measuring system, the residual temperature difference is proportional to the difference between the heating powers fed to sample and reference sample.

If the resulting temperature difference is due to differences in the heat capacity between sample and reference sample, or to exothermic/endothermic transformations in the sample, the heating power additionally required to keep this temperature difference as small as possible is proportional to the difference $\Delta\varphi_{SR}$ between the heat flow rates supplied to sample and reference ($\Delta\varphi_{SR}=\Delta C_P.\beta$), or proportional to the heat flow rate of transition $\Delta\varphi_{trs}$. [66].
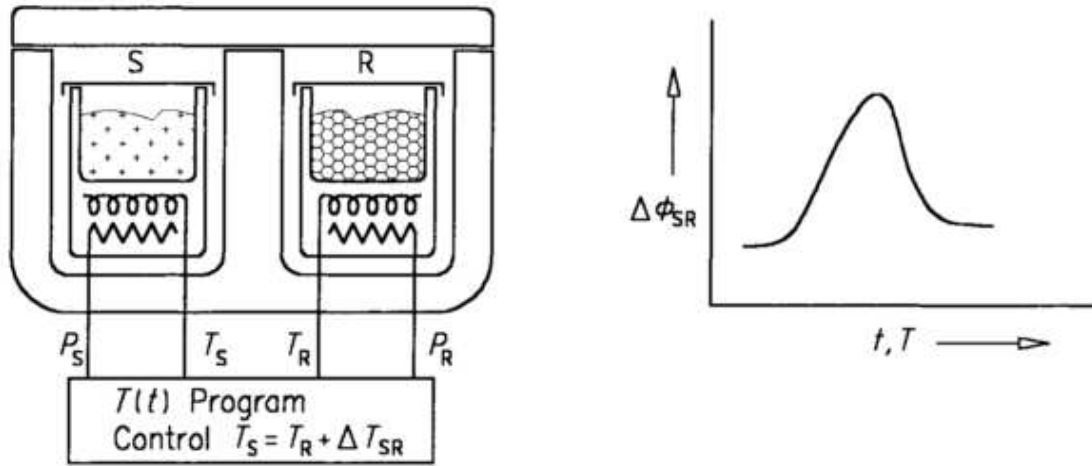
Figure 18 - Power compensating DSC [66]

2.2.3. Calorimetric signals

Contrary to simple thermal analysis which measures sample temperature as a function of time, DSC output presents heat flux difference of sample and reference. But DSC permits to convert these signals to temperature signals as well. For a better understanding of the calorimetric output peaks during a phase transition, the difference between temperature signals is shown in Figure 19. Figure 19-a illustrates the evolution of the sample temperature (T_S) and the reference temperature (T_R) according to the thermal program.

As it can be seen, at the beginning of the program, both T_R and T_S are kept at a same temperature and therefore their thermal evolution line is superposed. It is not until the occurrence of an isothermal phase transition that a step occurs in temperature curve. When melting begins (isothermal phase transition) the sample temperature (T_S) remains at the melting temperature as the solid and liquid are in equilibrium during the melting process. On the other hand, during this time, as the heat flow rate continues constantly, the temperature of the reference sample increases continuously. This deviation between the two temperatures causes a peak with a straight edge whose slope reflects the rate of energy transfer. The peak's maximum represents the end of the equilibrium region. Further heating, will result in an increase in the temperature of the fully melted sample and then as it is shown, the two temperatures become equal again.

Figure 19b, presents the same process in a differential form, in other words, by replacing *T* with *ΔT_SR* on the vertical axis, the lower diagram presents the differential evolution of temperature. This is a common method for representing temperature evolution in DSC as it

eliminates the instabilities caused by a reason other than phase transition and facilitates the graphic methods for calculating the peak temperature. For a perfectly pure material melting peak should be infinitely sharp and narrow, if there was no thermal gradient (resistance) across the sample. However, in reality because it takes time for heat (energy) to diffuse into the sample, the peak is broadened and reduced in height. The peak's maximum presents the end of melting process after which the liquid heats up to the reference temperature and therefore T_S curve returns back to the base line. Consequently, the resulting peak is not symmetric. Due to the nature of the corresponding phenomena, the descending edge of the peak has a linear shape (isothermal phase transition) and the ascending edge has an exponential shape (progressive phase transition).
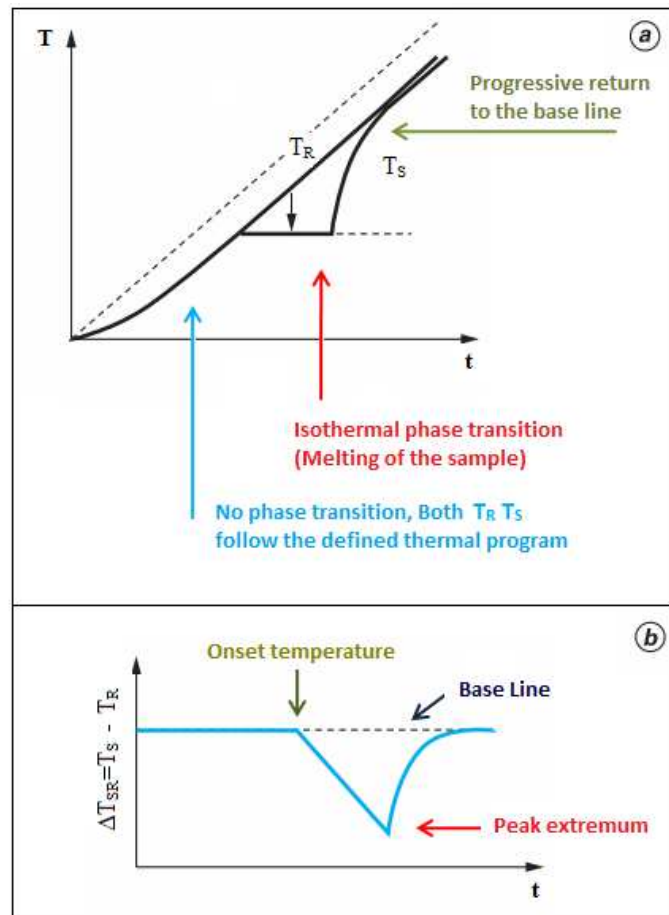
Figure 19 - Schematic presentation of temperature evolution in a DSC [69]

By definition the beginning of the phase transition, where the heat flux curve deviates from the base line is defined as the onset temperature. This is the point where peak begins and not the extremum value of the peak. It must be noted that in real experiments due to the impurities in the sample this onset point is not a sharp breaking point but it appears as a small roundness in the beginning of the melting step.

64

2.2.4. DSC principle

Fundamentals

All of the DSC apparatus obey the same principle. DSC in a simple form is an instrument that measures continuously the heat exchange between a sample and a thermostat according to a temperature program. Independent of whether a user obtains *T* or *ΔH* from the DSC, it is important to know the DSC principles and the functional relation between the measured signals which are the links to calculate different thermodynamic quantities. Firstly, for a preliminary presentation of DSC principle some simplifying assumptions must be considered:

1. The state of the system is assumed to be steady, and all the transformation are assumed to taken place in equilibrium state.
2. Only one thermal resistance between furnace and sample is taken into account, assuming no interaction between sample and reference sample.
3. Only the heat capacities of sample and reference are considered in calculation.
4. Sample is assumed to be homogenous all over the experiment which necessitates low heating rates, and small sample volumes.
5. The system is assumed to have a thermal symmetry in both sample and reference sides.
6. The whole system is assumed to be isolated in a way that there is no heat exchange with surroundings.

A schema of DSC is illustrated in Figure 20. According to the Biot-Fourier's equation for conduction heat transfer the amount of heat flux between two bodies is proportional to the temperature gradient between them:

$$\frac{dq}{dt} = -\gamma \frac{dT}{dx}$$

Equation (11)

In this equation *dq/dt* is the heat flux, the term *dT/dx* is the one dimensional temperature gradient and the coefficient γ is a proportionality factor (thermal conductivity).
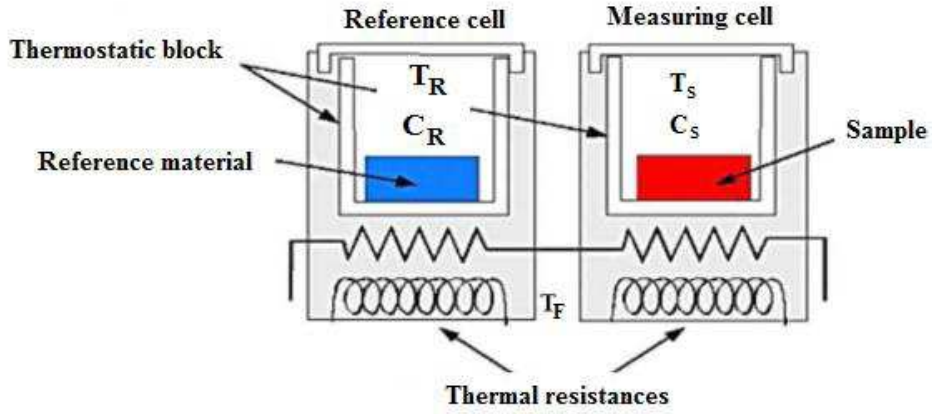
Figure 20 – Schematic illustration of DSC cells, T_R: reference temperature, C_R : heat capacity of reference, T_S : sample temperature, C_S : heat capacity of sample, T_F: furnace temperature [70]

For a one-dimensional heat flow in the sample the above equation can be rewritten as:

$$\varphi_{FS} = \frac{dq_{FS}}{dt} = -\frac{(T_F - T_S)}{R}$$
Equation (12)

Where φ_{FS} is the heat flux between sample and furnace, q_{FS} is the amount of heat exchanged between furnace and sample in the time t, T_F is the furnace temperature and T_S the sample temperature.

The same equation can be rewritten for the reference cell:

$$\varphi_{FR} = \frac{dq_{FR}}{dt} = -\frac{(T_F - T_R)}{R}$$
Equation (13)

Where φ_{FR} is the heat flux between reference and furnace, q_{FR} is the amount of heat exchanged between furnace and reference in the time t, T_F is the furnace temperature and T_R the reference temperature.

In these two equations R is the thermal resistance between cells and the thermostats.

By assuming a thermal symmetry in the system:

$$\frac{dq_{FS}}{dt} = \frac{dq_{FR}}{dt} \rightarrow T_S = T_R$$
Equation (14)

If a constant exothermic heat flow (φ_r)is produced in the sample crucible, the sample temperature (T_S) increases by ΔT_S and then consequently both the temperature gradient T_F-T_S

and φ_{FS} decrease. Under steady state condition this can be explained with a thermal balance as:

$$\Delta\varphi_{FS} = \varphi_r = -\frac{\Delta T_R}{R} \qquad \text{Equation (15)}$$

Knowing that no thermal phenomenon has happened in the reference side, the temperature difference between sample and reference will be:

$$\Delta T_S = \Delta T_{SR} = T_S - T_R \qquad \text{Equation (16)}$$

And hence:

$$\varphi_r = \Delta\varphi_{SR} = \varphi_{FS} - \varphi_{FR} \qquad \text{Equation (17)}$$

And therefore:

$$\varphi_r = -\frac{(T_S - T_R)}{R} = -\frac{\Delta T_{SR}}{R} = -K.\Delta T \qquad \text{Equation (18)}$$

In this equation K is a proportionality factor (heat transfer coefficient) and is a function of temperature, heat transfer surface area and the distance between sample and the reference. This formulation represents the direct proportionality between the measured φ_r and the measured signal ΔT, under a steady-state constant heat flow. It should be noticed that, this is only the case of an increase in the temperature of the sample without occurrence of any phase transition or reaction.

In the case of a non-steady state process (phase reaction or phase transition) ΔT will not be constant by time and this difference shows itself in the form of peaks, as discussed earlier. In this situation the heat flow rate produced inside the sample by a reaction or a phase transition $\varphi_r(t)$ is time dependent. By considering this time dependent heat flow rate, the heat balance for the sample side will be:

$$C_s\frac{dT_S}{dt} = \varphi_{FS} - \varphi_r \qquad \text{Equation (19)}$$

On the other hand, in the reference side, were no heat flow is produced or consumed ($\varphi_r = 0$):

$$C_R\frac{dT_R}{dt} = \varphi_{FR} \qquad \text{Equation (20)}$$

Now, by calculating the difference between the two balance equations:

$$\frac{dq}{dt} = \varphi_{FS} - \varphi_{FR} = \varphi_r + C_S\frac{dT_S}{dt} - C_R\frac{dT_R}{dt}$$

Equation (21)

Employing equations [Eq.3] and [Eq.4]:

$$\varphi_{FS} - \varphi_{FR} = \frac{dq_{FS}}{dt} - \frac{dq_{FR}}{dt} = \frac{dq}{dt} = -\frac{(T_R - T_S)}{R}$$

Equation (22)

And then by replacing T_r by T_s from the equation [Eq.13]:

Equation 1

$$\frac{dq}{dt} = \varphi_r + (C_S - C_R)\frac{dT_R}{dt} - RC_S\frac{d^2q}{dt^2}$$

Equation (23)

This is a fundamental equation of differential calorimetric analyses in which:

- $\frac{dq}{dt}$ is the heat flux measured by DSC

- $(C_S - C_R)\frac{dT_R}{dt}$: Term for elimination of asymmetry in measurement regarding the difference in specific heats of sample and the reference (Baseline signal)

- φ_r: Time dependent heat flow rate produced inside the sample (Enthalpy of reaction or phase transition)

- $-RC_S\frac{d^2q}{dt^2}$: heat exchange between sample and furnace in a transitory state.

In absence of any phase transition:

$$\varphi_r = 0$$

And by solving the first-order equation of differential calorimetric analyses:

$$\frac{dq}{dt} = (C_S - C_R)\frac{dT_R}{dt} - Ae^{\frac{-t}{RC_s}}$$

Equation (24)

where A is a constant. When *t* is sufficiently high comparing to RC_S, the second term on the right of the above equation can be neglected comparing to the first term:

68

$$\frac{dq}{dt} = (C_S - C_R)\frac{dT_R}{dt}$$

<div align="right">*Equation (25)*</div>

In this equation *dq/dt* represents the base line of the thermal output signal. In the absence of any phase transition in the sample, as C_S and C_R vary little, it presents a parallel line to the zero level line of the calorimeter. On the other hand, by occurring a phase change in the sample, C_S varies sensibly and therefore the base's slope changes rapidly.

2.2.5. Measurement of phase transition temperature

Knowing that in DSC the sample temperature is measured indirectly via measuring the furnace temperature (T_f) and the heat flow, more precision on the measurement procedure is needed. In this regard, the following operational conditions must be respected to obtain valid thermodynamic data:

- DSC apparatus must be carefully calibrated in several measuring points inside the experimental temperature range.
- The sample must be homogenous thermally, which necessitates slow heating and small amount of sample.
- The operational conditions must be repeatable and indeed all the experiments must be done in one apparatus with the same cells.
- Specific capacity of reference and sample cell must vary a little with temperature.

In this regard, for obtaining a mathematical relation for calculating the sample temperature equation [Eq.13] is rearranged as:

$$-R\frac{dq}{dt} = (T_R - T_S) = (T_F - T_S) - (T_F - T_R)$$

<div align="right">*Equation (26)*</div>

By replacing the term *($T_F - T_R$)* by help of equation [Eq.11]:

$$T_S = T_F - R\frac{dq}{dt} - C_R R\frac{dT_R}{dt}$$

<div align="right">*Equation (27)*</div>

Assuming that *t>>RC$_r$* :

$$\frac{dT_R}{dt} \approx \frac{dT_F}{dt}$$

<div align="right">*Equation (28)*</div>

Equation [Eq.18] can be rewritten as:

<div align="center">69</div>

$$T_S = T_F - R\frac{dQ}{dt} - C_S R\frac{dT_F}{dt}$$

Equation (29)

In which the term $C_S R \, dT_f/dt$ shows the thermal lag or the thermal inertia of the cell and *dQ/dt* represents the thermal signal deviated from the base line during a phase transition and is defined as:

$$\frac{dQ}{dt} = \frac{dq}{dt} - (C_S - C_R).\frac{dT_F}{dt}$$

Equation (30)

In this way, equation [Eq.20] can be used to calculate sample's temperature by knowing R, the thermal resistance of DSC and T_f the measured temperature of furnace.

However, often a graphical method is used to calculate sample's temperature. This methods is easier and faster and is based on this assumption that during a steady-state isothermal phase transition, the sample's temperature remains constant ($T_s=cte$). Moreover, it is assumed that furnace temperature varies by a constant rate ($dT_f/dt=cte$). By differentiating expression [Eq.21] with respect to *t*:

$$\frac{dT_F}{dt} = R\frac{d^2 Q}{dt^2}$$

Equation (31)

This equation can be developed by multiplying and dividing by the term dT_f:

$$\frac{dT_F}{dt} = R\frac{d\left(\frac{dQ}{dt}\right)}{dT_F} \times \frac{dT_F}{dt}$$

Equation (32)

And therefore, by eliminating the furnace temperature's evolution rate (dT_f/dt) :

$$\frac{1}{R} = \frac{d\left(\frac{dQ}{dt}\right)}{dT_F}$$

Equation (33)

According to this equation [Eq.24], the slope of the *dQ/dt* – T_f diagram is equal to the inverse of thermal resistance of DSC (1/R). This is shown on the endothermic heat flux curve of Figure 21. It should be reminded that thermal resistance (R) depends not only on the cell's material, but also it depends on sample's quantity and its contact area with cell's surface [68].
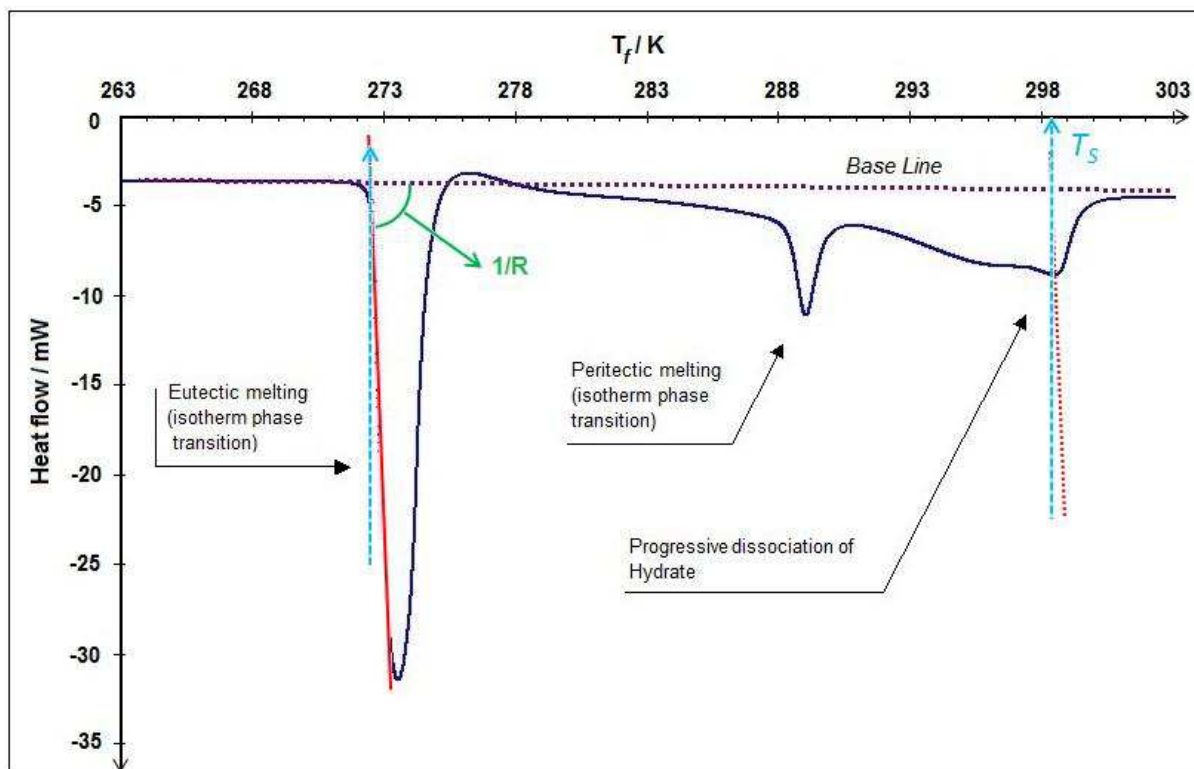
Figure 21 - Example of a heat-flux curve for calculation thermal resistance, R and the phase transition temperature

In this Figure the onset temperature as the beginning point of sample melting is precised by finding the intersection of the tangent line starting from the inflexion point of the peak with the baseline. During an isothermal phase transition, onset point gives the equilibrium temperature of the phase change.

Although this methods is useful for isotherm phase transitions, it may not be applicable to hydrate dissociation as they are known to have a progressive phase transitions. In this category of compounds, the resulting peak is not sharp at all to pass a tangent from its inflexion point. One practical method to overcome this problem is proposed by Gesellschaft für Thermische Analyse (GEFTA) [71]. This method suggest passing a line parallel to the tangent of isotherm peak, from hydrate peak and then projecting its intersection with the baseline to the temperature axis in order to find the corresponding temperature. This is shown in Figure 21. The method is valid for all the reversible phase transitions and can also be applied to non-isotherm transfers. In any point of the heat flux curve the temperature of the sample is obtained by drawing a line parallel to the tangent line, and finding its intersection with base line.

2.2.6. Calculation of sample enthalpy variation

According to equation [6], the heat absorbed or produced during a phase transformation is related to the power saved by calorimeter:

$$\frac{dh}{dt} = -\frac{dq}{dt} + (C_S - C_R)\frac{dT_F}{dt} - RC_S\frac{dq^2}{dt^2}$$

Equation (34)

and as it was described before it can be rearranged as:

$$\frac{dh}{dt} = -\frac{dq}{dt} + (C_S - C_R)\frac{dT_F}{dt} - Ae^{\frac{-t}{RC_s}}$$

Equation (35)

and when *t* is much bigger than R.C_S:

$$\frac{dh}{dt} = -\frac{dq}{dt} + (C_S - C_R)\frac{dT_F}{dt}$$

Equation (36)

and therefore the heat absorbed or produced during a phase change can be calculated by integrating the former equation:

$$\Delta h = \int \left(-\frac{dq}{dt} + (C_S - C_R)\frac{dT_F}{dt}\right)dt$$

Equation (37)

or according to equation [21]:

$$\Delta h = \int \left(-\frac{dQ}{dt}\right)dt$$

Equation (38)

and therefore, the phase change heat can be determined by calculating the surface under the base line of the heat flux curve.

2.2.7. Experimental procedure

For all of our calorimetric measurements a high pressure scanning calorimeter, HP-μ DSC VII (SETARAM, France) is used which is designed for a temperature range of 233 to 393 K and supports pressures up to 40 MPa. The pressure inside the high pressure *Hastelloy* cells were measured using pressure transducers GE DRUCK (PTX-7800) with a pressure range of 0 to 70 MPa with an accuracy of ± 0.01 MPa. A schema of this apparatus is presented in Figure 22

.
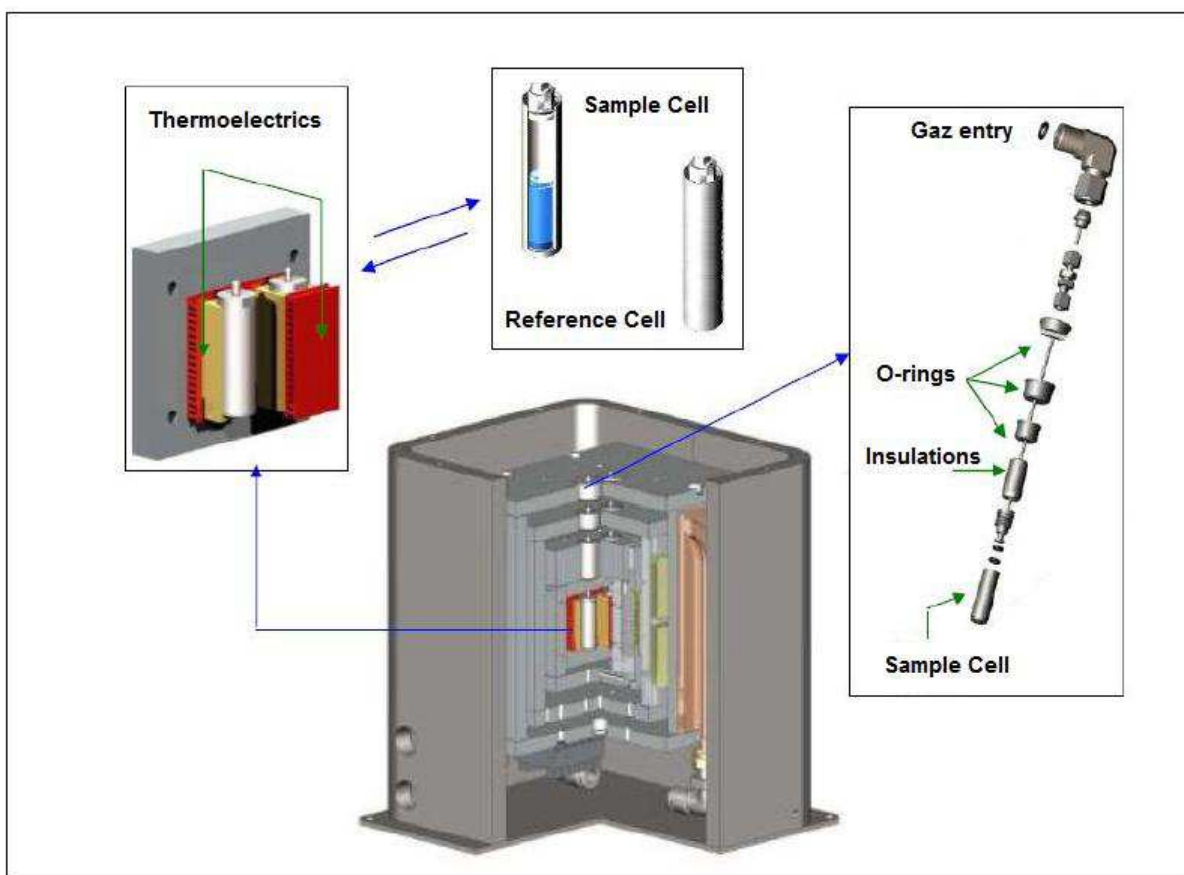
Figure 22 - A schematic presentation of HP-µ DSC VII (SETARAM)

As the temperature measurement is indirect in DSC, the calibration procedure is extremely important to achieve accurate results. Calibration of the apparatus heat flow sensitivity was made by manufacturer and was not modified. Temperature calibration had to be performed specifically with the cells used for our measurements, since thermal lag between sample and temperature probe in the DSC depend on the cell type being used. The best technique for calibrating temperature is measuring the melting temperatures of very pure metal or organic samples, and then computing a correction function that takes into account the deviation between measurements and known melting temperatures. This was done at various heating rates from $5^.10^{-2}$ K$^.$ min^{-1} to 5 K$^.$ min^{-1}, within the temperature range of interest for the study, using gallium ($x = 0.999999$, melting temperature = 302.9 K) and Diphenyl ether ($x = 0.999$, melting temperature = 300.01 K)   Temperature scale accuracy was verified by measuring the melting temperatures of pure water and it was found to be better than 0.2 K.

For all of systems, each time 0.04g ($\pm$ 0.001g) sample of the aqueous solution was injected into the sample crucible and weighted by an electronic balance (Metler Toledo AW205) with precision of 10^{-5} g before closing the vessel. The cell was purged several times with the

73

experiment gas (hydrogen or mixture) to assure the evacuation of air. At the end desired gas pressure was set.

As DSC cells are not equipped with agitators, in spite of the small quantity of sample, hydrate formation is hindered by limiting diffusion of gas through the liquid. The formation reaction is thus very slow and cannot be followed since no observation medium is provided. In order to overcome this inconvenience a multi-cycle program was adjusted and applied to all of the systems. These cycles consists in successively cooling the sample down to 248.15 K for providing a proper super-cooling (driving force). After keeping the sample at 248.15 K for a short time (usually 10 minutes) the samples were heated a temperature higher than 273.15 K, and lower than the dissociation temperature of hydrates. The sample is kept at this temperature for a while (10 minutes) and then again it is cooled down to 248 K. [Figure 23]. These cycles are repeated in order to accumulate the formed hydrate in cell by consuming the remained water. The last cycle in the thermal program consists in keeping hydrate at 248 K for a relatively longer period 100 min) for achieving at an equilibrium state and then dissociating the accumulated hydrate at a temperature rate of 0.5 K·min^{-1}. The number of cycles, the duration of keeping sample in lower and higher temperature limits and the cooling/heating rate are important factors which affect the amount of the formed hydrate and the resolution of the final peaks. These factor are usually set by experience.
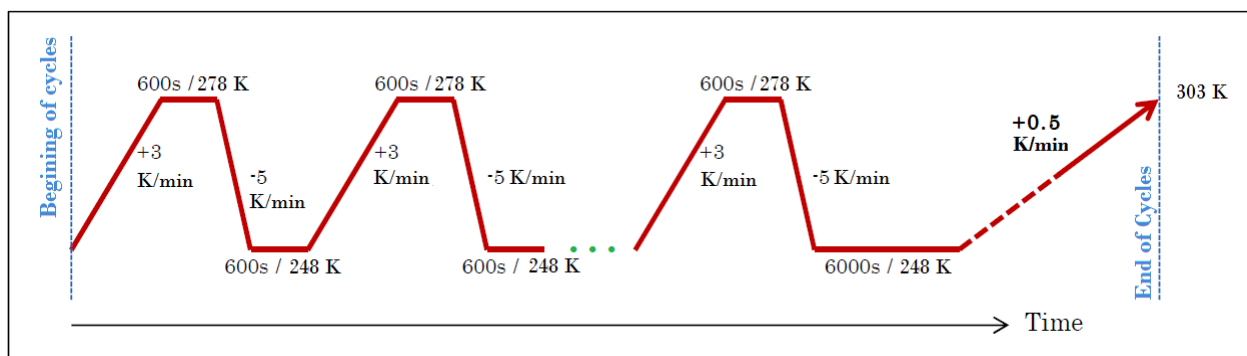
Figure 23 - A schematic presentation of multi-cycle thermal program for hydrate formation ending with hydrate dissociation.

The evolution of heat flux rate during the thermal cycles which corresponds to the conversion of water to hydrate can be seen in the Heat flux – time diagram illustrated in Figure 24. As it can be seen in this diagram, doing these cycles reduces the absolute value of heat flux of the sample. This can be interpreted as conversion of water into hydrate. As more hydrate is formed, less free water is remained in the cell, and therefore less energy is devoted for cooling

the remained water for making super-cooling. At the end, the heat flux seems to reach a constant value, which reveals appearance of an equilibrium state between water and formed hydrated at the corresponding gas pressure.
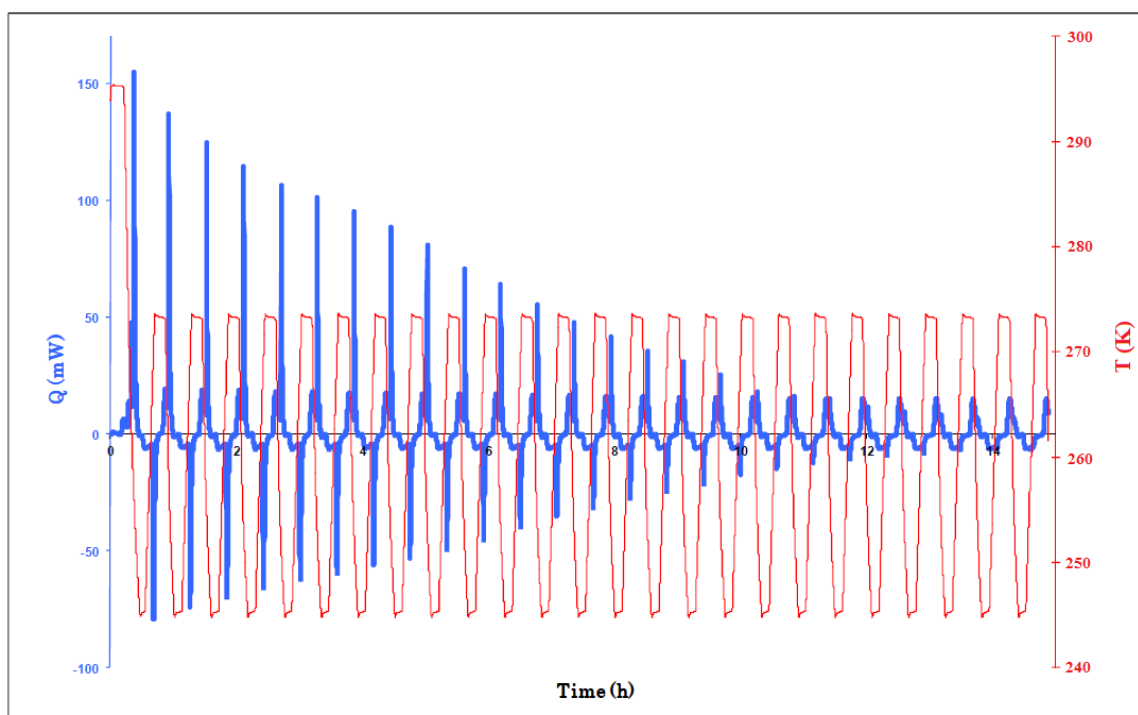
Figure 24 - Thermal cycling for a CO_2-H_2-H_2O system at 14 MPa (equimolar gas composition)

2.3. Isochoric reactor

2.3.1. Description

A high pressure reactor (ARMINES, FRANCE) is used to realize the p-V-T measurements in order to investigate gas hydrate phase equilibrium. Strong agitation system, compositional analysis of both gas phase and liquid phase and the visual observation through the sapphire window makes the reactor a suitable apparatus for measuring hydrate phase equilibrium. The main part of the reactor is a cylindrical cell made of austenitic steel to bear operational pressures up to 40 MPa and a temperature range of 233-373 K. A schematic diagram of the reactor is given in Figure 25. The equilibrium cell has an inner volume of 206.0±1.5 mL, with two sapphire windows in front and the back. It is equipped with a strong agitation system which facilitates hydrate formation. Pressure is measured by two calibrated pressure transducers (GE DRUCK, type PTX611), one for low pressure ranges *i.e.* 5 MPa (± 0.15 % full scale) and the other for high pressure ranges *i.e.* 40 MPa (± 0.15 % full scale). A platinum temperature probe (PT 100) installed inside the cell with uncertainty of ±0.02K permits to

measure the interior temperature of the reactor. Both the pressure transducer and temperature probe were connected to a data acquisition unit to record the temperature, and pressure variation versus time. The temperature of the cell is controlled by a thermostatic bath (Tamson Instruments, TV4000 LT).
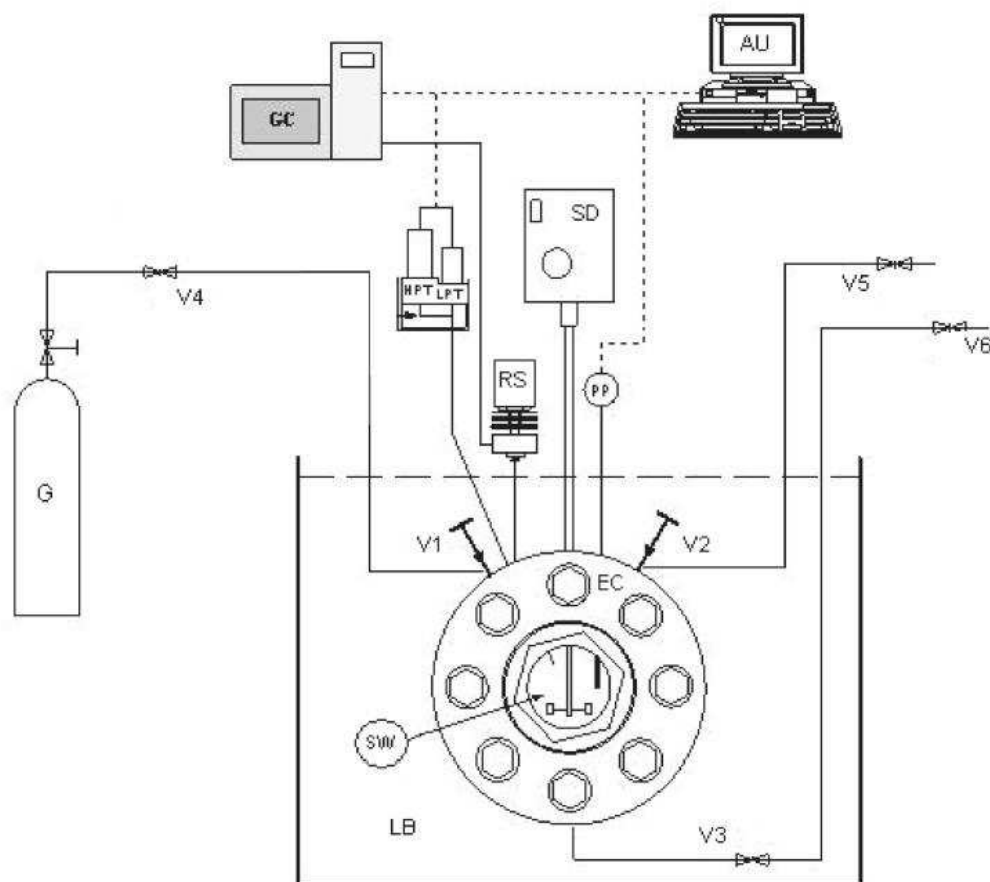
Figure 25 - Schematic of hydrate cell (with courtesy of Ecole des Mines de Paris, CEP/TEP). DAU, data acquisition unit; DW; EC, equilibrium cell; G, gas cylinder; GC, gas chromatograph; HPT, high pressure transducer; LB, liquid bath; LPT, low pressure transducer;

2.3.2. Experimental procedure

Hydrate phase equilibrium and storage capacity of gas hydrate were studied using the isochoric reactor. For each measurement (50 ± 0.1) mL of aqueous solution was injected into the cell through valve V3, using an ISCO syringe pump and then the reactor was charged with the desired pressure of gas through valves V4 and V1. The whole set up was then submerged in the thermostatic cooling bath of silicone oil. The temperature was slowly decreased until the hydrate was formed. Hydrate formation was detected either visually through the two sapphire windows installed on the front and rear of reactor or by the pressure drop and

76

temperature increase due to exothermic formation of hydrate. The temperature was then kept constant for obtaining temperature and pressure stability and the maximum hydrate formation. From this part two different approaches could be taken:

I. *Measuring the dissociation temperature of gas hydrate:*

For measuring the dissociation temperature of hydrate, the temperature was increased by 0.1 K steps. At each step, the reactor was given time to reach the equilibrium state. By saving the data of each step, a set of pressure-temperature data was gathered which was presented in a form of a P-T diagram. A schematic P-T diagram of this kind is illustrated in Figure 26.
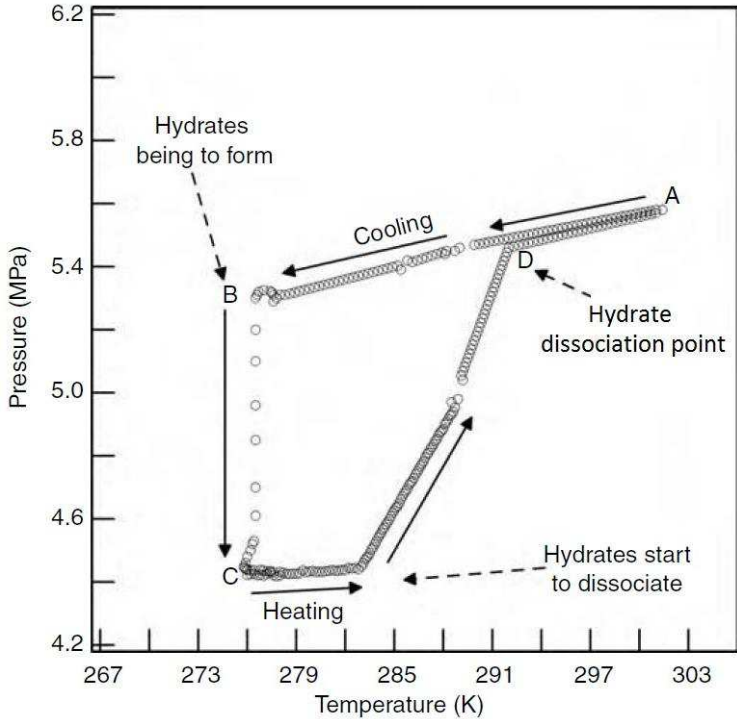
Figure 26 - A schematic T-P diagram of hydrate
Formation - dissociation process in an isochoric reactor [30]

As it can be seen, by submerging the cell in the thermostatic bath (*point A*) the cell's interior temperature decreases until hydrate forms at *point B* where due to the hydrates formation and filling of hydrates cavities by gas molecules, pressure dropped drastically. By heating hydrates from its equilibrium state (*Point C*) hydrates started to dissociate until at *point D* the slope of the pressure-temperature diagram changes sharply. This is the dissociation point of hydrates where the last crystal of hydrate in equilibrium with aqueous phase dissociates.

77

II.   *Measuring the gas storage capacity of hydrate*

To analyze the hydrate storage capacity, the amount of the formed hydrates and pressure-temperature equilibrium data are needed. The laters can be obtained by the help of pressure transducers and the temperature probe connected to the acquisition centre, but the amount of the formed hydrate can not to be measured directly. One solution is to first measure the amount of remained aqueous solution in the cell at *point C* and then by knowing the density of hydrate structure, calculate the amount of the formed hydrate by making a mass balance of water in aqueous phase and hydrate phase. For this purpose a dilute concentration of LiCl (4 mg/L) was used as a trace molecule in order to measure the amount of the remained aqueous solution. As LiCl is a water soluble salt that does not enter the hydrate structure, its concentration in the remaining aqueous phase increases after hydrate formation. With the help of atomic absorption analysis LiCl concentrations in the initial solutions, and in the liquid remaining at the end of hydrate formation experiments could be measured. The amount of liquid consumed by the hydrate formation can then be calculated by the relation [Eq.39]:

$$\Delta V_L = V_{L,0} - V_{L,eq} = V_{L,0}\left(1 - \frac{C_{Li,0}}{C_{Li,eq}}\right)$$

Equation (39)

where V_L and C_{Li} respectively stand for the volume and Li$^+$ ions concentration of the liquid phase in the reactor. Underscores 0 and *eq* indicate the initial and final conditions, respectively. Assuming that the mass of liquid consumed was converted into hydrates, the volume of hydrates formed may be approximated by:

$$V_{H,eq} \approx \Delta V_L \frac{\rho_L}{\rho_H}$$

Equation (40)

In equation [Eq.40] the density of the liquid phase ρ_L was supposed constant over the range of compositions and temperatures, and equal to 1000 kg.m^{-3}. This assumption is justified by the low concentration of salt in the solution used for the measurements. The volumes of vapour phase at initial and final conditions are given by equations [Eq.41] and [Eq.42], respectively:

$$V_{V,0} = V_R - V_{L,0}$$

Equation (41)

$$V_{V,eq} = V_R - V_{L,eq} - V_{H,eq}$$

Equation (42)

Where the volume of the reactor has been determined previously to be $V_R = (206.0 \pm 1.5)$ mL, including the liquid transfer lines. Finally the amount of hydrogen stored in the hydrate can be obtained from pressure and temperature measurements using equation [Eq.43] :

$$n_{H_{eq}}^{H_2} = \frac{p_0 V_{V,0}}{ZRT_0} - \frac{p_{eq} V_{V,eq}}{ZRT_{eq}}$$

Equation (43)

At the pressures investigated for our measurements, 20 MPa or less, the compressibility factor Z of hydrogen was assigned a value of 1,1. The number of moles entrapped was further converted to a percentage of the hydrate mass in order to compare the storage capacity with other media.

2.4. Gas phase composition analysis: Gas Chromatography

The gas phase composition analyzing system was possible by a Rapid Online Sampling Injector (ROLSI) developed and constructed at École des Mines de Paris, Fontainebleau, France. ROLSI is from one side connected to the isochoric reactor for taking samples and from the other sided connected to a Gas Chromatographer (GC) for sending the samples to the GC through an isothermal transfer line [Figure 27]. A permanent stream of career gas in the open cycle of ROLSI makes online sampling possible. Absence of dead volume in the sampler, possibility of taking samples as small as 0.1 mg, wide range of operational temperatures from cryogenic conditions to 553 K and pressures up to 60 MPa makes ROLSI a very practical sampler for studying hydrate phase equilibrium [72].

The gas chromatograph is a PERICHROM PR2100 which uses a Thermal Conductivity Detector (TCD) and a PORAPAK-Q packed column (length, 2 m; o.d., 1/8 in., 80/100 mesh). The TCD was calibrated for propane, carbon dioxide and hydrogen. For this purpose, firstly a career gas was selected for two systems of H_2-C_3H_8 and H_2-CO_2 by comparing the thermal conductibility of these gases. Table 8 presents the thermal conductibility of some common career gas in gas chromatography in a wide range of 273 to 378 K. For the system H_2-C_3H_8 the thermal conductibility of nitrogen produces a good resolution and was selected as the carrier gas of the system.

Table 8 - Thermal conductivity of common career gases

Gas	Thermal conductivity / $W \cdot m^{-1} \cdot K^{-1}$
Ar	1624,478
N_2	2378,101
He	$1,668439 \cdot 10^4$
H_2	$1,657972 \cdot 10^4$
CO_2	1419,325
C_3H_8	1507,247

An efficient carrier gas in a TCD detector must have a thermal conductibility value different from all the analyzing compounds (here H_2, CO_2 and C_3H_8) to produce a chromatograph peak with a good resolution. As it is given in table 8, for the H_2-CO_2 system no gas exists with this condition. The thermal conductibility of all of these gases is either close to the thermal conductivity of hydrogen or carbon dioxide. For this reason, two carrier gases were selected for this system. Helium was selected for CO_2 calibrating and nitrogen for H_2 calibration. In the sampling processes by changing the carrier gas each time two samples were taken to assure the accuracy of the analysis.
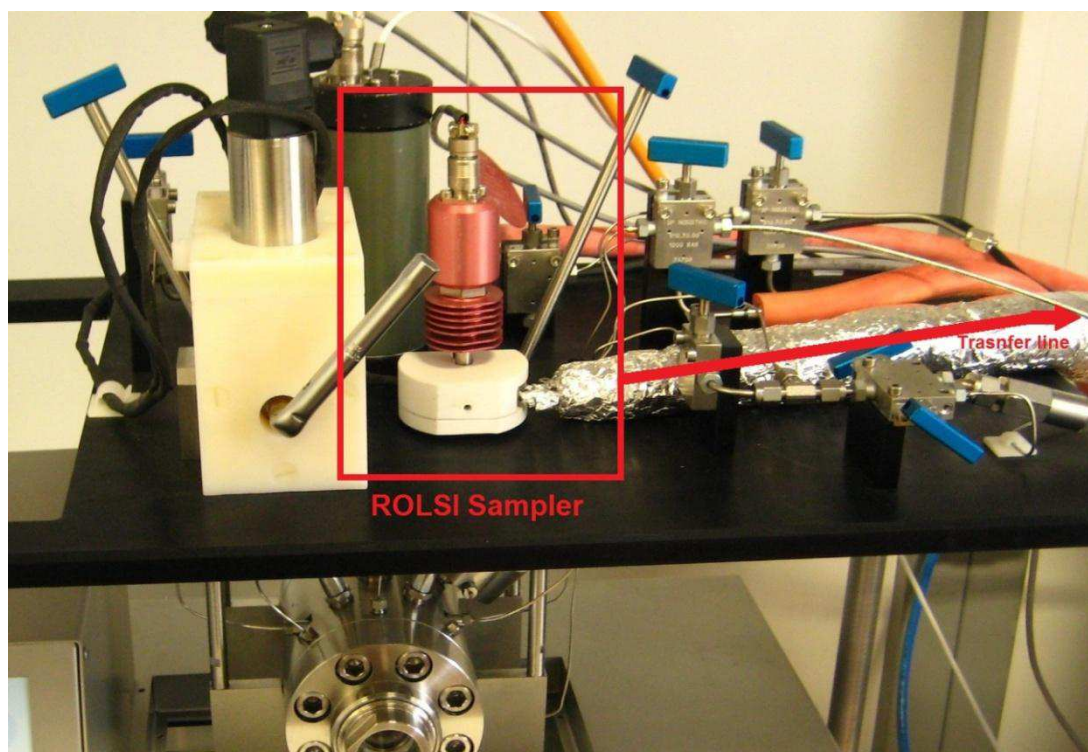
Figure 27 - The ROLSI sampler connected to the reactor

The obtained calibration curves were fitted to second-order polynomial equations. The composition of the gas phase at a given equilibrium condition was determined from the peak area ratio of the unknown sample and the coefficients of the corresponding polynomial equation for each compound. In this way, the gas phase composition was analyzed by gas chromatography for H_2-CO_2 and H_2-C_3H_8. The fitted parameters for each gas component are presented in Table 9. The calibration curves follow the general form of ax^2+bx+c.

Table 9 - Polynomial parameters of calibration curves

Gas component	Career gas	Polynomial equation parameters		
		a	b	c
Hydrogen	Nitrogen	$-2{,}40269 \cdot 10^{-13}$	$2{,}03371 \cdot 10^{-9}$	0
Propane	Nitrogen	0	$1{,}49097 \cdot 10^{-9}$	0
Carbon dioxide	Helium	$-1{,}65165 \cdot 10^{-11}$	$2{,}16556 \cdot 10^{-8}$	0

2.5. Liquid phase analysis: Atomic Absorption Spectrometry

In order to calculate the amount of enclathrated gas in the hydrate structure, firstly the amount of formed hydrate must be measured. For this purpose, lithium chloride was used as a tracer for measurement the amount of the free water. Because lithium chloride does not participate in hydrates structure, salt concentration will increase in the unconverted free water increases after hydrate formation. By measuring the initial and final salt concentration in the aqueous solution the amount of hydrates can be calculated. This was done by help of an atomic absorption spectrometry apparatus (SOLAAR, Thermo Electron Corporation). For each experiment, the aqueous solution introduced into the cell contained 4 mg/L of lithium chloride concentration in order not to affect the hydrate dissociation conditions. After formation of hydrate, thanks to the liquid sampling equipment on the reactor, remained free water inside the reactor was analyzed. For each analysis a set of standards was used to calibrate the atomic absorption spectrometer.

2.6. Materials

Table 10, presents materials and chemicals used in the present work with their purities and name of their suppliers. DSC samples and p-V-T cell aqueous solutions were prepared through gravimetric method, using an accurate electronic balance (Metler Toledo AW205) with precision of 10-5 g.

2.6.1. Preparation of TBAOH samples

For preparation of TBAOH-H_2O mixtures the starting material TBAOH·$30H_2O$ hydrate (98 wt.% purity) was purchased from Alfa-Aesar. Solid starting material was solved in distilled water in the calculated ratio and closed in bottles. Prior to the measurements all mixtures were degassed by evacuation of the air from the closed bottle. For the differential scanning calorimetry (DSC) investigations ~40 mg of the solution were used and for p-V-T measurements, 50 ml of the aqueous solution was used each time.

Table 10 - Chemicals used in the measurements, with their purities and their suppliers

Chemical	Supplier	Purity
Hydrogen	Linde	99.9999%
Hydrogen – carbon dioxide (50%-50%)	Air liquide	Purity of each gas > 99.99%
Carbon dioxide	Air liquide	99.995%
Nitrogen	Linde	99.999%
Helium	Air liquide	Purity of gas > 99.9
TBAOH.$30H_2O$	Sigma Aldrich	98 wt%
TBPB	Alfa Aesar	99 wt%
NaBH$_4$		
TBPBH$_4$*	Synthesized in Lab.	
Acetic Acid	Sigma Aldrich	99.7wt%

For each measurement, distilled and deionised water was used

2.6.2. Preparation of TBPBH$_4$ samples

The TBPBH$_4$-H_2O mixtures were prepared using freshly synthesized TBPBH$_4$. This compound was obtained by reacting sodium borohydride (NaBH$_4$, 98 wt. % purity) with TBPB (99 wt. % purity) according to the reaction:

$$TBPB + NaBH_4 \rightarrow TBPBH_4 + NaBr \downarrow$$

Equation (44)
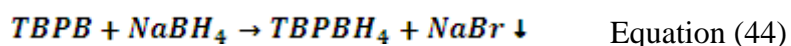
This reaction was carried out in a solution of ethanol, followed by solvent evacuation and sample crystallization. To prevent the hydrolysis reaction of TBPBH$_4$ during the preparation of the TBPBH$_4$-H$_2$O mixtures, a 0.5 M water solution of NaOH was used instead of pure distilled water. Such concentration was investigated experimentally by observation of the hydrogen release in the mixtures with different amount of NaOH. At this concentration of sodium hydroxide no hydrogen release was observed. To avoid a slow hydrolysis reaction which can be invisible, all TBPBH$_4$ -H$_2$O mixtures were prepared separately in the DSC sample holder prior to each measurement. At the end, for investigating the hydrogen release from the TBPBH$_4$ hydrolysis reaction, acetic acid was used.

Chapter three:

Results & Discussions (1)

- Semi-clathrate systems -

As it was discussed earlier one of the main properties of hydrogen clathrate hydrates is their severe formation / dissociation conditions. In order to overcome these severe conditions, many researches have been carried out in recent years and consequently some organic additives have been presented, among which THF is the most famous. Although additives such as THF [42-47] reduce the formation pressure of hydrogen hydrates and increase their dissociation temperature, their volatility and toxicity cause inevitable operational problems.

In this aspect, further investigations were contributed to the semi-clathrate of quaternary salts capable of hosting hydrogen molecules in more stable structures. Unfortunately, the major disadvantage of these semi-clathrates is their low storage capacity [52-64] which does not meet the technical and commercial requirements for a mobile storage system. However, they appear to be an imaginable future for in-place storage systems.

Accordingly, in this work hydrogen semi-hydrates of two quaternary salts were investigated. Effect of Tetra-n-butyl phosphonium borohydrate (TBPBH4) as a quaternary phosphonium salt and Tetra-n-butyl ammonium hydroxide (TBAOH) as a quaternary ammonium salt on hydrogen storage has been investigated for the first time. Their phase diagrams have been established and their storage capacities have been measured. Eventually efficiency of these salts is evaluated by comparing the results with other hydrogen hydrate systems.

3.1. Investigation of TBPBH$_4$ semi-clathrate system

3.1.1. Introduction

As previously stated, hydrogen storage in sII clathrate hydrates is constrained by severe formation conditions. Subsequent use of promoter molecules such as tetrahydrofuran (THF) created new prospects for corssing these barriers and therefore to shift the phase equilibrium boundaries to lower pressures and higher temperatures region. In this regard, special attention has been given to the hydrates of tetraalkylonium salts. Several experimental evidences show hydrogen enclathration in cavities of tetra-*n*-butylammonium bromide (TBAB) semi-clathrate [73-78]. It is shown that binary H$_2$-TBAB semi-clathrate hydrate demonstrates greatly increased thermal and low-pressure stability when compared with H$_2$ and H$_2$-THF clathrate hydrates. Moreover, when tetra-*n*-butylammonium fluoride (TBAF) is used instead of TBAB, the stability can be increased even further [79].

Since the discovery that hydrogen molecules can be stored in semi-clathrate hydrates of quaternary ammonium compounds, other members of the "quaternary ammonium/ phosphonium salts" family have been subject of many investigations. One major disadvantage of this approach is that the total amount of hydrogen stored in semiclathrate hydrates is too small to be compared with the mass fractions required for the practical usage.

On the other hand, some hydrolysable materials such as hydroquinone [80] and NaBH$_4$ [91] are attracting the attentions for a hydrogen storage scheme. The common point between these two different storage methods is the presence of water as an essential component. Therefore, if a hydrolysable compound be able of forming hydrates (semi-clathrate) a further hydrolysis of this compound will result in a higher hydrogen production. This new approach is called *hybrid storage* of hydrogen. An early investigation of hybrid hydrogen storage in tetra-n-butylammonium borohydride semiclathrates shows that the additional hydrogen produced from the hydrolysis of BH4$^-$ increases the gravimetric hydrogen storage capacity by 170% [81]. The hydrolysis reaction can be summarized as:

$$NaBH_4 + 2H_2O \rightarrow NaBO_2 + 4H_2 \qquad \qquad \textit{Equation (45)}$$
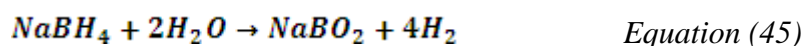
Theoretically the hydrolysis of sodium borohydride has an ideal gravimetric storage capacity of 10.8 wt%, however by taking into account NaBO$_2$ as a by-product, the actual hydrogen capacity reduces to less than 2.9 wt% [82].

As it has been demonstrated earlier, [78] the tetra-alkylphosphonium salts increase the hydrate stability more than their ammonium partners. This behaviour may be present also in the case of TBPBH$_4$ salt in comparison to TBABH$_4$. In this regard, tetra-n-butylphosphonium borohydride [(n-C$_4$H$_9$)$_4$PBH$_4$] salt has been chosen for the purpose of hydrogen hybrid storage investigations. Using different pressures of N$_2$ and H$_2$ the effect of the gas nature and hydrate stabilization kinetics has been analysed. The dissociation temperatures and phase diagram of the system has been investigated and finally quantitative measurement of the chemically bonded hydrogen was obtained by gas volumetric analysis.

3.1.2. Investigations of the synthesized TBPBH$_4$ salt

In order to achieve the optimal conditions for the synthesis of the TBPBH$_4$ salt different parameters such as volumes of the solvent (ethanol), time and atmosphere of the reaction were studied. The favourable synthesis procedure was chosen by comparing the results of the gas volumetric analysis. The highest hydrogen release during the hydrolysis revealed the best reaction conditions. Table 11 presents the results of 4 sets of operational conditions that were tested during the study. The conditions of reaction number 1 are more favourable in comparison to the others. It is noticeable that the reaction atmosphere does not influence the efficiency of synthesis and in contrary, the time of mixing and volume of solvent are of great importance. Therefore, in our investigations TBPBH$_4$ salt was synthesized under the conditions of reaction number 1. The 1.73 mol of hydrogen, which was released from 1 mol of TBPBH$_4$ corresponds to 1.26 wt. % of chemically bonded hydrogen in TBPBH$_4$. This amount is much higher than hydrogen storage in the hydrates stabilized by other tetraalkylonium salts. For instance, H$_2$ + TBACl and H$_2$ + TBPB semiclathrate hydrates can release 0.12 wt% and 0.14 wt. % of hydrogen respectively [78], which is almost 10 times lower than the hydrogen storage properties of the TBPBH$_4$. In additions to the chemically stored hydrogen, there is a possibility of physical entrapping of hydrogen molecules into the structure of the semiclathrate hydrates of this salt. Thereby the hydrogen content of this material will increase even more.

Table 11 - Results of the gas volumetric analysis of the TBPBH₄, synthesized at different conditions

Reaction	Reaction atmosphere	$V_{(ethanol)}$ /ml	Time of reaction / hr	Gas volumetric ratio $n(TBPBH_4) : n(H_2)$
1	Air	30	24	1 : 1.73
2	Air	50	216	1 : 1.31
3	Argon	100	24	1 : 1.52
4	Argon	30	24	1 : 1.51

The prepared samples were subjected to NMR measurements for identification of the tetra-*n*-butylphosphonium borohydride salts after their synthesis. The proton spectrum of the TBPBH₄ is presented on the Figure 28.
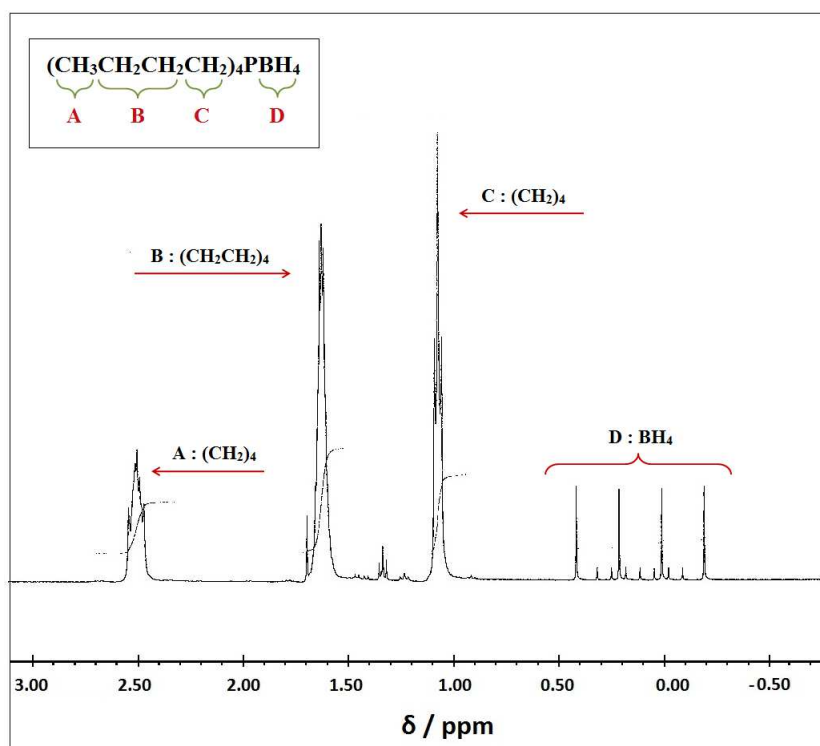
Figure 28- The H¹ NMR spectra of the TBPBH₄ compound

The ¹H NMR spectra of TBPBH₄ salt has not been previously published. 4 series of peaks, which identify TBPBH₄ structure are present on this spectrum. These peaks which are marked as "A", "B", "C" and "D" correspond to $(CH_2)_4$ (between the 2.44 and 2.60 ppm), $(CH_2CH_2)_4$ (between the 1.56 and 1.72 ppm), $(CH_2)_4$ (between the 1.0 and 1.18 ppm) and BH_4 (between the –0.2 and 0.4 ppm) groups, respectively. The proton spectrum of the BH_4^- group of the TBPBH₄ compound is close to that recorded for sodium borohydride and hydroxyborohydride

[83], showing similar B-H coupling region. The small peaks in the -0.3 to 0.5 ppm region correspond to BH resonances and are formed due to the existence of two boron isotopes, both of which are NMR active: ^{10}B, with a nuclear spin I = 3 and natural abundance of 19.9%, and ^{11}B, with I = 3/2 and natural abundance of 80.1%. In the same region the four peaks with large intensity correspond to the heteronuclear coupling between ^{11}B and hydrogen atoms, attached to boron. The other seven low intensive peaks are due to the coupling between hydrogen and ^{10}B atoms.

3.1.3. Investigations of TBPBH$_4$ – H$_2$O system

As a preliminary step, stability of TBPBH$_4$ semi-clathrate hydrates was verified. Under atmospheric pressure, the dissociation temperatures of the TBPBH$_4$ hydrates were measured in a salt concentration range from 0.36 to 12.5 mol %. Figure 29 presents the DSC heat flux curve of the 2.44 mol% solution of TBPBH$_4$ after 20 cycles of cooling-heating program.
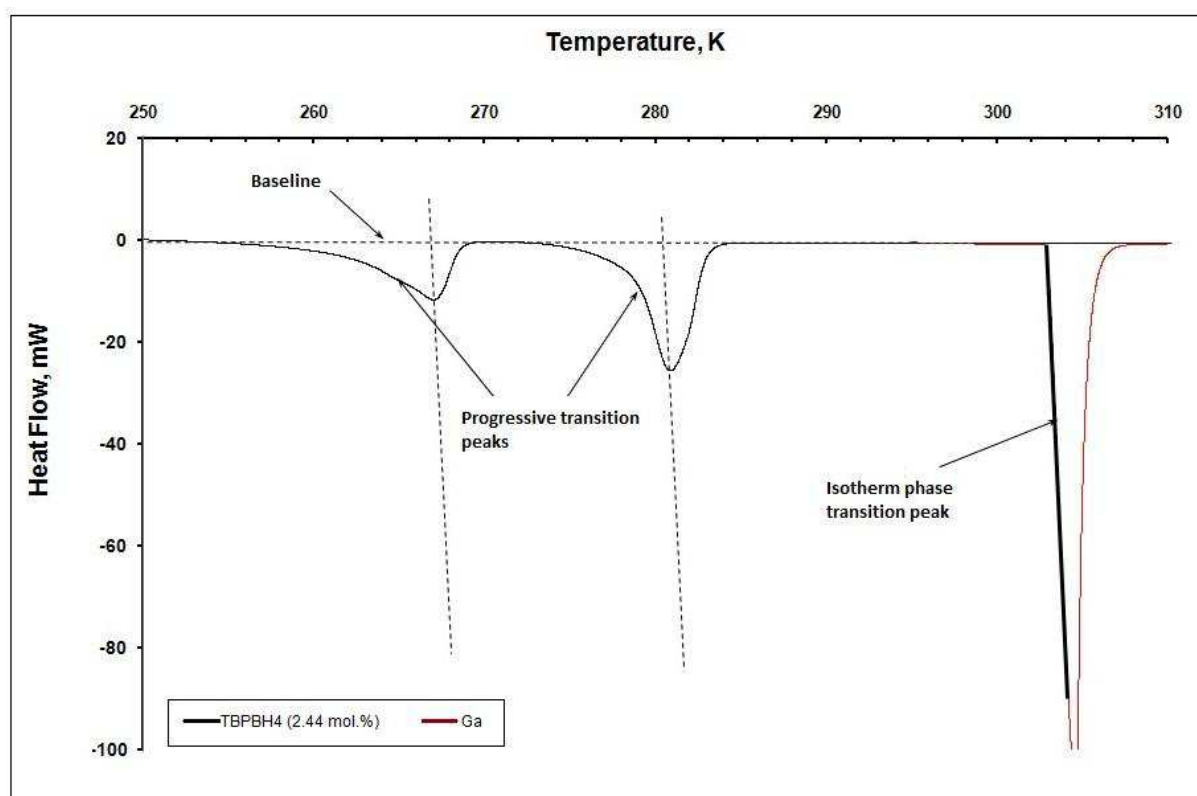
Figure 29 - DSC heat flux curve for the dissociation of 2.44 mol% of TBPBH$_4$

As it is shown, two peaks appeared during the final heating phase. The first peak at 280.5 K, is attributed to the endothermic dissociation of the TBPBH$_4$ semi-clathrate phase. The second peak at 266.9 K is due to the solution of the remaining water and NaOH, which was added to prevent premature reaction. As it is visible, these two dissociation peaks have progressive

90

character. Their dissociation temperature was measured using the line taken from the slope of the Ga melting peak.

All further investigations of dissociation temperatures were carried out in the same manner, as presented on this heat flux curve. Figure 30, presents the heat flux curve of the TBPBH4 hydrates under ambient pressure in the salt concentration of 0.36 to 4.75 mol%. As it can be seen in this figure, approximately for all the solutions in this salt concentration range, hydrate dissociation temperature remains constant at around 280.5 ± 0.5 K however, diluting the solution results in reduction in the quantity of the formed hydrate. This can be seen by the reduction in the area under the semi-clathrate peak and increase in the area under NaOH + ice peak.
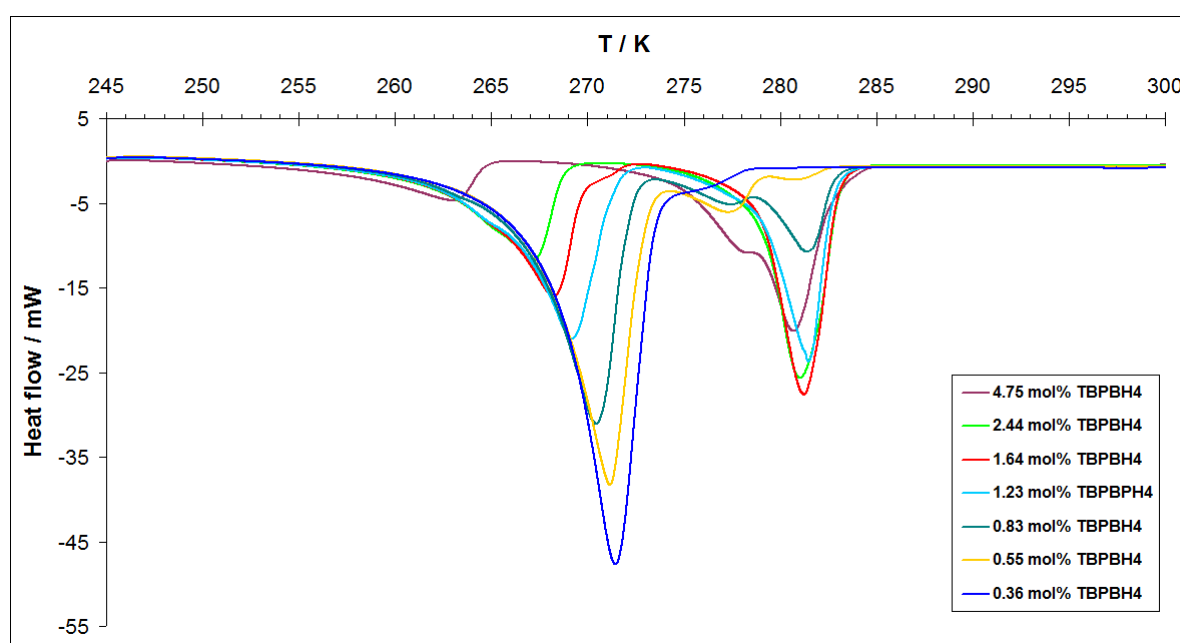
Figure 30 - DSC heat flux curve for TBPBPH$_4$ hydrates under ambient pressure in a salt concentration range of 0.36 to 4.75 mol%

In the present work detail investigations were performed for the TBPBH$_4$-H$_2$O hydrates at high water content. A complete set of results in the range of TBPBH$_4$ concentration from 0.36 mol% to 12.5 mol% was obtained in the same manner through DSC measurements and are listed in the Table 12. The existence of a hydrate of the TBPBH$_4$ salt, with approximately 26 molecules of water in its composition, was inferred from visual observation of the crystallization of solutions of variable concentrations. This composition is subject to uncertainty of at least ± 2 H$_2$O molecules per TBPBH$_4$ and would require further structural analysis to be validated. This hydrate undergoes non congruent dissociation at a temperature

of around 280.6 K (Figure. 31). The peritectic transition from one solid phase to a mixture of two immiscible liquids L_1 and L_2 was observed visually by heating of the frozen samples up to 373 K.

The limits of existence of the demixtion zone were not determined precisely, even though the constant melting temperature is an evidence of the existence of invariant equilibrium conditions over a wide range of compositions (at least from 0.5 to 4.5 mol% $TBPBH_4$).

Table 12 - Dissociation temperatures of TBPBH$_4$ hydrates as a function of salt concentration.

C_{TBPBH4}, mol, %	T_{diss} / K
12,5	$274,2 \pm 0.2$
8,33	$276,7 \pm 0.2$
5,88	280 ± 0.2
4,76	$280,3 \pm 0.2$
3,85	$280,6 \pm 0.2$
3,23	$280,2 \pm 0.2$
2,78	$280,3 \pm 0.2$
2,44	$280,5 \pm 0.2$
1,64	$280,8 \pm 0.2$
1,23	281 ± 0.2
0,83	281 ± 0.2
0,55	$280,6 \pm 0.2$
0,36	$275,9 \pm 0.2$

It was observed that demixtion exists at temperatures even higher than 373 K in the 1.64 mol. % solution. For the construction of a more precise phase diagram, investigations of additional points are needed. That is why all equilibrium lines are built using dashed lines.

This type of phase diagram is comparable with the diagrams of related systems. Thus very similar phase behaviour was observed by Dyadin et al. [84] for the i-AmAB-H$_2$O (i-AmAB is iso-amilammonium bromide) and i-AmPB-H$_2$O (i-AmPB is iso-amilphosphonium bromide) systems, where hydrates were formed by peritectic reactions from two liquid phases. The approximate ionic radii of the BH_4^- and Br^- (2.03 and 1.96 Å respectively) can be one of the factors of similarity in the phase behaviour.
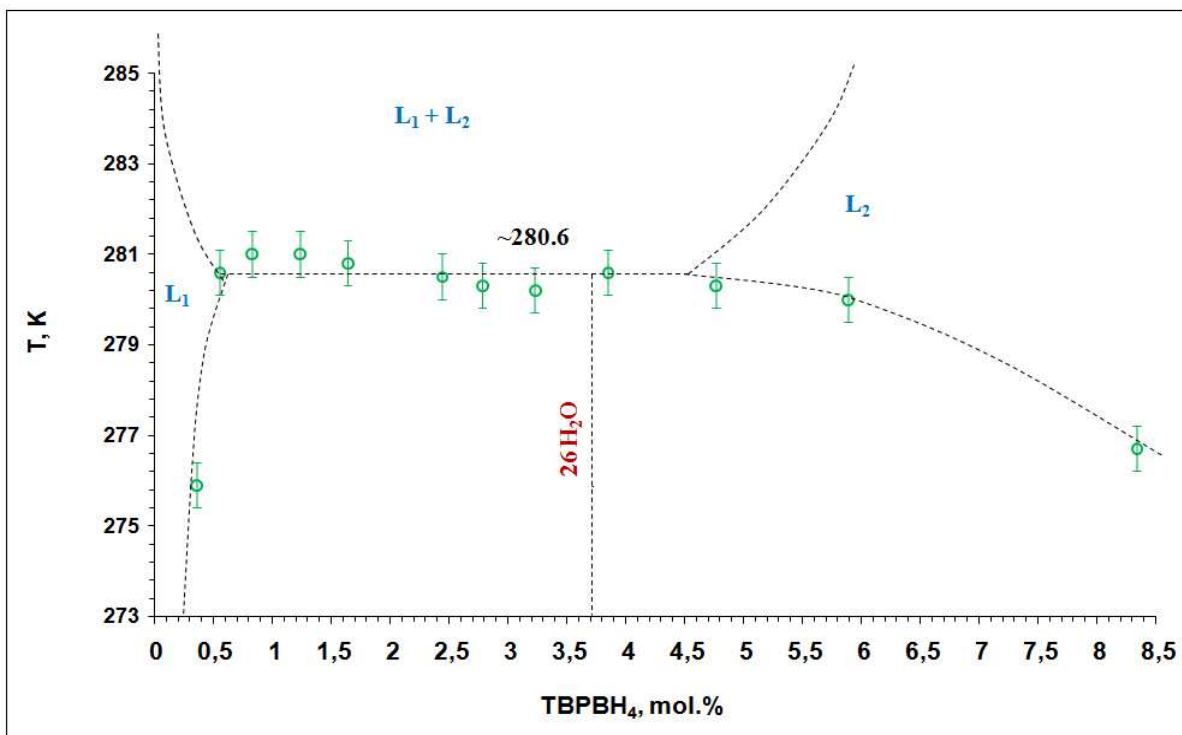
Figure 31 - The phase diagram of the TBPBH₄ + H₂O binary system in the region of crystallization of high water content semi-clathrate polyhydrate. (Dashed lines – equilibrium behaviours can vary. Solid line – data more clear).

For the investigations of gas absorption and its influence on the stability of the clathrate hydrates, TBPBH₄ solutions with concentrations less than 3.2 mol. % were selected. This region was selected with the view that higher water content could promote the formation of a larger amount of cavities, and thereby, larger content of trapped gas.

3.1.4. Investigation of the H₂-TBPBH₄ – H₂O system

TBPBH₄ semi-clathrate hydrate stability under hydrogen pressure was investigated using DSC measurements at different gas pressures and different salt concentrations. Figure 32 presents the effect of hydrogen pressure on the heat flow curves obtained with a TBPBH₄-H₂O system at a salt concentration of 1.96 mol%.

As it can be seen in this figure, by increasing hydrogen pressure of the system, the dissociation peak of the hydrate shifts to higher temperatures, which means that hydrogen molecules stabilize the semi-clathrate structure, by occupying the small cavities of the hydrate. On the other hand, the peaks corresponding to NaOH + ice melting shift to lower temperatures. Assuming the concentration of NaOH to be negligible, this is in accordance

93

with the phase behaviour of water at solid-liquid equilibrium, where pressure has a reverse relation with temperature.
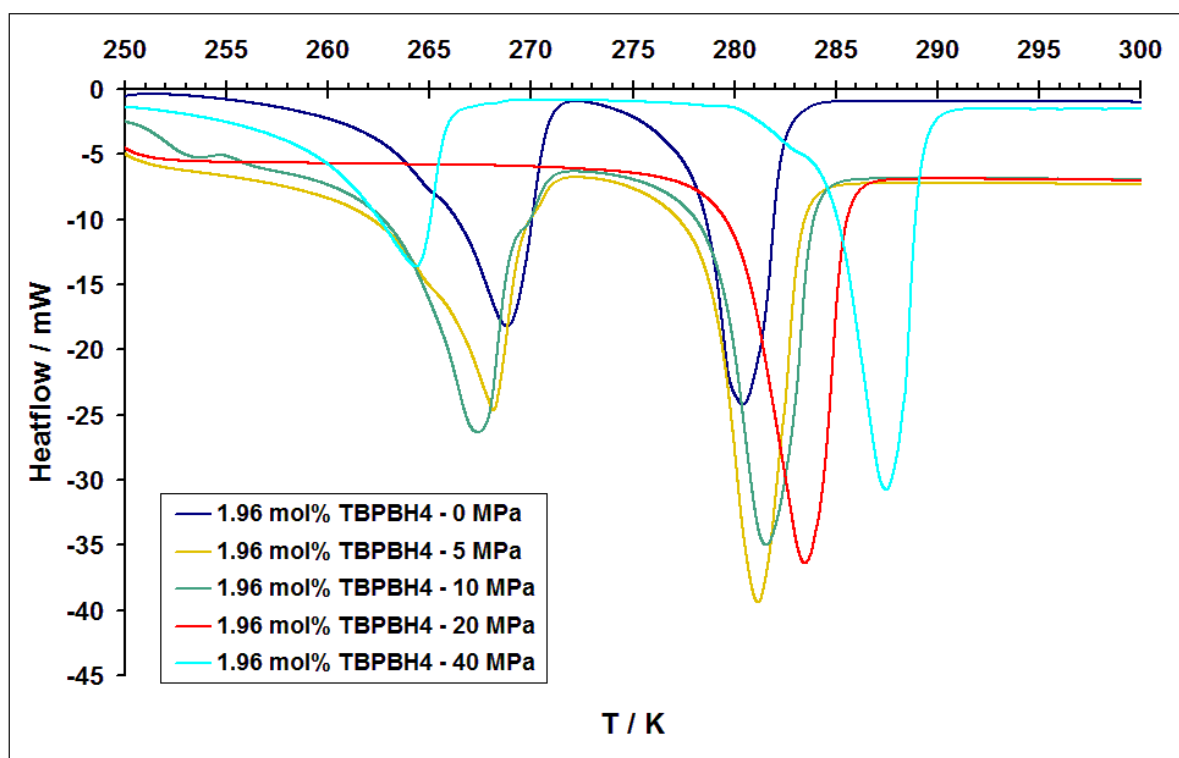
Figure 32 - DSC heat flux curve of the 1.96 mol% solution of TBPBH$_4$ under different hydrogen pressures

Table 13 presents the measured dissociation temperatures of the H$_2$ + TBPBH$_4$ semi-clathrate hydrate for the same solution (1.96 mol. % TBPBH$_4$) at different gas pressures.

Table 13 - Temperatures of dissociation of the G + TBPBH$_4$ semiclathrate hydrate at different gas pressures (G = H$_2$ or N$_2$)

P / MPa	T_{diss}/ K
H$_2$ + TBPBH$_4$ (*1.96 mol. %*)	
3.0	281 ± 0.5
12.2	282.9 ± 0.5
20.0	284.2 ± 0.5
36.8	286.1 ± 0.5

The *P-T* data obtained from these measurements are presented in Figure 33 and are compared with the equilibrium data for hydrogen hydrates with different promoters, such as THF, TBAB, TBACl (tetra-*n*-butylammonium chloride), TBPB, taken from literature.
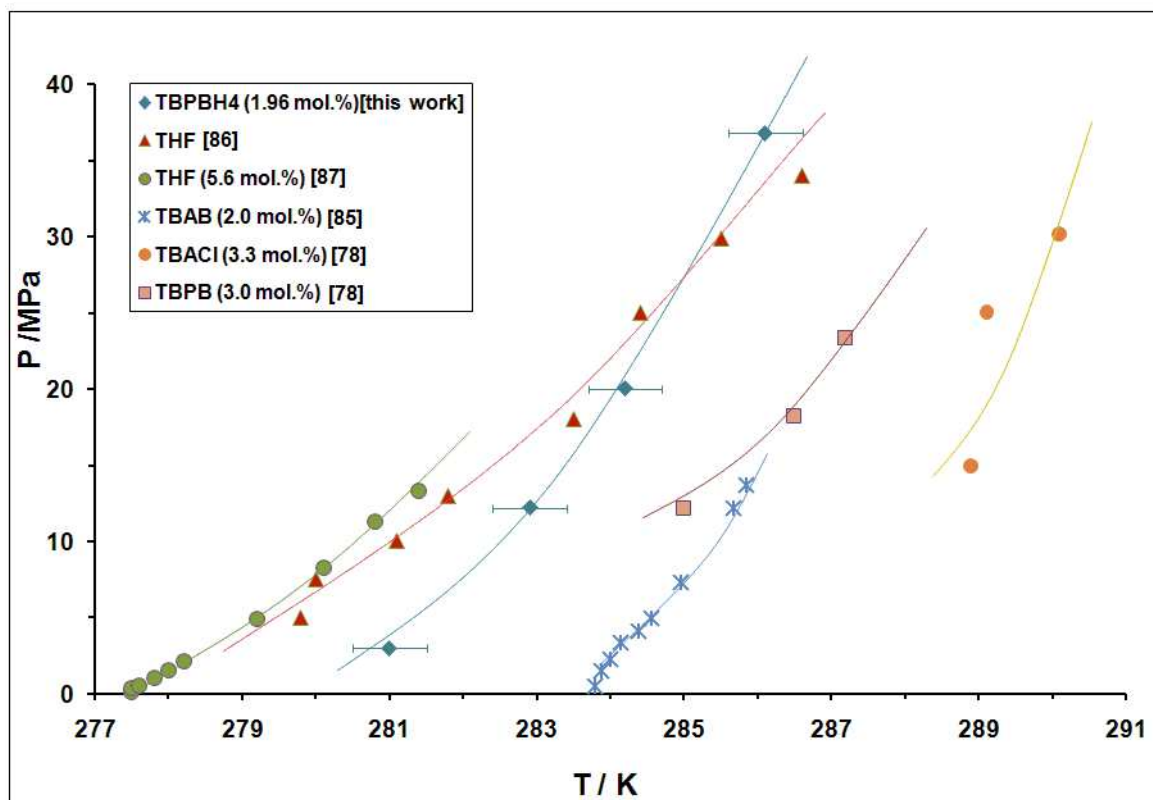
Figure 33 – P-T data for additive + water + H$_2$ systems. (The type of additive, its concentration and the source of data are presented on the diagram. Error bars represent the uncertainties on phase change temperatures, based on repeated determinations of melting points of gallium. Lines represent exponential fits of experimental points)

Furthermore, the dissociation temperature of the TBPBH$_4$ semiclathrate hydrate of hydrogen has been measured as a function of salt concentration at different gas pressures. The results obtained are listed in Table 14 and represented in Figure 34. As shown in this figure, in the concentration range from 0.55 to 3.23 mol%, the TBPBH$_4$ hydrate of hydrogen is more stable than the hydrate without gas enclathration. The hydrogen has efficient stabilizing effect on the hydrate structure and leads to the increase of dissociation temperatures up to 6 K. Except this temperature shift, the phase behaviour of H$_2$O + TBPBH$_4$ + H$_2$ systems in this concentration region remains the same as it was in the absence of gas.

Table 14 – Dissociation temperature of TBPBH₄ semi-clathrates under different hydrogen pressures

C_{TBPBH4} mol. %	*No gas* T_{diss}/ K 0 MPa	Hydrogen		
		T_{diss}/ K 10 MPa	T_{diss}/ K 20 MPa	T_{diss}/ K 40 MPa
3.23	280.2	282.6	284.4	286.8
2.44	280.5	-	-	286.8
1.96	280	-	284	286
1.64	280.8	-	-	286.8
1.23	281	282.6	284	286.5
0.55	280.6	282.5	284.5	286.3

The influence of hydrogen on the hydrate stability is clearly visible in Figure 34. The dissociation temperature of the hydrate increased up to 6 K at 40 MPa of hydrogen pressure. Furthermore, the stability of TBPBH₄ semi-clathrate hydrates of gas increased with pressure.
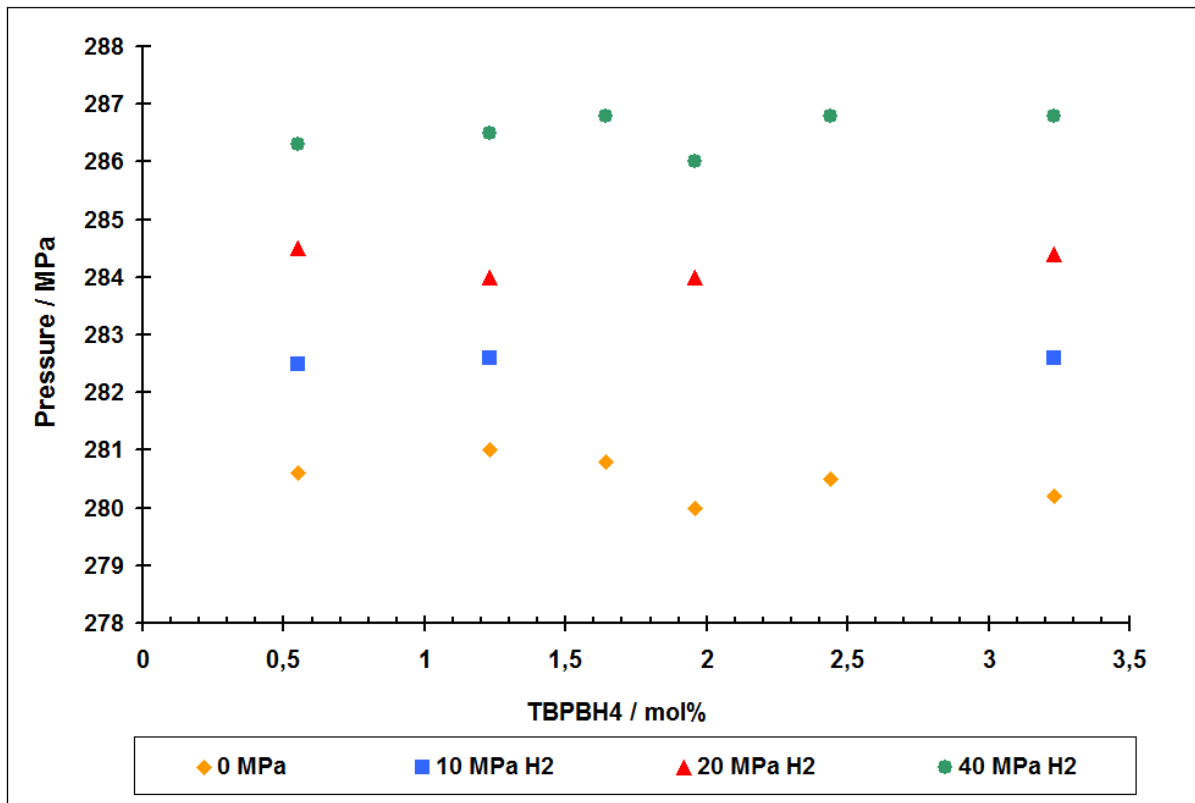
Figure 34 – Effect of pressure on TBPBH₄ clathrate of different salt concentrations

3.1.5. Investigation of the N_2 -TBPBH$_4$ – H$_2$O system

The measured equilibrium data of the TBPBH$_4$ semiclathrate hydrate with nitrogen for the 1.64 mol. % solution are listed in Table 15.

Table 15 - Dissociation temperature of TBPBH$_4$ hydrates as a function of concentration in different pressures of N$_2$

C_{TBPBH4} mol. %	*No gas* T_{diss}/ K 0 MPa	Nitrogen		
		T_{diss}/ K 10 MPa	T_{diss}/ K 20 MPa	T_{diss}/ K 40 MPa
2.44	280.5	290	291.3	295.2
1.64	280.8	289.4	292	295.1
1.23	281	289.6	292	295.4
0.55	-	289.6	291.4	295.7

The *p-T* phase behaviour for other nitrogen hydrates taken from the literature are also presented with these data in Figure 35. It is noticeable that all presented additives improve stability of the pure nitrogen hydrate. The best thermodynamic stability shows the nitrogen hydrate in the presence of THF, which shows the higher dissociation temperature at the same pressures. The two other mixed hydrates (TBAB and TBPBH$_4$) exhibit almost the same temperature change associated with the increase of nitrogen pressure. They differ only in their stability, which is higher for the TBPBH$_4$ hydrate for approximately 2 K at the same nitrogen pressure.

The dissociation temperature of the TBPBH$_4$ semiclathrate hydrate of hydrogen and nitrogen has been compared as a function of the salt concentration at different gas pressures. The results obtained are presented in Figure 36. As it is shown in this figure the influence of the nitrogen on the hydrate stability comparing to the stabilization effect of hydrogen is clearly visible. The dissociation temperature of the hydrate increased with the gas pressure augmentation, reaching up to 14.4 K at 40 MPa of nitrogen pressure. These results show strong differences in the stabilizing effect of gases of different natures and validate the assumption of gas enclathration into available cavities of the TBPBH$_4$ semi clathrate structure.
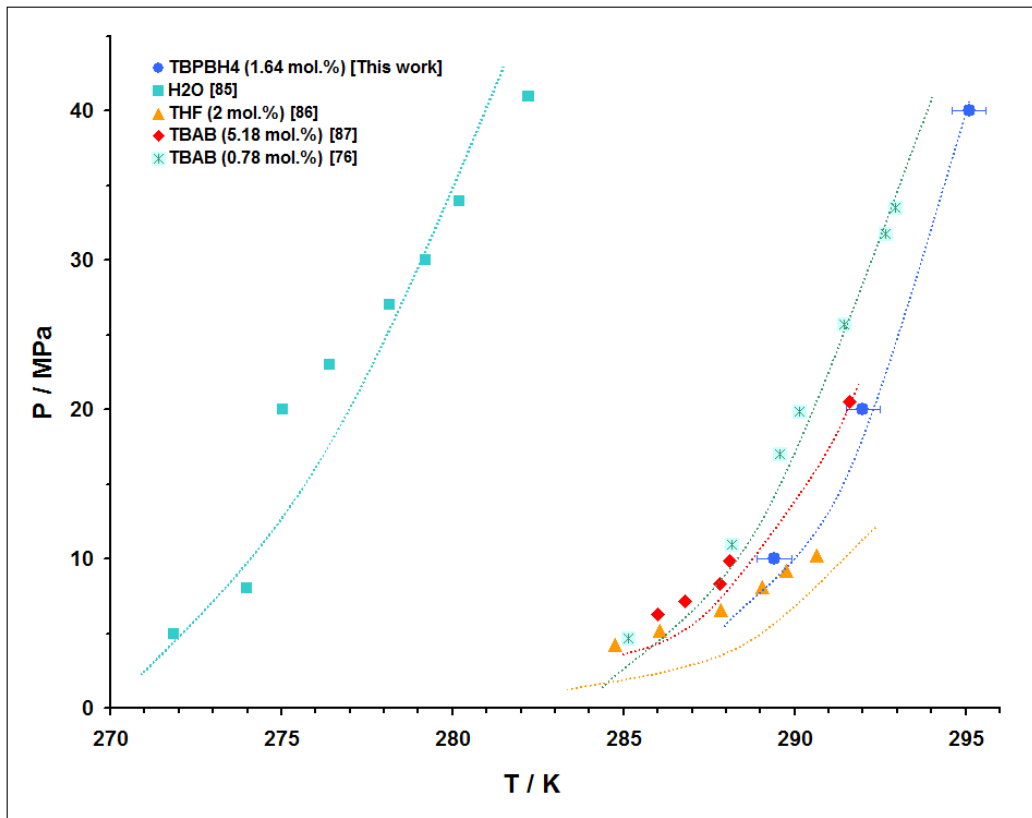
Figure 35 - P-T phase diagram of additive+water+N₂ system
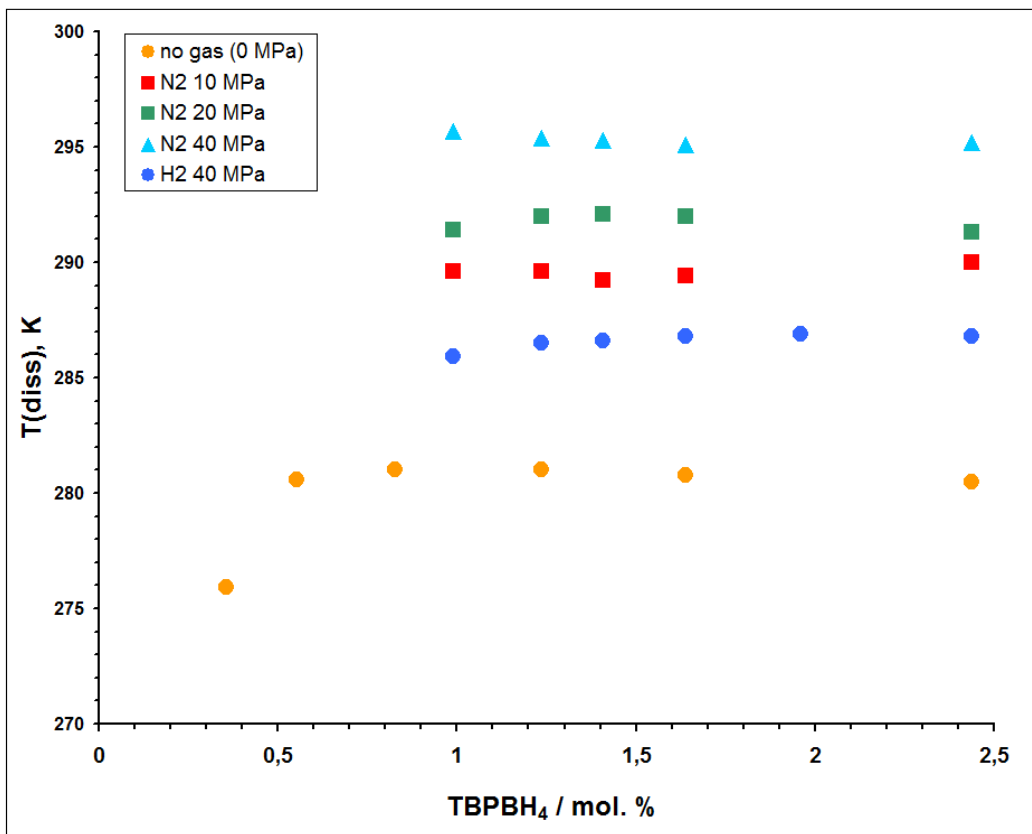
Figure 36 - Comparison of hydrogen and nitrogen pressure on the phase diagram of TBPBH4

3.2. Investigation of TBAOH semi-clathrate

3.2.1. Introduction

The idea of using semi-clathrate as a hydrogen storage medium was pursued using tetra-n-butylammonium hydroxide ($C_{16} H_{37} NO$). TBAOH hydrate structure has been studied earlier by Dyadin and Udachin and has shown to have a relatively high dissociation temperature [84]. According to these investigations, TBAOH-H_2O system forms two different hydrate structures. As it is shown in Table 16 the more stable structure (hereafter hyd1) which possesses 28.3 moles of water per mole of tetrabutylammonium hydroxide ($Bu_4NOH.28.3$ H_2O) melts congruently at 300.55 K. The second structure (hyd2) which possesses 32.3 moles of water per mole of tetrabutylammonium hydroxide ($Bu_4NOH.32.3$ H_2O) melts incongruently at 292.15 K.

Table 16 - Properties of TBAOH hydrate structures

Hydrate	T_{diss} / K	Melting type	Density / $kg.m^{-3}$
$Bu_4NOH.28,3$ H_2O	300,55	*Congruently*	1063
$Bu_4NOH.32,3$ H_2O	291,15	*Incongruently*	1046

Due to these high dissociation temperatures hydrate-based hydrogen storage could reach near ambient conditions, which would be of great interest for most applications. At a first step, the phase diagram of TBAOH semi-clathrate was studied at atmospheric pressure in the absence of hydrogen; then the possibility of hydrogen enclathration and the phase equilibria of H_2 – TBAOH – H_2O system was investigated.

3.2.2. Investigation of TBAOH – H_2O system

Series of DSC analysis have been carried out to investigate the TBAOH-H_2O phase diagram at atmospheric pressure in absence of hydrogen. Figure 37 present the resulting heat flux curve of dissociation of a 1.23 mol% TBAOH solution after 30 cycles at a rate of 1 K/min. As it can be seen in this figure, three peaks are detectable in this curve. The first one from the left corresponds to the melting of the eutectic phase transition of Ice + hyd2 into liquid phase. A eutectic phase transition is an invariant phenomenon which takes place at a constant temperature and therefore results in appearance of a sharp isotherm peak on the heat flux curve. The temperature corresponding to this phase transition is given by the onset of the heat

flux peak, around 272 K. The small peak at 288 K also shows an isotherm phase transition which is attributed to peritectic dissociation of hyd2 phase into a mixture of hyd1 and liquid.

Eventually, the last peak in this curve (right) presents the progressive dissociation of hyd1 hydrate structure. The non-isotherm nature of the phase transition of this hydrate structure is due to the presence of a liquid with a composition different from hyd1 in equilibrium with hydrate. The method applied for calculating the dissociation temperature of this kind of phase transition is the *Gesellschaft für Thermische Analyse (GEFTA)* [71] which was described earlier in 3.1.

The isotherm nature of the two first peaks implies that their corresponding phase transition temperature is independent of the salt (TBAOH) concentration. This fact can be seen in Figure 38, where the peak evolution for four TBAOH solutions is shown. It can be seen that the peak corresponding to the peritecitc dissociation remains at constant temperature in this range of concentrations and the progressive dissociation peak of hyd1 shifts to the higher temperatures by an increase in concentration of salt where at 3.23 mol% (around the congruent concentration) only one sharp peak appears.
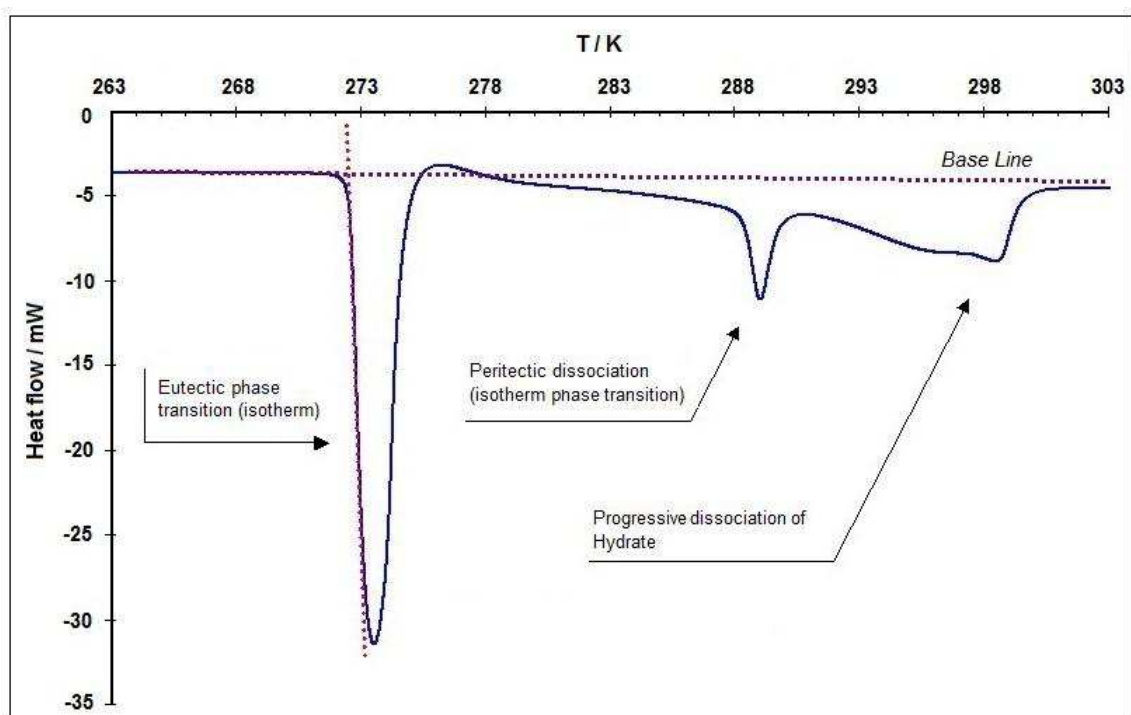
Figure 37 - DSC heat flux curve of dissociation of 1.23 mol% solution of TBAOH
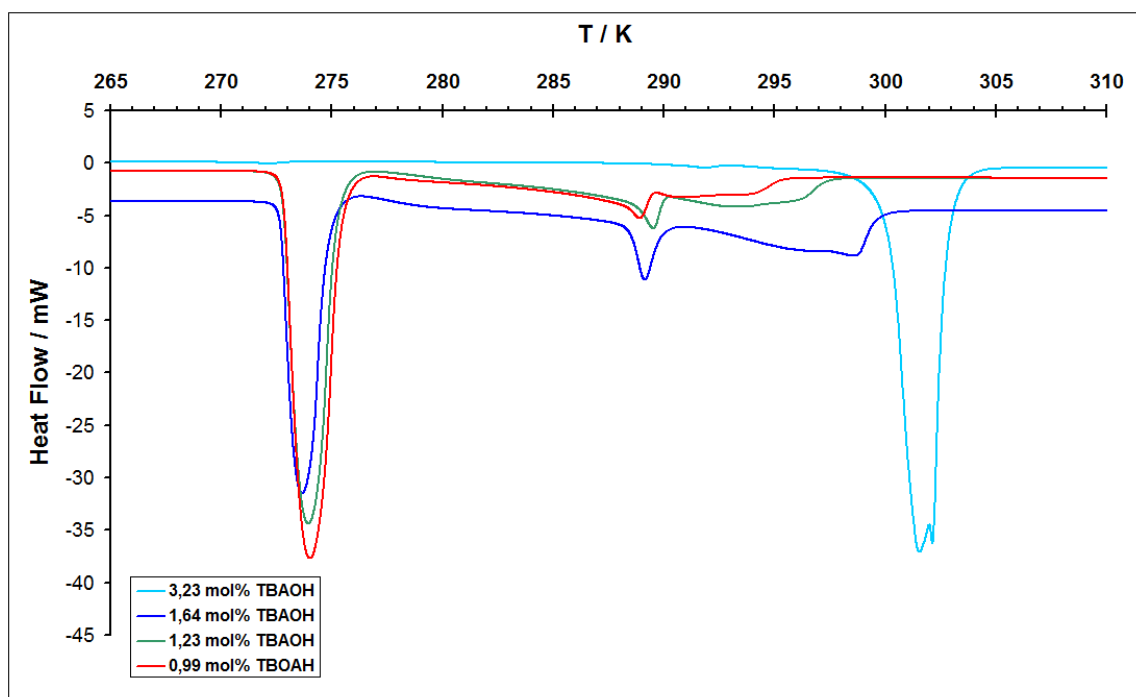
Figure 38 –Heat flux curve of TBAOH hydrate in different salt concentration at ambient pressure

Table 17 gathers the measured dissociation temperatures of 9 compositions ranging from 0.83 to 3.41 mol % TBAOH. The onset of the first peak for all samples between 0.83 and 2.44 mol % is at 272.3 ± 0.5 K; the onset of the second peak between 0.99 and 3.23 mol % is at 288.9 ± 0.7 K. The uncertainty ranges given here correspond to twice the standard deviation of the mean values. They may be compared to the uncertainty of temperature measurements using DSC, which is generally of 0.5 K.

Table 17 - Temperatures of (Ice + hyd2) eutectic melting, TE, (hyd1 + hyd2) peritectic melting, TP, and hyd2 dissociation, Tdiss, in the system H$_2$O + TBAOH at variable salt concentrations

C_{TBAOH} mol%	T_E/K	T_P/K	T_{diss}/K
3.23	-	289.64	300.14
2.44	272.44	288.44	299.54
1.96	272.64	288.54	299.14
1.64	272.74	288.94	298.44
1.41	272.14	288.74	297.14
1.23	272.14	288.54	295.14
1.1	272.24	289.04	294.14
0.99	272.04	288.94	292.94
0.83	272.14	-	291.44

The resulting *x-T* phase diagram of the (TBAOH + H₂O) at ambient pressure is demonstrated in Figure 39. As it can be seen in this diagram, at point *C* hydrate with composition of TABOH.28,3H₂O coexists with the liquid phase of the same composition which reveals the existence of a congruent melting point. This is in accordance with the data reported by Dyadin and Udachin [84]. Point *M* represents the metastable equilibrium of (hyd2 + Liquid) phases reported by Dyadin, while our measurements show the peritectic invariant corresponding to (hyd1 + hyd2 + Liquid) equilibria, at a slightly lower temperature. As the concentration of TABOH salt reduces in the solution, the dissociation temperature of hyd1 decreases until at point *P* it coincides with the dissociation of hyd2. This point is the peritectic point of the phase diagram. Further dilution of the solution brings to point *E* which represents the eutectic melting of (Ice + hyd2) mixture. This is shown in Figure 39 in a schematic way, by extrapolating the equilibrium points. Compositions of these dashed points have not been obtained as in highly diluted concentration of TBAOH solution, the corresponding peak heights were reduced dramatically which made the graphical methods very difficult and inexact to find the dissociation point.
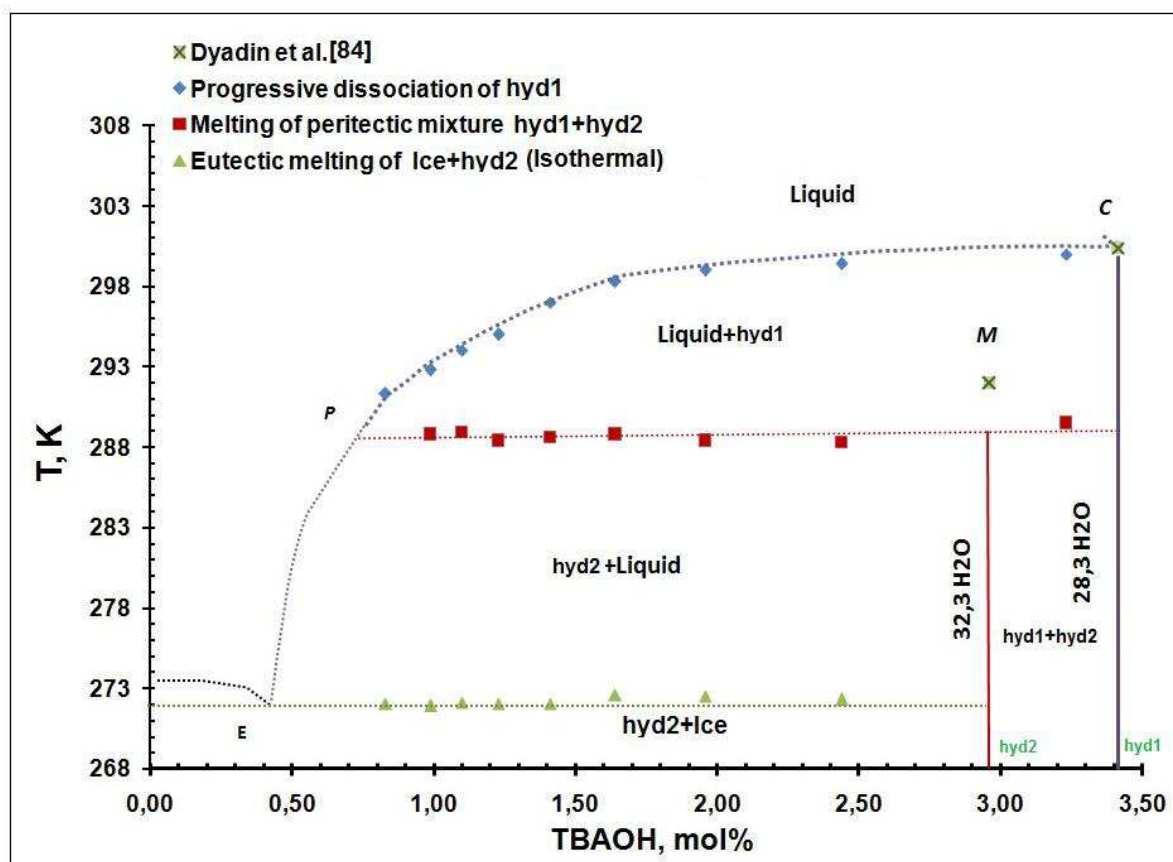
Figure 39 - The phase diagram of TBAOH-H₂O binary system

3.2.3. Investigation of the H_2 – TBAOH – H_2O system

Stabilization of TBAOH-H_2O semi-clathrate hydrates in presence of hydrogen was investigated using DSC measurements in different TBAOH concentrations. For this purpose, TBAOH solutions in a concentration range of 0.83 mol% to 2.44 mol% were chosen. There were two constraints for choosing this concentration range, firstly because the purchased TBAOH salt was in form of TBAOH crystals containing 30 molecules of H_2O and therefore working in more concentrated solutions was not possible, and on the other hand, highly diluted solutions did not produce dissociation peaks with sufficient resolution. The effect of hydrogen pressure can be seen on Figure 40 in which the heat flux curves of dissociation of semiclathrates in a salt concentration of 1.23 mol% are presented. As it can be seen in the figure, the peak corresponding to the dissociation of the second hydrate structure (hyd2) shifts to higher temperatures (from 288 K to 295 K) by increasing pressure to 40 MPa. On the other hand, the progressive peak of hyd1 is almost constant around 294 K and seems to be independent of hydrogen pressure.
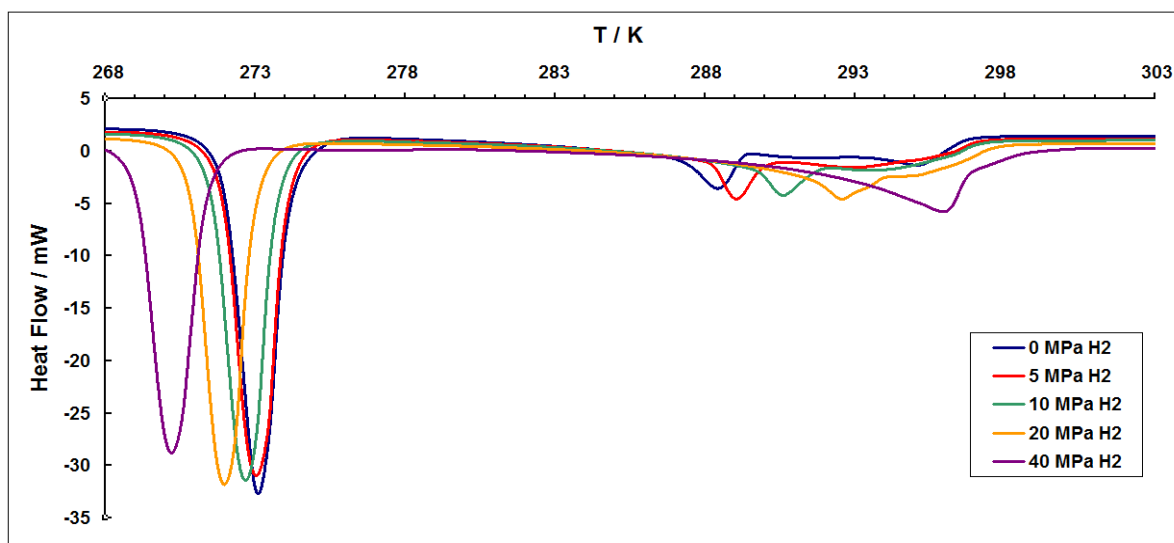
Figure 40 - The heat flux curve of 1.23 mol% TBAOH hydrate at different hydrogen pressures

A set of complete results of the dissociation temperatures of the two hydrate structures under four different hydrogen pressures are presented in Table 18 and are represented in Figures 41 and 42 to easily compare the effect of hydrogen pressure on the two hydrate structures.

103

Table 18 - Dissociation temperatures of H2-TBAOH-H2 semi-clathrate under different hydrogen pressures

C_{TBAOH} mol%	Hydrate structure hyd2					Hydrate structure hyd1				
	H₂ pressure/MPa									
	0	5	10	20	40	0	5	10	20	40
2.44	288.44	289.14	290.94	292.74	296.74	299.54	300.14	300.34	301.44	303.54
1.96	288.54	290.54	291.74	293.34	296.94	299.14	299.14	299.34	299.74	301.34
1.64	288.94	289.94	291.34	293.94	296.54	298.44	297.34	297.94	298.14	299.14
1.41	288.74	289.74	291.04	292.94	295.84	297.14	295.14	296.54	296.44	298.14
1.23	288.54	288.94	290.54	292.44	294.74	295.14	294.44	294.54	295.04	295.84
1.10	289.04	289.04	290.14	292.64	292.64	294.14	295.14	295.44	294.94	294.74
0.99	288.94	288.74	290.34	291.84	292.24	292.94	294.34	294.64	291.84	292.64
0.83	286.74	287.74	288.64	290.04	296.74	291.44	291.64	-	290.04	292.24
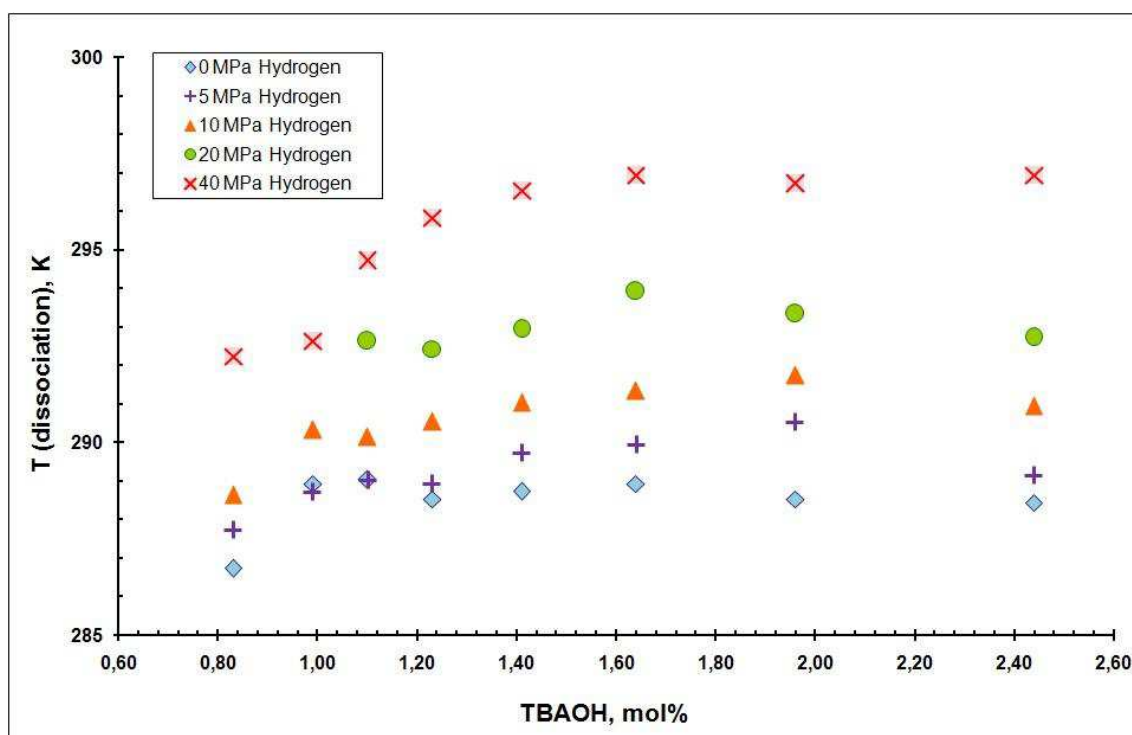
Figure 41 - Effect of hydrogen pressure on dissociation temperature of the second hydrate structure of TBAOH-H₂O system (hyd2)

As it is shown in Figure 41, dissociation temperature of the hyd2 structure is almost independent of TBAOH concentration in this concentration range, while it highly depends on the hydrogen pressure. For instance, for an increase of pressure from 0 to 40 MPa in a

solution of 1.6 mol% of TBAOH, the corresponding dissociation temperature of hyd2 increases by about 8K.

In contrary, Figure 42 demonstrates a strong dependence of the hyd1 dissociation temperature on the salt concentration, while the effect of pressure is much less sensible in this structure. As an example, the dissociation temperature of the first structure for the same salt concentration (1.6 mol %) increase around 1 K by under 40 MPa increase of the system pressure.
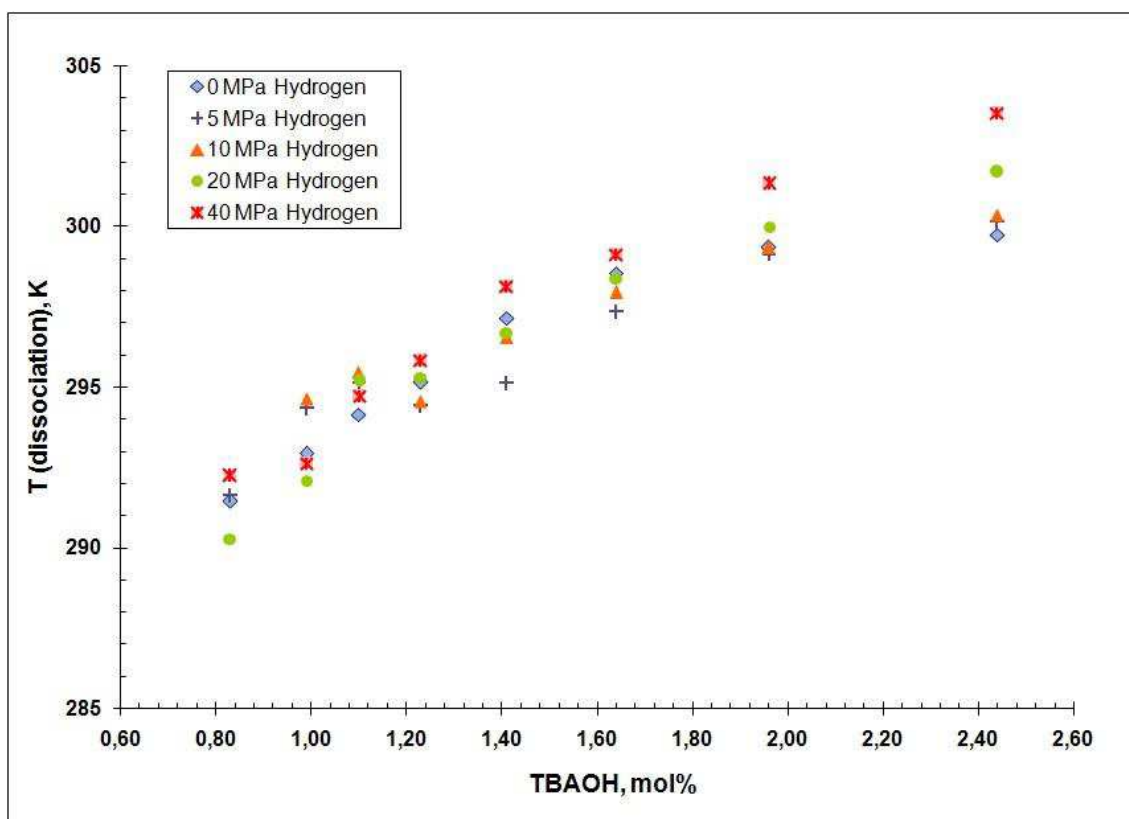
Figure 42 - Effect of hydrogen pressure on dissociation temperature of the first hydrate structure of TBAOH-H$_2$O system (hyd1)

These results demonstrate that hydrogen pressure is in favour of stabilization of the hyd2 hydrate structure, which consequently means that hydrogen molecules occupy available cavities in this second hydrate structure. Dissociation temperatures of TBAOH-H$_2$O hydrate are compared with some other quaternary semi-clathrate in Figure 43. For this comparison, the dissociation temperatures of hyd2 structure of TBAOH semi-hydrate with salt concentrations of 0.83, 1.23 and 1.96 mol % are selected, as well as those of hyd1 structure with the concentration of 1.23 mol%.
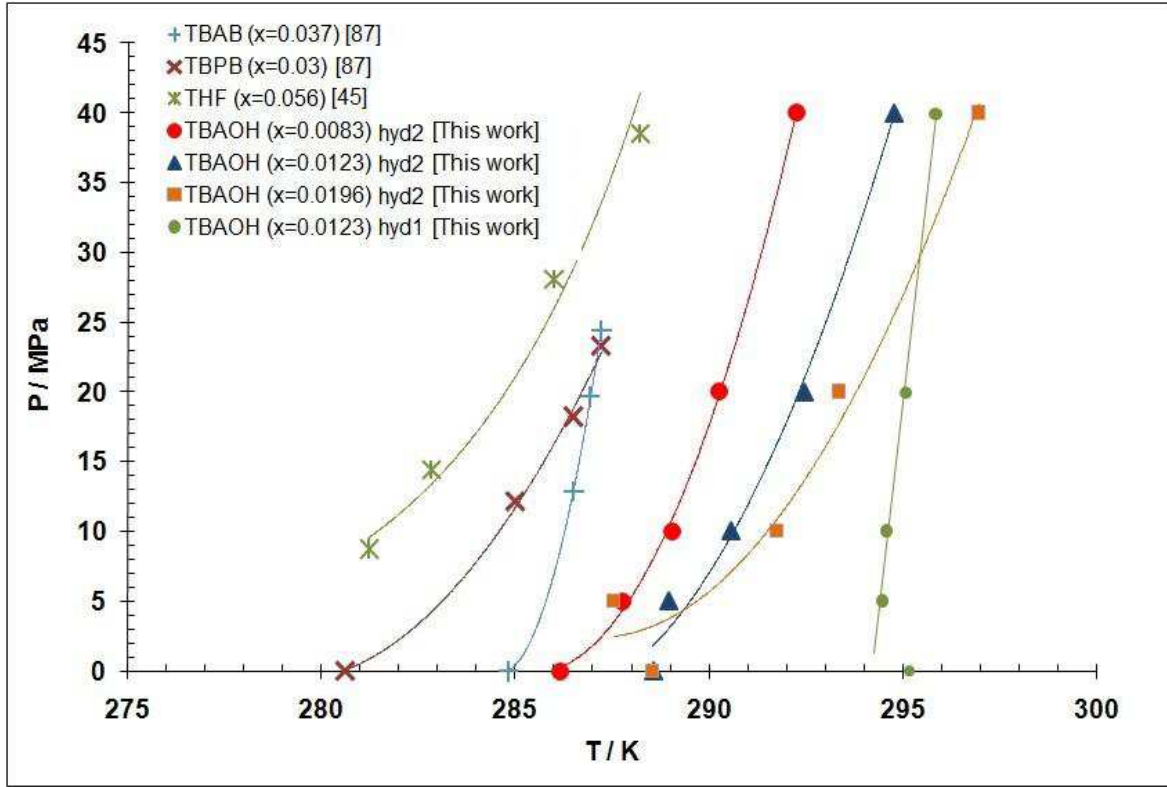
Figure 43 – comaprison of P-T equilibrium data of various H$_2$+semi-clathrate hydrates

T-p curves of THF, TBAB, TBPBP and hyd2 TBAOH hydrates obey approximately a similar trend and may be fitted by exponential curves. On the other side, *T-p* curve of hyd1 structure is almost perfectly linear. This observation may be explained by considering the Clapeyron relation between the *p* and *T* differentiates on the equilibrium curves:

$$\Delta_{diss}Vdp = \Delta_{diss}HdT$$

Equation (45)

In equation 2, $\Delta_{diss}V$ (resp. $\Delta_{diss}H$) represents the variation of volume (resp. enthalpy) of the system upon hydrate dissociation. $\Delta_{diss}H$ is independent of pressure. For a hydrate that contains no gas entrapped, $\Delta_{diss}V$ is the difference in volume between the hydrate and the corresponding amount of solution, which are nearly independent of pressure. $\Delta_{diss}V$ is thus constant, leading to a linear *T-p* curve. If the hydrate contains gas entrapped, $\Delta_{diss}V$ includes the volume of gas released, which varies as $1/p$. In that case the classical exponential-type *T-p* curve of H-L-V equilibria is obtained.

3.2.4. *p-V-T* measurements and hydrogen storage capacity

In order to calculate the hydrogen storage capacity of TBAOH hydrates from reactor experiments, it is assumed that only hyd2 hydrate structure was formed, because the TBAOH

concentration and temperature conditions were located in the (hyd2 + Liquid) domain of the phase diagram. The p-T diagram of TBAOH hydrate formation and dissociation is presented in Figure 44.
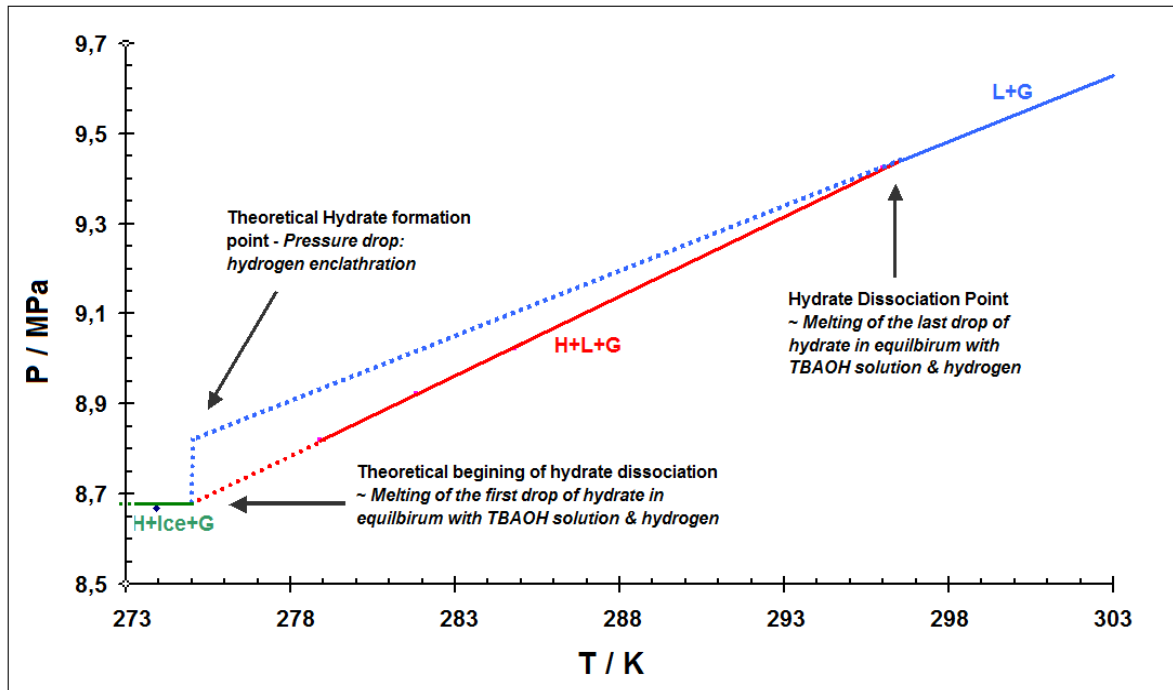
Figure 44 - p-V-T measurement of a 1.41 mol% solution of TBAOH under 10 MPa hydrogen [The dot lines in this diagram are just extrapolating of the data and they do not present confirmed measurements]

As it is shown in this diagram, by cooling down the TBAOH solution under hydrogen pressure, hydrate formation occurs by a sharp pressure drop. After reaching stability in temperature and pressure (green line), hydrates is heated by 0.1 K temperature steps (red line) until the last drop of hydrate dissociates and the two phase equilibrium between aqueous phase and gas phase appears. This change in equilibrium state of the system, results in slope variation of the *p-T* diagram. The intersection of former slope (red line) and the new slope (blue line) presents the hydrate dissociation point.

In our calculations in equation 43, the initial pressure of the system is the corresponding pressure of the system at 298 K and the final pressure of the system is the corresponding pressure of the system at 278 K. This temperature is taken high enough to permit the sampling of the aqueous phase. A value of 1046 kg.m^{-3} was thus taken for the hydrate density in equation 43. Our results at 10 MPa and 20 MPa show a hydrogen storage capacity of 0.35 wt% and 0.47 wt% respectively, while only 40 % of aqueous solution was converted to hydrate. This percentage capacity is compared with the storage capacity of other hydrogen

hydrate systems in Table 19. As it is given in this table, while pure hydrogen hydrate system shows maximum storage capacity of 5.5 wt% under severe thermodynamic conditions i.e. 220 MPa, stabilized semi-clathrate hydrates with moderate formation conditions show lower storage capacity (0.14 to 3.44 wt%).

Table 19-Hydrogen storage capacity of common hydrates and their formation conditions

System	H_2 content/wt%	p/MPa	T/K	Reference
H_2+H_2O	3.7	220	200-270	[88]
$H_2+THF+H2O$	3.44	75	255	[47]
$H_2+MCH*+H_2O$	1.38	149	273-279	[45]
$H_2+TBAB+H_2O$	0.6	16	287	[34]
$H_2+TBACl+H_2O$	0.12	14.9	288.9	[35]
$H_2+TBPB+H_2O$	0.14	12.1	285	[35]
$H_2+TBAOH+H_2O$	0.47	20	290	Present work

Regarding the relatively low storage capacity of hydrogen in TBAOH system, application of TBAOH semi-clathrate for mobile hydrogen storage applications does not seem economic. However, due to its stable structure, relatively low formation pressure and high (near to ambient) dissociation temperature, TBAOH semi-clathrate system have a potential to be developed as a in-place storage medium and for industrial hydrogen storage. It is evident that commercialization of this system needs further economic plant studies, including the cost of the equipments, power and labour work.

Chapter four:

Results & Discussions (2)

- clathrate hydrates in presence of gas mixture -

This chapter presents hydrogen hydrates phase equilibria in presence of gas mixtures, without any soluble organic salt in the aqueous phase. These gas mixtures are selected with two different approaches:

(1) The first system that comprises a gas mixture of propane – hydrogen is chosen to investigate the effect of small concentrations (partial pressure) of propane on the stability of hydrogen sII hydrate (Tuning Phenomenon)

(2) The second system is chosen in order to investigate the efficiency of hydrate clathrate as a separation medium in a gas mixture of CO_2-H_2. The phase equilibrium of the system has been studied and the gas phase molar composition has been analyzed.

4.1. Propane + Hydrogen + Water ternary system

4.1.1. Introduction

In spite of the stability of the semi-clathrate hydrogen systems, their major inconvenience is their low hydrogen storage capacity in comparison to pure the hydrogen-water systems. In order to mitigate the severe formation conditions of pure hydrogen hydrates, and to avoid the low capacity of semi-clathrate systems, Lee et al. [43] proposed for the first time the concept of *tuning*. They showed that for sII hydrate to be stable relative to ice, the only condition to be satisfied is that the occupancy of the large cage would be close to 1. In their investigations, by introducing THF as an auxiliary guest in the large cages of sII hydrate they increased the stability of hydrate structure. Subsequently, by tuning THF concentration in the aqueous solution they demonstrated that there exists an optimum concentration in which both hydrogen and THF will enter the large cavities.

Although tuning method was proposed for water soluble sII hydrate formers, the effect could be extended to a large number of hydrate formers such as hydrocarbon gases, and especially natural gas constituents. Among the natural gas components, propane is known to occupy large cages of sII hydrate and therefore is considered as a type II hydrate former [30-31].
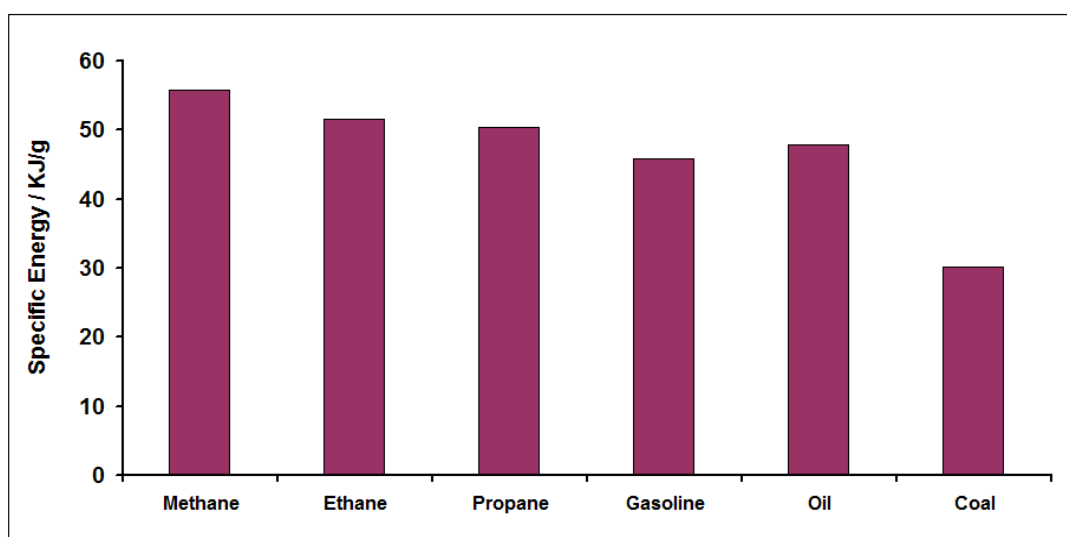
Figure 45 – Comparison of specific energy of propane with different common fuels

Moreover as it is shown in Figure 45, comparing to other constituents of natural gas propane has a relatively high specific energy. Gas mixture of hydrogen and propane can be used in industrial burners, internal combustion engines and in fuel cell where the presence of propane

is not a critical issue. In this regard it is potentially an ideal candidate to be tuned with hydrogen in order to stabilize sII clathrate hydrate by occupying the large cavities and leaving the small cages for hydrogen molecules.

4.1.2. Pure Propane – H_2O system

The first system that was studied in this work is propane + water system. Propane hydrate formation condition has been discussed earlier in several literatures and its phase equilibrium has been reported by different sources [89-95]. According to these investigations, propane forms hydrate structure II with a composition of $8G^1.136\ H_2O$ or $G.17\ H_2O$. The unit cell of this hydrate structure consists of 136 water molecules, with 16 small cavities and 8 large cavities which accommodate propane molecules [96].

Like all other hydrocarbon + water systems, the phase behaviour of propane + water system differs significantly from normal hydrocarbon mixtures. Firstly, because the hydrate phase is an important part of all hydrocarbon + water phase diagrams, and secondly because of the presence of two distinct liquid phases which are low soluble in each other.

Another significant difference of propane + water system is the relatively high critical temperature (369.9 K) of propane in comparison to the other constituents of natural gas. This can be seen in Table 20 which compares the critical temperature of some hydrate forming gases with respect to the triple point of water. The relatively high critical temperature of propane causes the intersection of pure propane vapour pressure line (V-L_{C3H8}) with the three phase hydrate equilibrium line (L_W-H-V) which consequently results in appearance of a second quadruple point (Q_2) in the phase diagram of these systems [30].

A schematic pressure-temperature diagram of systems with a higher quadruple point is illustrated in Figure 46. As it can be seen in this diagram, the L_W-V-L_{HC} equilibrium line which departs from Q_2 is very steep which is due to the presences of three incompressible phases in the equilibrium. Being almost vertical, the L_W-V-L_{HC} equilibrium line is usually considered as 'the limit of hydrate formation' or 'the maximum temperature of hydrate formation' because it practically limits the temperature range of hydrate existence [30]. The same phase behaviour can be observed for $H_2O + C_2H_6$ and $H_2O + i\text{-}C_4H_8$.

---

[1] G= Gas molecule

Table 20- Critical point of some hydrate forming gases with respect to the triple point of water

Constituent	T_C / K	P_C / MPa
Methane	190.6	4.59
Ethane	305,4	4.87
Propane	369.9	4.25
iso-butane	407.7	3.62
Nitrogen	126.3	3.39
Hydrogen	33.3	1.29
	Triple temperature / K	Triple pressure / MPa
Water	273.16	0.00603

If the critical temperature of a gas is considerably lower than the triple point temperature of water, *e.g.* methane and nitrogen, the vapour phase is supercritical and will not condense in higher pressures. Consequently these systems do not have an upper temperature limit for hydrate formation which is the case for $H_2O + CH_4$ and $H_2O + N_2$ systems.
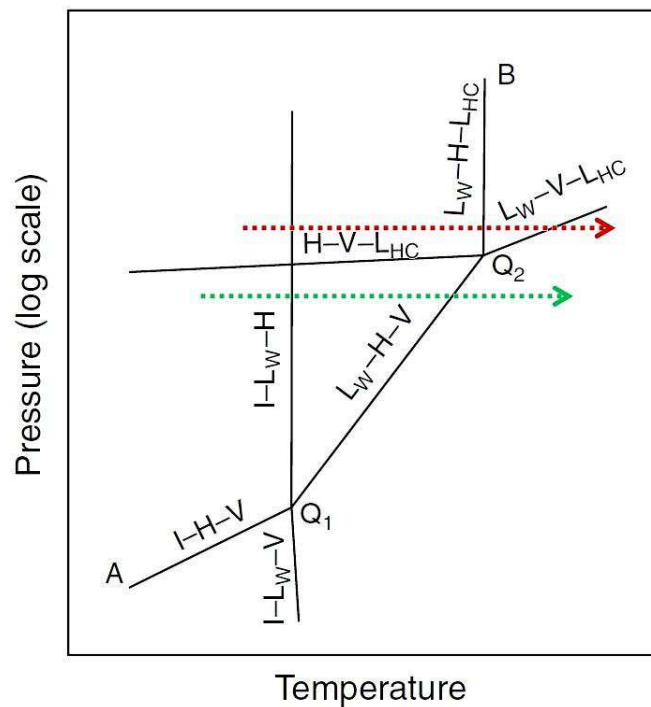
Figure 46- P-T diagrams for hydrocarbon+water systems with higher quadruple points [30]

If the critical temperature of a gas is considerably lower than the triple point temperature of water, e.g. Methane and nitrogen, the vapour phase is supercritical and will not condense in

higher pressures. Consequently these systems do not have an upper temperature limit for hydrate formation which is the case for $H_2O + CH_4$ and $H_2O + N_2$ systems.

Due to the importance of determination of the upper quadruple point, which is the temperature limit of hydrate formation, the first part of this work is dedicated on investigating Q_2. Propane hydrate equilibrium data were evaluated using HP-DSC measurements and the upper quadruple point was investigated.

a) Investigation of the upper quadruple point of the C_3H_8-H_2O system

Several studies have been done in order to find the exact value of the quadruple point for propane system. Table 21 lists these reported data in literature for Q_2. As it can be seen, a disagreement exists between reported temperature and pressure of Q_2. In this work, in order to investigate the upper boundary of the H-L_W-V line *i.e.* Q_2, a series of DSC measurements have been conducted in a pressure range of 0.3 to 0.6 MPa. The choice of this pressure range was made by considering Table 21 and reconsideration of Figure 46. According to Figure 46, on pressures above Q_2 and on pressures below Q_2 different phases co-exist which can be detected on DSC heat flux curves. By approaching these two pressures, *i.e.* by reducing pressures above Q_2 and increasing pressures below Q_2 a point in which four phases are in equilibrium appears. This point is the quadruple point of the system and its degree of freedom is zero.

Table 21- Second quadruple point (Q_2) of Propane-water system

Temperature / K	Pressure / MPa	Reference
278.8	0.55	30
279	0.60	92
278.2	5	90

Figure 47 shows the heat flux curve obtained upon warming up a sample of the propane-water system at 0.57 MPa after 30 cycles with a heat rate of 1 K/min. There are three picks detectable in this curve. The existence of these three peaks shows that the system is not at the quadruple point and according to the data on Table 21; it must be in a pressure range above the quadruple point. Following the red arrow on Figure 46, the corresponding peak for each phase transition with the same order in the heat flux curve can be found.
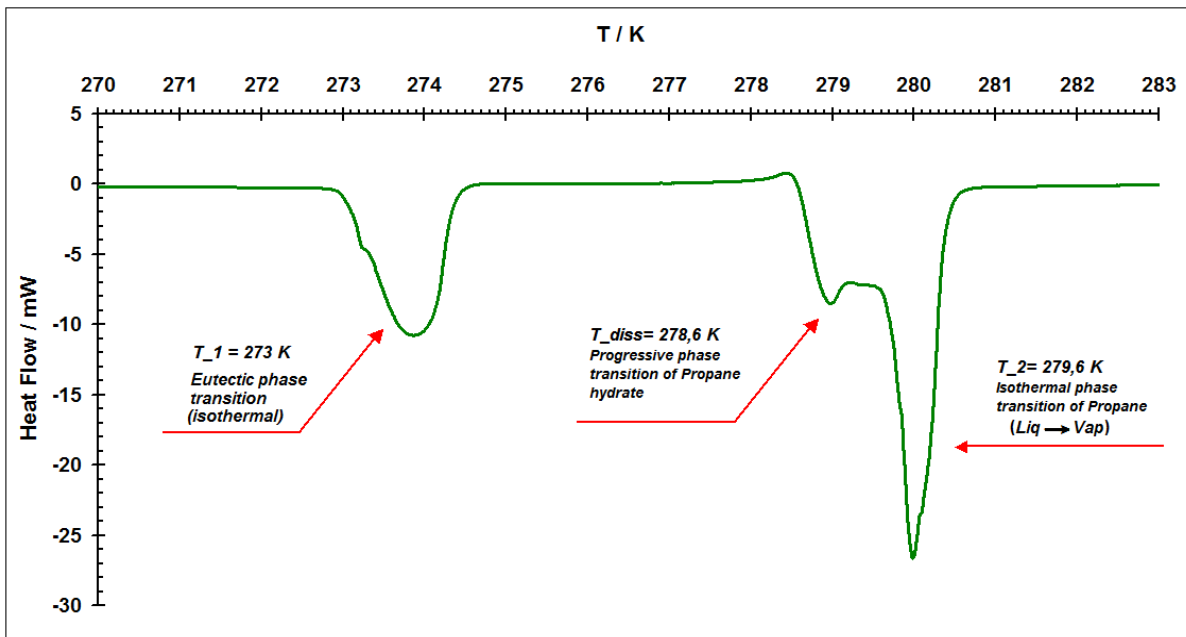
Figure 47 - DSC heat flux curve of propane-water system at 0.6 MPa (30 cycles)

The first peak from left corresponds to the eutectic mixture of ice + hydrate phases. Melting of an eutectic mixture is an invariant phase transition that takes place at constant temperature and therefore results in a sharp isothermal melting peak. The melting temperature is given by the onset of the heat flux peak around 273 K. The second peak at 278.6 K corresponds to an isotherm phase transition which is attributed to hydrate dissociation. This temperature is in fact the limit of hydrate formation at this pressure. According this phase diagram (Figure 46) the last peak which corresponds to the evaporation of liquefied propane has a progressive nature. It seems that this peak should have had wider shoulders but due to the small difference between hydrate dissociation temperature and liquid propane evaporation temperature, the corresponding peaks have been mixed in each other.

For pressures lower than the quadruple pressure, due to the closeness of hydrate dissociation temperature and liquefied propane evaporation temperatures, the corresponding peaks are not distinguishable. This can be seen in Figure 48 which presents the heat flux of propane + water system under pressure of 0.4 MPa. With the same approach in this example, by following the green arrow in Figure 46 the nature of the appeared peaks on the heat flux curve can be interpreted, but these peaks are so much mixed that calculating their corresponding temperatures are practically impossible.

115
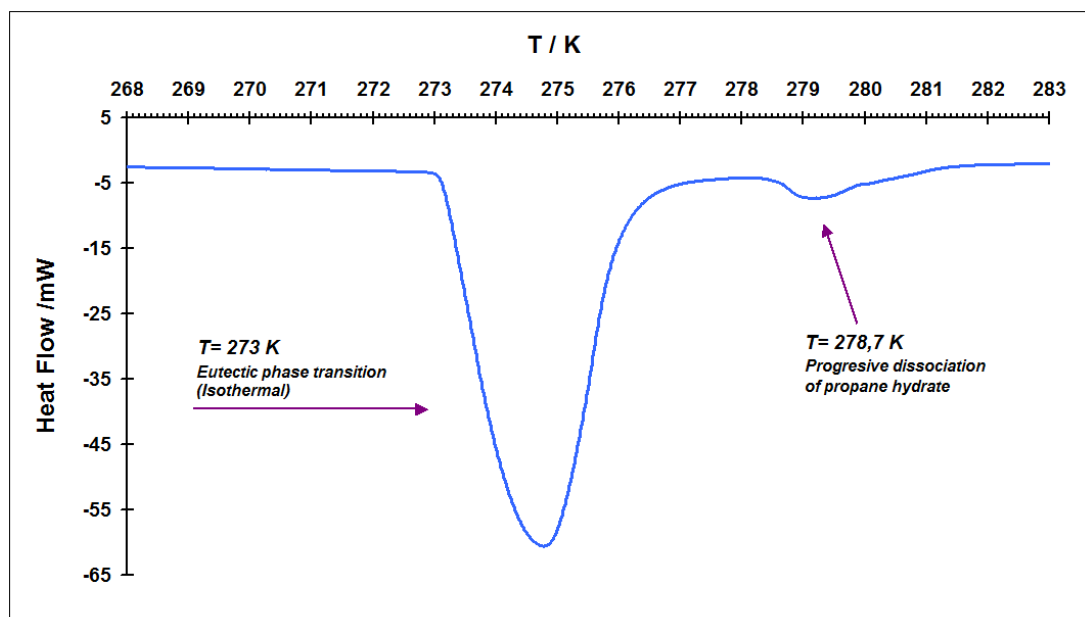
Figure 48 - DSC heat flux curve of propane-water system at 0.3 MPa (3 cycles)

The corresponding heat flux curve is presented in the Figure 49, which is the result of propane hydrate dissocitaion under 0.51 MPa propane pressure, after 30 cycles. As it can be seen, no peak for eutectic melting is detectable, this means that during the 30 cycles all of the water content of the system has converted into hydrate. The resulting peak, demonstarates that even at a pressure of 0.51 MPa, where are still at a region up to Q_2.
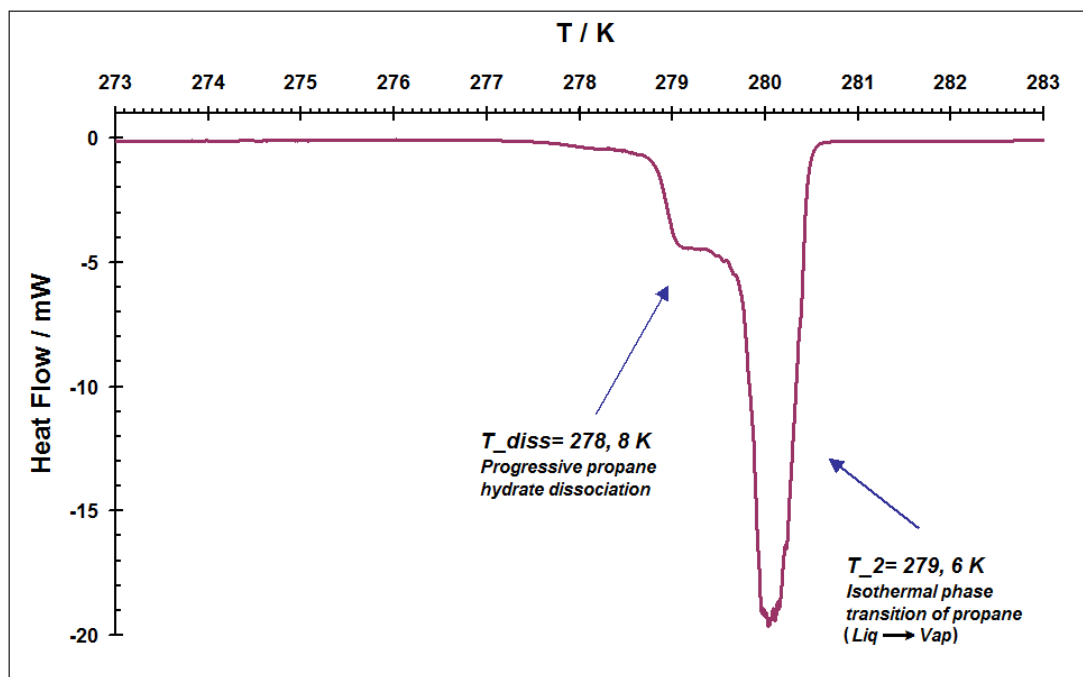
Figure 49 - DSC heat flux curve of dissociation of propane hydrate at 0.51 MPa

116

The main inconvenience with DSC measurements for the propane-water system at pressures lower than 0.5 MPa is the inaccuracy in calculation of dissociation temperature. As it is shown in Figure 50, for the propane hydrate at 0.4 MPa, the peak corresponding to the eutectic melting and progressive dissociation of hydrate are not easily distinguished. This is due to the low dissociation temperature of hydrate. In this example, after 40 cooling/heating cycles a considerable amount of hydrate has been formed and therefore the resulting peak for hydrate dissociation overlaps the eutectic melting peak.

On the other front, when a small amount of hydrate is produced in a short cycling program (3 cooling/heating cycles) the calculated dissociation temperature is very inaccurate. This can be seen in Figure 48 where the calculated dissociation temperature for hydrate at 0.3 MPa is 278.7 K, about 1 K greater than the expected dissociation temperature.
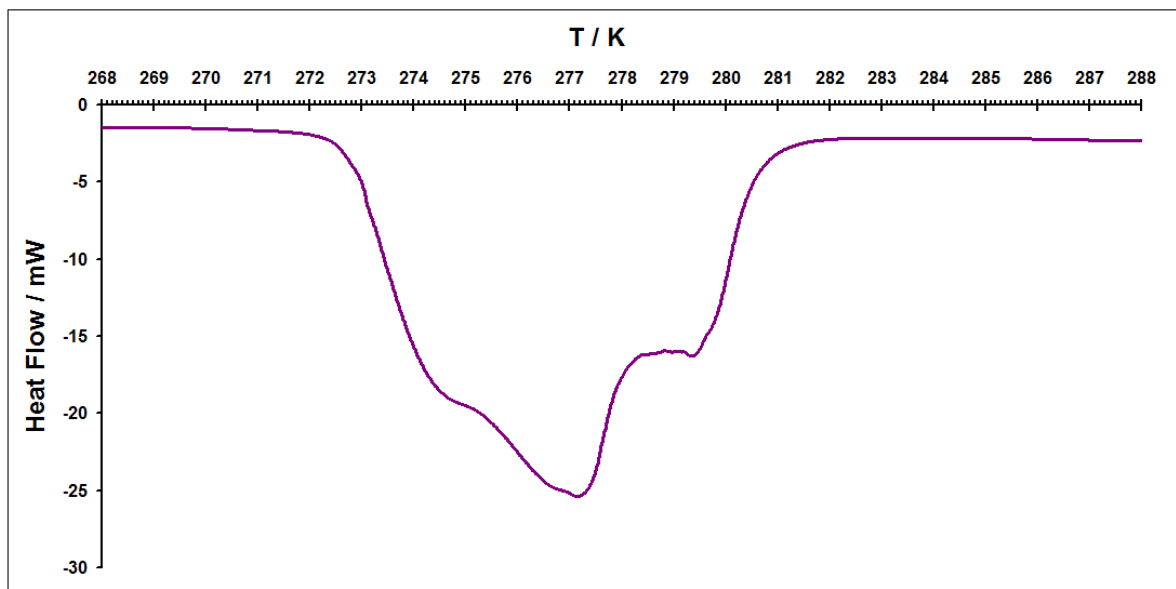
Figure 50 - DSC heat flow curve for propane system at 0.4 MPa

In this situation, the most exact measuring method is direct *p-V-T* measurements. The p-T diagram of propane + water system which is obtained by *p-V-T* measurements is illustrated in Figure 51. Hydrate formation equilibrium points are shown on blue curves and the red curve presents hydrate dissociation equilibrium data. The inflection point on the red curve which is in fact the intersection of two equilibrium curves H-V-LW and V-LW is the dissociation point of this system. In this example, the calculated hydrate dissociation temperature was 277.41 ± 0.1 K at 0.46 ± 0.015 MPa.
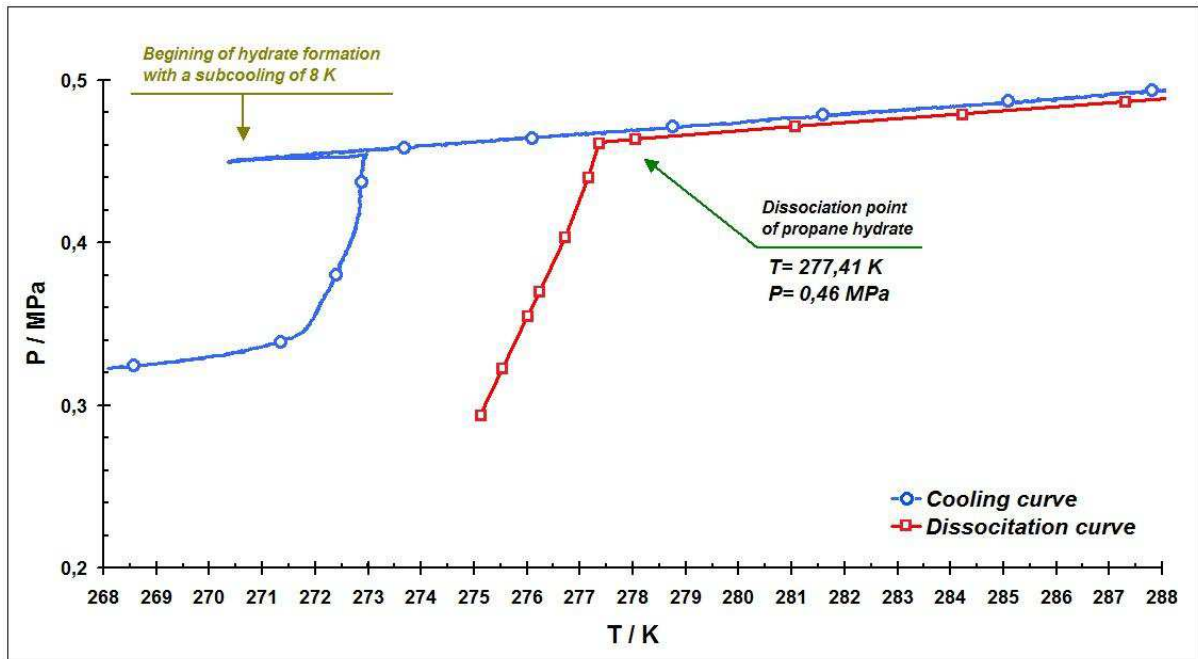
Figure 51 - P-T diagram of propane hydrate formation dissociation at 0.46 MPa obtained by p-V-T measurements

Our DSC results accompanied by p-V-T measurements, suggests the presence of an upper quadruple point Q_2 at a pressure of 0.5 MPa with a temperature of 279.65 ± 0.2 K.

b) Investigation of phase equilibrium of $C_3H_8 + H_2O$ system

Following the same approach, hydrate existence zone *i.e.* different equilibrium points on L_W-H-V and L_W-H-L_{C3H8} equilibrium curve, as well as equilibrium points on L_W-V-L_{C3H8} curve were measured. According to our results the propane hydrate formation boundary was around 279 K. To be more exact, the intersection of the mentioned equilibrium curves gave the upper quadruple point of the system to be 278.8 ± 0.5 K at pressure of 0.56 MPa. The measured data are presented in Table 22 and are compared with the data reported in literature. The range of uncertainty of our data (± 0.5 K) corresponds to twice to the standard deviation of the mean values.

Table 22 - The phase equilibria of propane + water system

Reference	T / K	P / MPa	Reference	T / K	P / MPa
LW-H-V			LW-H-V		
Miller & Strong [97]	273,2	0,165	*Deaton & Frost [98]*	273,7	0,183
	273,4	0,172		274,8	0,232
	273,5	0,176		275,4	0,27
	273,7	0,186		275,9	0,301
	273,9	0,19		277,1	0,386
	276,8	0,365	*Reamer et al. [95]*	277,2	0,4137
	277,1	0,39		275,7	0,3047
	277,2	0,393		274,3	0,2406
	277,8	0,459		274,26	0,207
	278	0,472	*Verma et al. [99]*	274,82	0,241
Kubota et al.[100]	273,25	0,172		276,37	0,331
	273,35	0,174		277,82	0,455
	273,55	0,181		278,87*	0,552*
	273,65	0,187	*Robinson & Menhta [101]*	274,26	0,207
	273,95	0,199		274,82	0,241
	274,15	0,207		276,37	0,331
	274,65	0,232		277,82	0,455
	274,85	0,239		278,87*	0,552*
	276,15	0,323	*Thakore and Holder [102]*	274,2	0,217
	276,75	0,371		275,2	0,248
	277,65	0,455		276,2	310
	278,05	0,5		277,2	0,45
	278,15	0,517		278,2	0,51
	278,35	0,542	*Mooijer-van den Heuvel et al. [103]*	275,43	0,52
	278,45	0,552		277,38	0,56
This work	277,55	0,4			
	277,51	0,46			

	278,8*	0,56*			
L_W-H-L_{C3H8}			**L_W-H-L_{C3H8}**		
Wilcox et al. [104]	278,9	0,807	*Mooijer-van den Heuvel et al. [92]*	278,71	0,643
	278,6	1,296		278,75	0,893
	278,6	1,758		278,75	1,393
	278,8	2,034		278,75	1,891
	279,2	2,902		278,78	1,893
	278,8	4,247	*Kubota et al. [100]*	278,45	0,616
	278,9	6,115		278,45	0,81
This work	278,95	0,58		278,45	0,921
	278,85	0,585	*Reamer et al. [95]*	278,8	2,0464
	278,75	0,59		278,7	1,4769
	278,85	0,594		278,6	0,684
	278,85	0,6			
L_W-V-L_{C3H8}			**L_W-V-L_{C3H8}**		
This work	279,65	0,58	*Kubota et al. [100]*	279,15	0,579
	279,95	0,585		279,85	0,59
	280,25	0,59		280,55	0,603
	280,45	0,594		280,65	0,605
	280,65	0,597		283,65	0,659
Mooijer-van den Heuvel et al. [103]	279,43	0,59			
	281,45	0,622			
	283,47	0,66			
	285,49	0,7			
	287,45	0,74			

* Upper quadruple point of propane + water system

These data are also illustrated in the form of a *p-T* diagram in Figure 52 to give a better understanding of the hydrate formation limit and the quadruple point of the system. As it can be seen in this figure, further increase on the pressure of the system, has a negligible effect on the dissociation temperature of propane hydrate. In other words, Q_2 is the limit of propane hydrate formation.
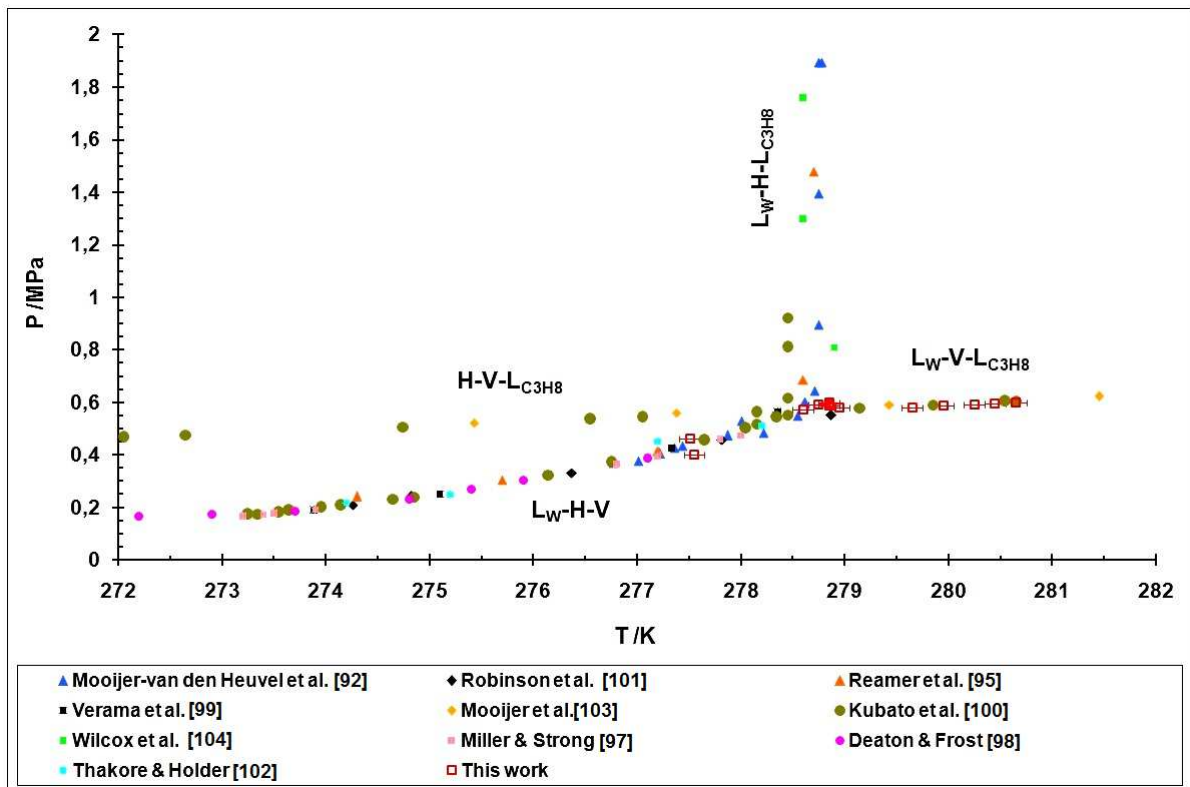
Figure 52 - The phase diagram of propane + water system

4.1.3. Hydrogen + Propane + Water system

To evaluate hydrate equilibria in the system hydrogen + propane + water firstly the phase diagram of the binary system hydrogen + propane in presence of excess water [2] must be considered. There are very few data published on hydrate phase equilibria in the binary system of hydrogen + propane [105-107]. Almost all of these data are produced under relatively low pressures *i.e.* less than 5 MPa [Figure 53] or in very high range of pressure *i.e.* more than 100 MPa.

Figure 54 presents investigation of hydrogen + propane system in a wide range of pressure to 250 MPa. As it can be seen in this figure, in the low pressure range, the decomposition curve of double hydrate of propane + hydrogen has dissociation temperatures of about 3 to 4 K greater than the pure propane hydrate. However, by increasing the pressure up to 250 MPa, the difference in dissociation temperature increases up to 20 K.

---

[2] Water is present in excess in this system and the composition of hydrogen phase is relative only to propane content.
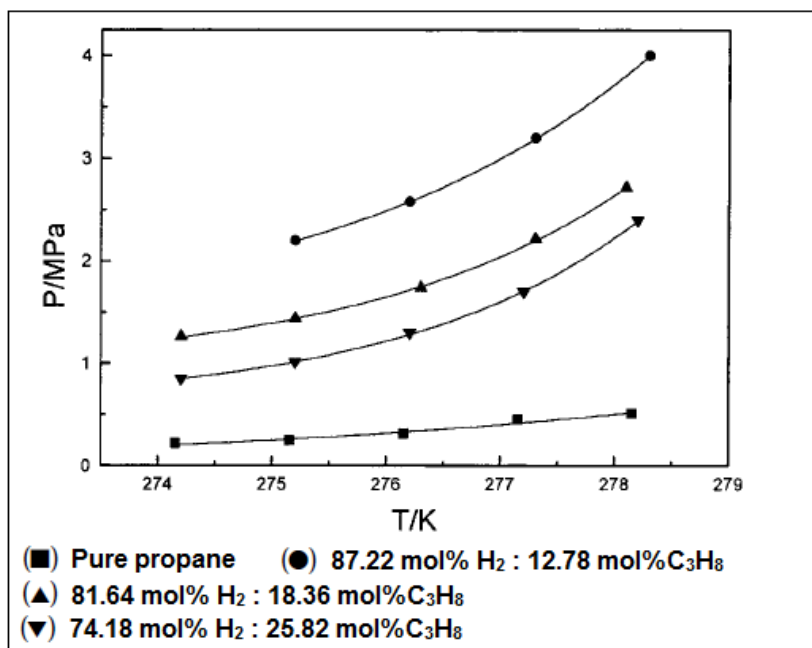
Figure 53 - Hydrate formation conditions for hydrogen + propane hydrate [92]
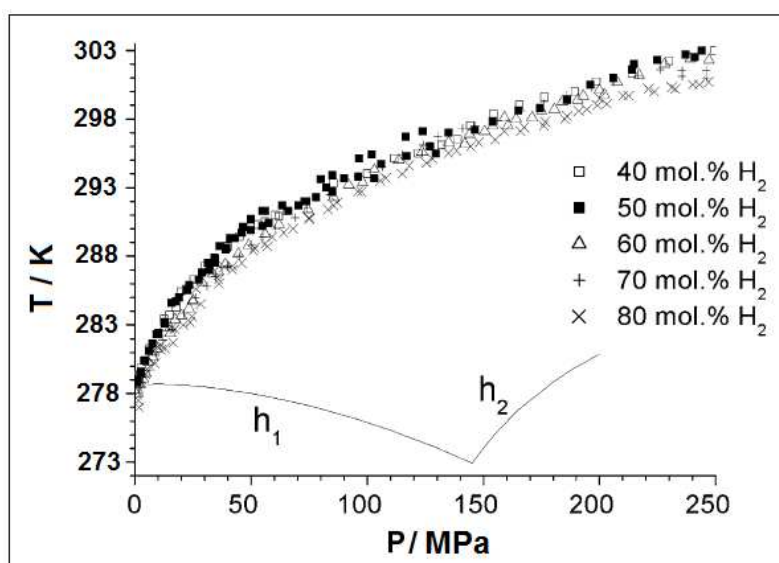
Figure 54 - Decomposition curve of propane + hydrogen propane double clathrate hydrates. h_1: cubic structure II of pure propane hydrate, h_2: propane hydrate with an unknown structure [91]

One important point investigated in this work [92] is the structure of the formed hydrate. Although both hydrogen and propane stabilize sII hydrate structures, in the case of gas mixture, the possibility of appearance of a new structure exists. Ballard et al. [90] demonstrate that for the binary system of methane + ethane in which both of the molecules form sI hydrate structure, at very high pressures and incipient ethane fractions, hydrate structure sII appears and coexists with hydrate sI. Moreover, as it can be seen on Figure 54 at pressures around 150

MPa, an unknown hydrate structure appears which can reveal the possibility of the same pattern in the binary system of propane + hydrogen. This phenomena can be interpreted as *pseudo-retrograde* [30] of propane hydrate, in which the sII hydrate dissociates by pressurization at a constant temperature.

Although Skiba et al [106] have not presented the *x*-T phase diagram of the system, they have reported that the temperature-composition projection of their results at a constant pressure, demonstrates that the liquids curves are in the form of a cupola with flattened top, proving that only one gas hydrate is formed in the system. Moreover, the results of their Raman spectroscopy confirm the formation hydrate II structure.

a) Investigation of H_2 + C_3H_8 + H_2O system

In our investigation four H_2-C_3H_8 compositions with propane molar fraction of 10%, 5%, 3%, 1% in a pressure range of 4 to 40 MPa was studied. Prior to the experimental investigations, the phase envelope of the hydrogen + propane system is obtained by *Simulis Thermodynamic* software [Figure 55]. By investigating this phase envelope one can see that at pressures above 15 MPa no hydrocarbon in vapour phase exists and therefore no phase transition happens. Accordingly for our DSC measurements at pressures above 20 MPa no peak for pure hydrocarbon phase transition is expected.
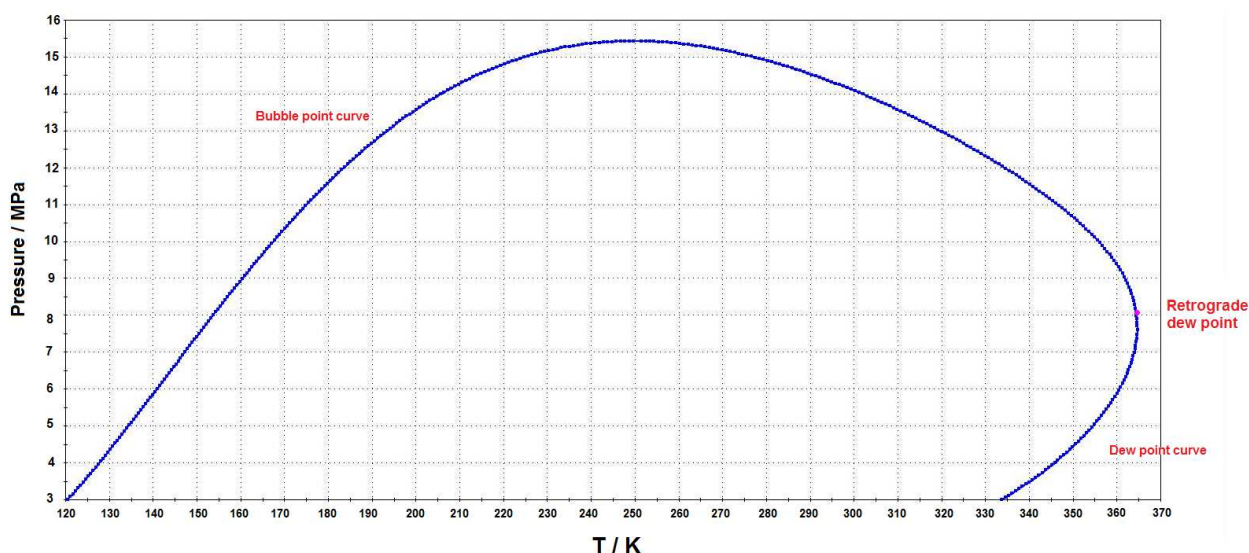
Figure 55 - Phase envelope of the system Hydrogen + Propane

An analogy with the phase envelope of a typical natural gas [Figure 56] shows that in the moderate pressure and temperature range, hydrate locus intersects the phase equilibrium. In

this domain, the only phase transition that is observed is hydrate formation /dissociation. Outside this phase envelope, in pressures above the bubble point, all the hydrocarbon fraction exist in the liquid form and again no phase transition happen.
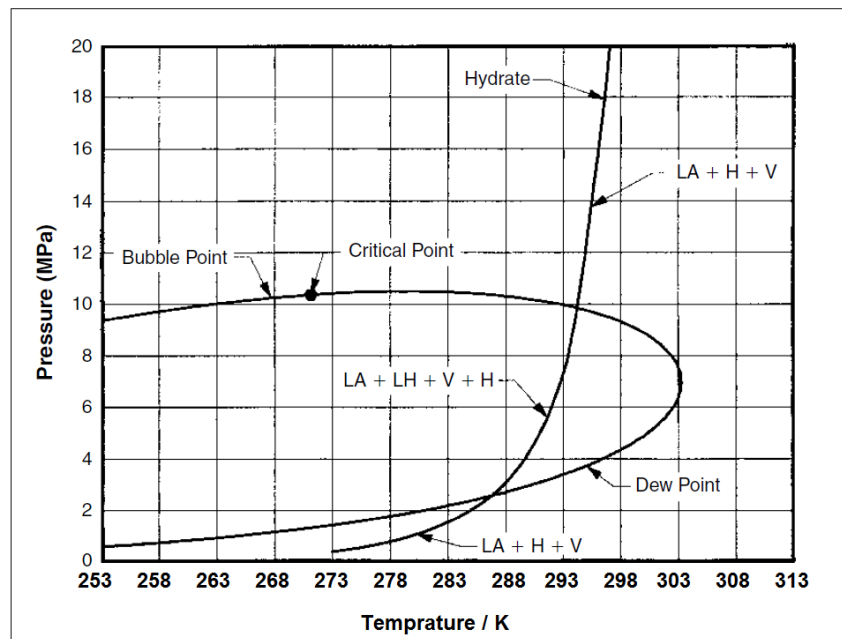
Figure 56 - Phase diagram of natural gas with a composition of methane: 70.85 mol%, ethane 11.34 mol%, propane: 6.99 mol%, isobutane 3.56 mol%, and n-butane: 4.39 mol% and carbon dioxide: 2.87 mol% [31]

The obtained heat flux curves for the H_2-C_3H_8 system with a molar fraction of 1 mol% of propane is shown in Figure 57. The heat flux curve obtained under pressure of 5 MPa shows the existence of two series of peaks. The right peak, in the temperature range of 280 to 282 K is attributed to the isotherm phase transfer of hydrocarbon component in the binary system of hydrogen + propane. This is in accordance with the phase envelope presented in Figure 55 for pressures below the dew point pressure.

The peak on the left basically consists of two peaks: one eutectic melting around 273 K and one progressive dissociation of hydrate around 273-277K. As it can be seen these two do not have a good resolution. This is because of the relatively small amount of the hydrate formed with resulted in a small peak. Therefore, this small hydrate peak is mixed with the big peak corresponding to eutectic phase transition of the solid phase. As a result measuring the dissociation temperature of hydrate seems impossible. This is the case for most of the samples and therefore, most of the dissociation temperatures had to be confirmed by p-V-T measurements in this section.
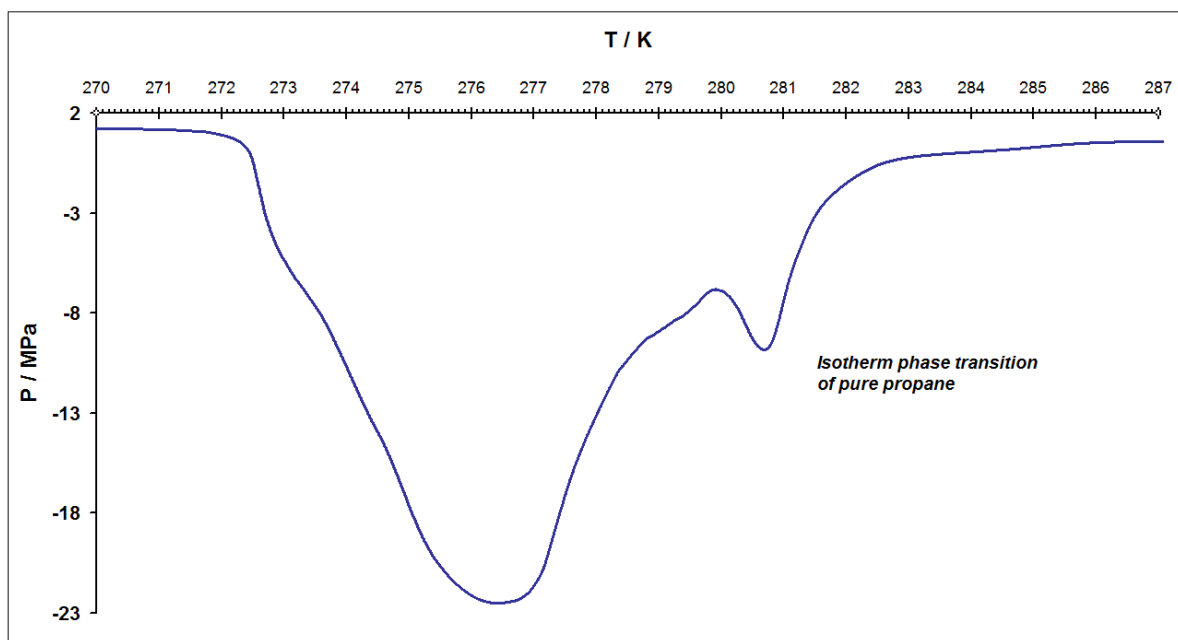
Figure 57 - DSC heat flux curves of the 1 mol% fraction of propane in the propane + hydrogen - water system under pressure of 5 MPa

The resulting dissociation temperatures of hydrates measured by DSC and the reactor are presented in Table 23. These results are represented in Figure 58 in a form of a P-T phase diagram, to compare the effect of pressure and mole fraction of propane in stability of hydrate phase.

Two conclusions can be made from these results. First of all, addition of propane has a great stability effect on sII hydrate structure in comparison to pure hydrogen hydrate of the same structure. Secondly, all the phase equilibrium temperatures in the propane + hydrogen system increase with the increase of propane mole fraction in the gas mixture. The interesting point in this figure is that at propane molar fractions of 5 mol% and 10 mol% propane + hydrogen hydrate is even more stable than pure propane hydrate. This indicates that H_2 molecules enclathrate in the hydrate formed from hydrogen + propane + water which results in an increase in the stability of the hydrate. As mentioned earlier, propane + hydrogen mixture are used in industrial burners. For the development of hydrate as a storage medium for this mixture, further quantitative investigations are needed to measure the amount of gas stored in the hydrate, composition of hydrate phase and the calorific capacity of the storage system.

125

Table 23 - The dissociation temperatures of propane + hydrogen hydrates as a function of gas composition and pressure

y_{H2} /mol%	Total pressure of system / MPa	Partial pressure of hydrogen / MPa	Eutectic melting temperature of ice / K	Dissociation temperature of hydrate / K
0.90	4	3.6	272.55 ± 0.1	279,50 ± 0.5
0.90	5	4.5	272.55 ± 0.1	280,13 ± 0.5
0.95	4	3.8	272.55 ± 0.1	279,75 ± 0.5
0.95	5	4.75	272.55 ± 0.1	280,05 ± 0.5
0.95	10	9.5	272.45 ± 0.1	280,10 ± 0.5
0.97	4	3.88	272.75 ± 0.1	274,30 ± 0.5
0.97	5	4.85	272.35 ± 0.1	276,15 ± 0.5
0.97	10	9.7	272.15 ± 0.1	277,65 ± 0.5
0.97	20	19.4	271.55 ± 0.1	278,45 ± 0.5
0.99	5	4.95	272.35 ± 0.1	275,55 ± 0.5
0.99	10	9.9	272.15 ± 0.1	276,50 ± 0.5
0.99	20	19.8	271.05 ± 0.1	277,20 ± 0.5
0.99	40	39.6	269.55 ± 0.1	280,40 ± 0.5
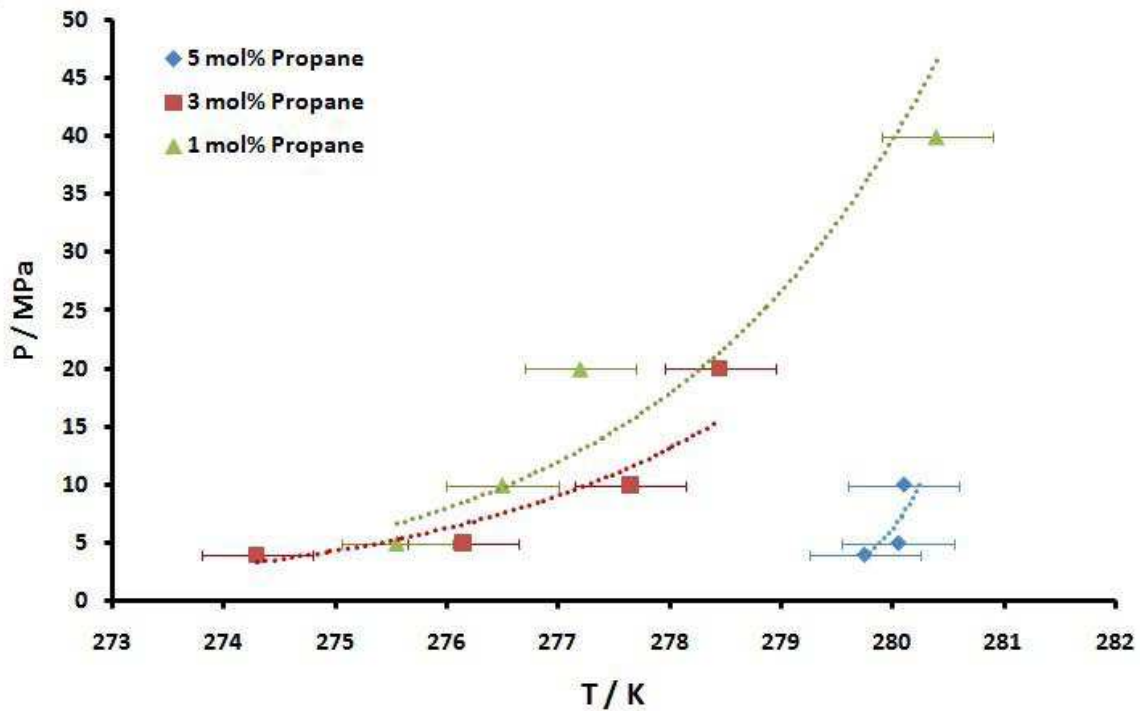
Figure 58 - P-T phase diagram of Propane + Hydrogen - Water system under different pressures for different component compositions

126

It must be noted that, further p-V-T investigations for measuring the amount of hydrogen stored in this system was not successful. Our ROLSI sample is not effective for sampling low pressures of gas (*i.e.* less than 1 MPa). In all of our experiments, propane partial pressure in the mixture is less than 1 MPa and therefore in spite of several sampling experiments, no peak corresponding to propane was detected on the output chromatogram.
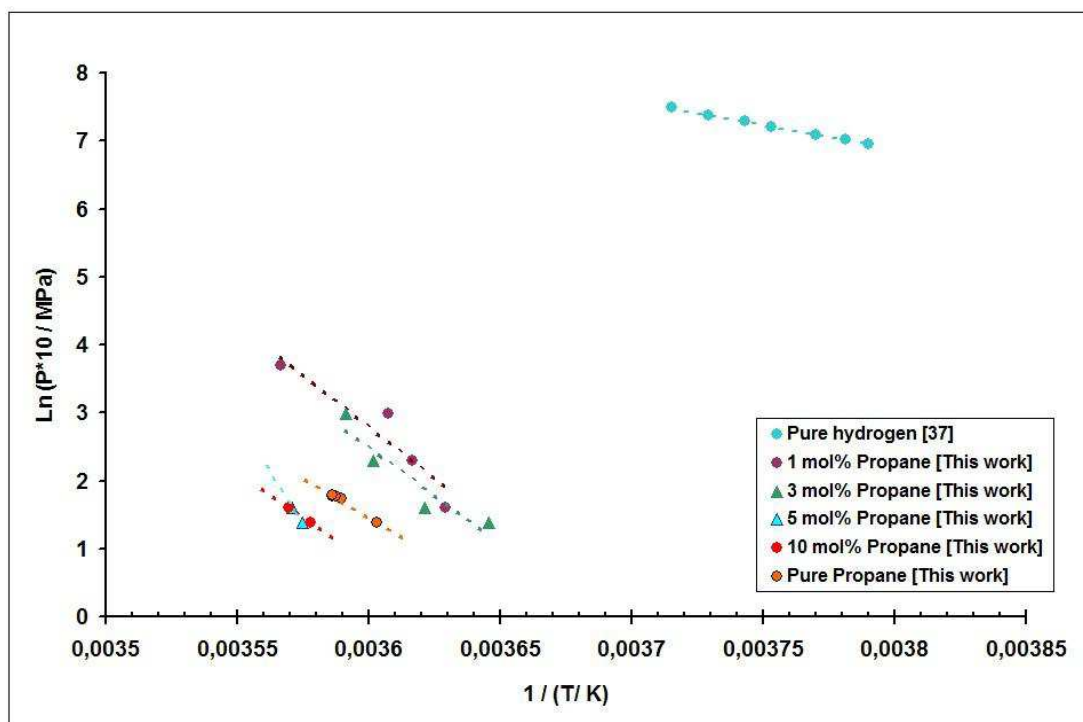
Figure 59 - Clapeyron equation presentation of Propane - Hydrogen hydrate dissociation

4.2. Carbon dioxide – Hydrogen system

4.2.1. Introduction

The emission of carbon dioxide from the burning of fossil fuels is known as major contributor to the global warming and climate change. Particularly, one third of the CO_2 emissions worldwide are being produced by fossil fuel electric power [108].

A promising solution to reduce greenhouse gas emissions is CO_2 capture and storage. CO_2 capture can be accomplished through two methods: either carbon can be removed before the fuel's combustion (pre-combustion capture) or CO_2 can be removed from the flue gas (post-combustion capture). In post-combustion processes the CO_2 has to be separated from the flue gas which consists mainly of a CO_2/N_2 mixture whereas in pre-combustion processes one has to consider CO_2 separation from CO_2/H_2 mixtures [109]. The recent, IGCC[3] power plants propose new potentials for CO_2 capture by converting the gas from the gasifier into a stream of H_2 and CO_2 through a shift reaction [110]. After separation, the CO_2 can be captured and the remaining H_2 could be used as an energy carrier [111]. In this regard, the separation of CO_2 from CO_2/H_2 gas mixtures plays a major role in chemical industry. The objective of this section is the investigation of equilibrium data for hydrate clathrate formed under pressure of CO_2/H_2 mixtures and the efficiency of a hydrate separation unit in gas separation.

4.2.2. A discussion on the phase diagram of H_2-CO_2-H_2O

Prior to investigations on H_2-CO_2 hydrates, phase equilibrium of pure CO_2 hydrate has been investigated [112-130]. Carbon dioxide is known to form hydrate structure sI at moderate pressure between 1 to 4 MPa. The equilibrium data of CO_2 hydrates, and its comparison with pure hydrogen equilibrium [Table 24] shows that in a mixture of hydrogen and carbon dioxide, carbon dioxide forms a more stable hydrate structure and therefore it is the dominant guest molecule (hydrate former). These data reveals that in a H_2-CO_2 gas mixture carbon dioxide is more likely to enter the clathrate hydrates cavities by forming sI clathrate hydrates leaving a rather purified H_2 gas stream. Therefore, one may assume that presence of H_2 in the gas mixture has only an impact on the total pressure of the system but not on the nature and the character of the formed hydrates. The validity of this assumption will be studied in the next part, by comparing the phase equilibrium data of CO_2-H_2 and pure CO_2.

---

[3] Integrated Coal Gasification Cycle

Similar to propane, carbon dioxide has also a relatively high critical temperature [Table 24] which causes the appearance of a second quadruple point in its phase diagram at 283.1 K and 4.50 MPa. In our investigations, hydrate equilibrium data is measured in a pressure range of 4 to 14 MPa for a 50-50mol% gas mixture. Accordingly, in interpolating the DSC heat flux curves, one must locate the thermodynamic state of the system on the P-T phase diagram of the system. For instance, Figure 61 presents the resulting DSC heat flux curve of the CO_2-H_2-H_2O system under a pressure of 4 MPa. As it is expected, three peaks are detectable here. One isothermal peak (left) resulted from eutectic melting of the solid phase. One isothermal peak (middle), corresponding to phase transition of pure carbon dioxide under 4 MPa pressure. And finally a small progressive peak, spread in a wide temperature range of (278-282 K) corresponding to the progressive dissociation of hydrates. As the amount of the hydrates formed is small, the hydrate peak does not have a good resolution which makes confirming the nature of these peaks difficult. But as it was discussed earlier, by considering the fact that our operational pressure in this example is lower than the second quadruple point (Q_2) of corresponding peak to the phase transition of pure carbon dioxide must be located right after the eutectic peak of the solid phase.

Table 24 - Phase equilibrium data of pure carbon dioxide hydrate and pure hydrogen hydrate

$CO_2 - H_2O$		$H_2 - H_2O$	
$H - L_W - V$ [113]		$H - L_W - V$ [45]	
T / K	P / MPa	T / K	P / MPa
277.2	2.04	269.15	178.41
279.2	2.58	268.15	160.76
280.9	3.22	267.15	146.80
281.9	3.68	266.45	134.97
283.1	4.50	265.25	120.75
$H - L_W - L_{CO2}$ [115]		264.45	111.38
283.2	4.5		
284.2	13		
285.2	24.3		
286.2	37.2		
287.2	52.2		
288.2	69.6		
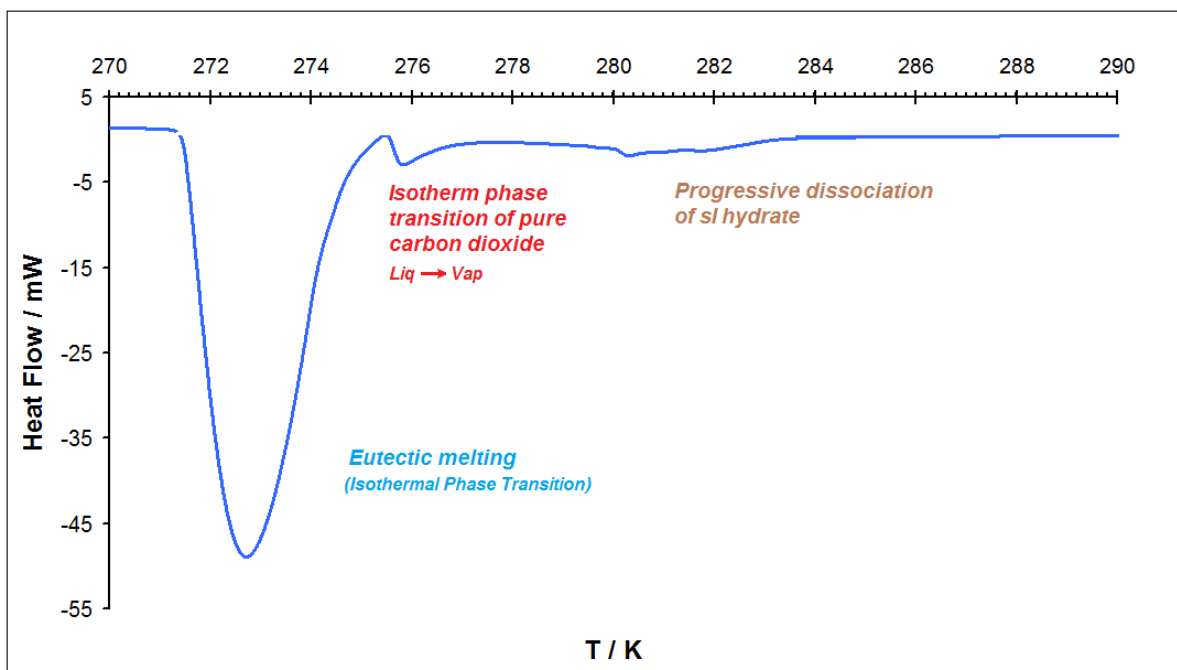
Figure 60 - DSC heat flux curve for H$_2$-CO$_2$-H$_2$O system at pressure of 4 MPa

This can be seen in Figure 62 where the schematic presentation of CO$_2$-H$_2$O phase diagram is shown. As it can be seen here, under a constant pressure phase transition, by increasing the temperature, the red arrow (a) firstly crosses the I-L$_W$-H equilibrium line (eutectic melting). By continuing heating, the arrow (a) crosses the H-L$_W$-L$_{CO2}$ curve which corresponds to isothermal phase transition of pure carbon dioxide (L$_{CO2}$ →V). Subsequently the last equilibrium line that is crossed is the H- L$_W$-V which corresponds to the progressive dissociation of hydrates.
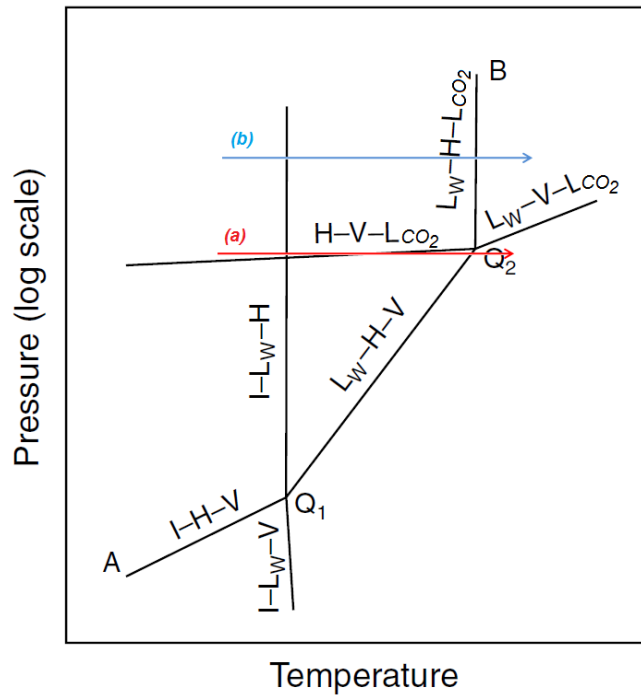
Figure 61 - Schematic presentation of P-T phase diagram of CO₂-H₂O system [30]

Figure 64, presents another case, which correspond to the heat flux curve of the system H_2-CO_2-H_2O under a pressure of 7 MPa (Higher than Q_2 pressure). In this diagram, as it is expected the isothermal peak of pure carbon dioxide, appears on the right side of the progressive peak of hydrate dissociation[4].
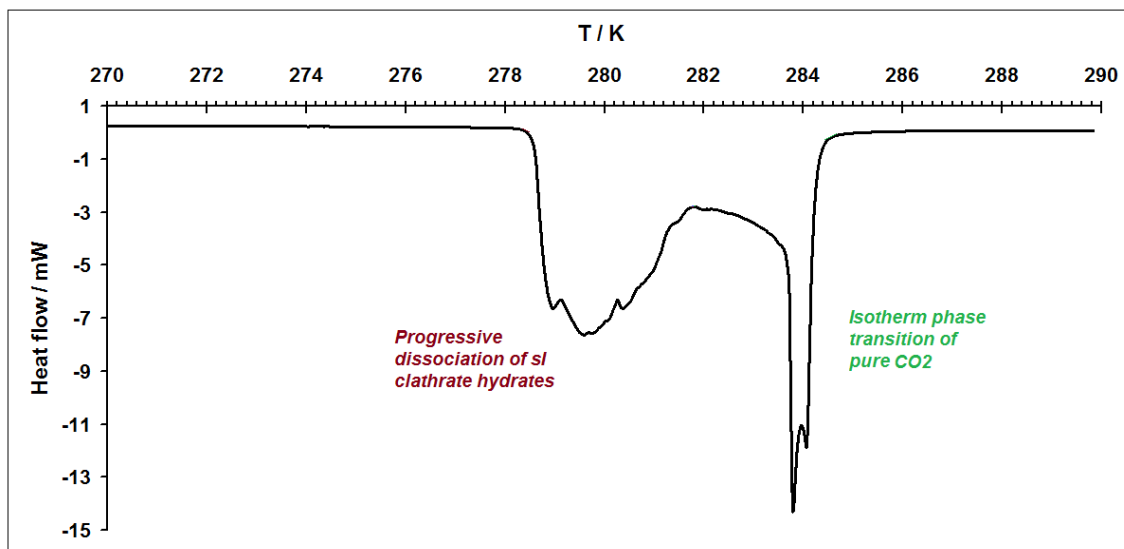
Figure 62 - DSC heat flow curve of H₂-CO₂-H₂O system under pressure of 7 MPa

---

[4] It is noticeable that in this example, all of the excess water is converted into hydrates and therefore no peak for eutectic melting of the solid phase exists in the corresponding heat flux curve.

This can be understood by following the blue arrow (b) on Figure 62. By increasing the temperature, after crossing the I-L_W-H equilibrium curve (eutectic melting) the blue arrow (b) will cross the L_W-H-L_{CO2} (isotherm phase transition of CO_2). All over this work, the same pattern has been applied for exploiting the dissociation temperature of CO_2-H_2-H_2O hydrate.

4.2.3. Investigation of H_2-CO_2-H_2O phase equilibrium

Table 25 presents the resulting dissociation temperature of hydrates obtained from DSC measurement with an accuracy of $\pm$ 0.5 K.

Table 25 - Phase Equilibria data of H_2-CO_2-H_2O system

Pressure / MPa	Hydrate dissociation temperature / K	Isotherm phase transition of carbon dioxide / T
H-V-L_{HC}		
4	275.65	-
L_W-H-L_{HC}		L_W-V-L_{HC}
5	276.75	281.2
6	278.55	282.35
7	279.35	283.65
8.5	281.35	283.67
140	283.75	-

These results are compared in Figure 64 with other published data for a 50-50 mol% mixture of CO_2-H_2 as well as the phase equilibrium data of pure hydrogen hydrate and pure carbon dioxide hydrate. As it can be seen in this diagram, addition of carbon dioxide is in favour of hydrate stabilization in comparison to pure hydrogen hydrate. However, this figure shows that pure CO_2 is more stable than a H_2-CO_2 gas mixture, both in dissociation temperature and formation pressure.

In order to investigate the effect of pressure and the possibility of hydrogen enclathration in hydrate cavities, partial pressure of CO_2 in 50-50 mol% gas mixture is compared with the pure CO_2 data.
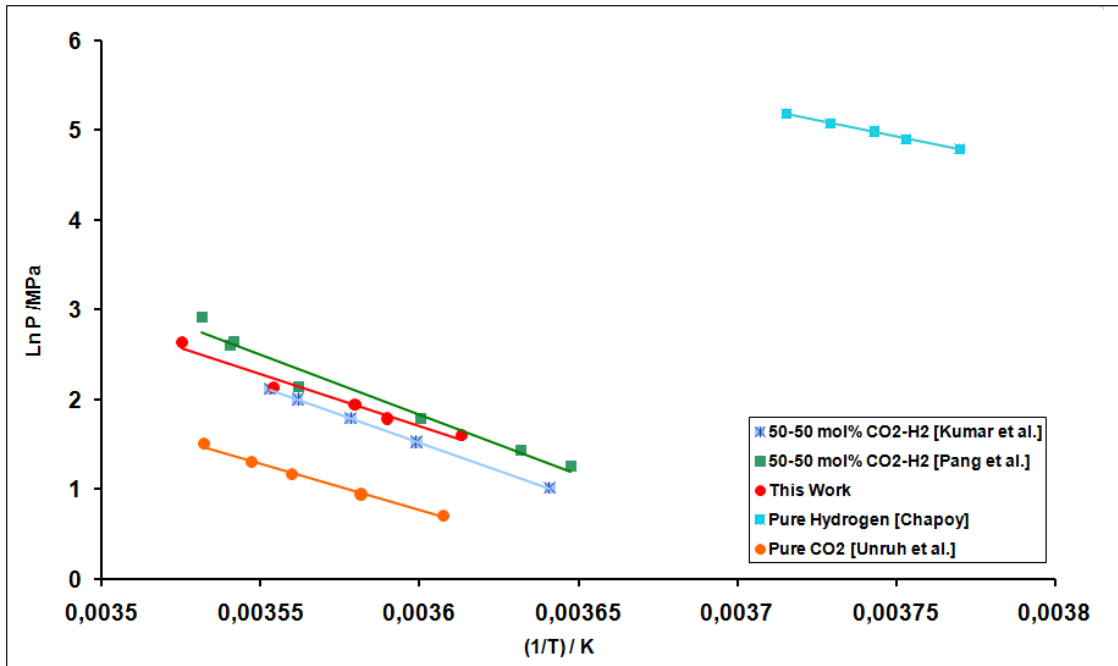
Figure 63 - Comparison of equilibrium data of CO_2, H_2 and H_2-CO_2 system
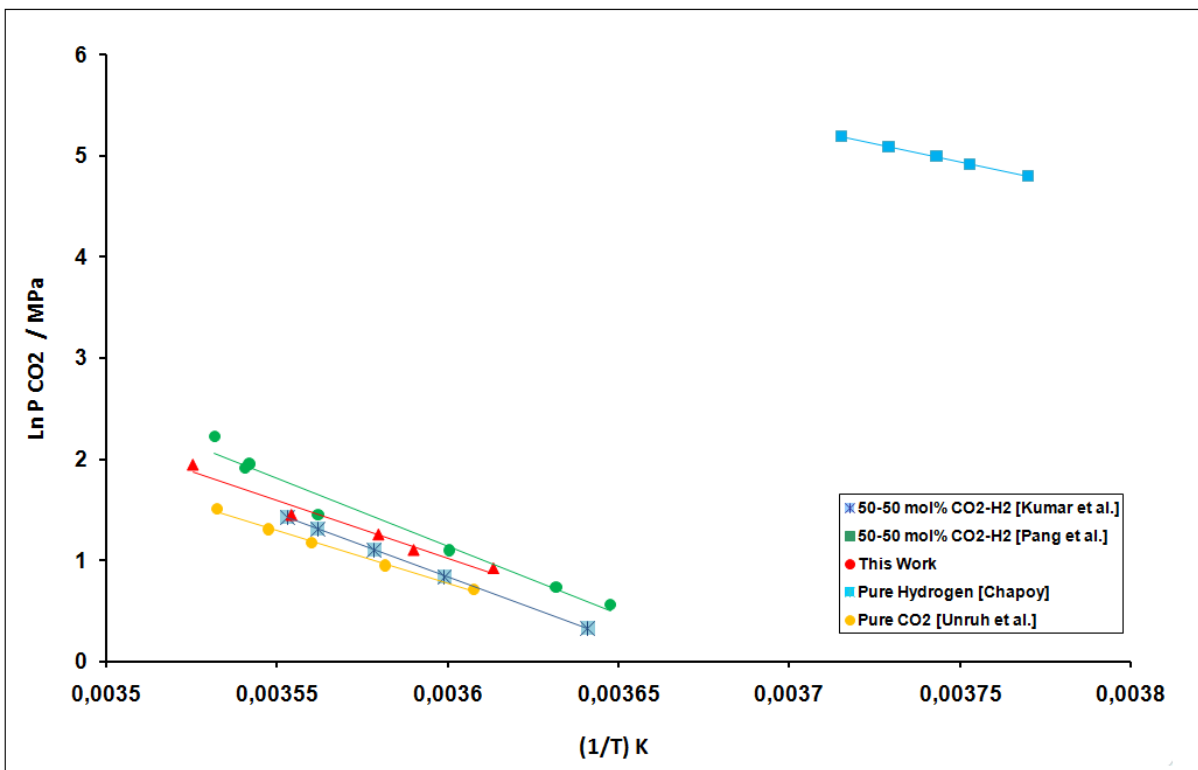
Figure 64 - Comparison of equilibrium data of CO_2, H_2 and partial pressure of CO_2 in the H_2-CO_2 system

Figure 64 illustrates the result of this comparison. According to this Clapeyron diagram, after removing the effect of H_2 pressure, the resulting lines are approximately superposed and are located in the same pressure range, this reveals that hydrogen molecules do not enter the hydrate structure and only carbon dioxide hydrates are formed. This fact is specially observed

in lower pressures, which provide convenient operational conditions for an industrial application of this method.

4.2.4. Composition analysis of CO_2-H_2O hydrate

Using p-V-T measurements, composition of a sample 50-50 mol% of CO_2-H_2 gas mixture was analyzed after hydrate formation in order to investigate the efficiency of CO_2 capture.

Experimental determination of the compositions of the existing phases in equilibrium with gas hydrate by the p-V-T method is usually not an easy procedure. Some major technical inconveniences are:

- Long metastable periods
- Difficulties of sampling without disturbing the thermodynamic equilibrium
- Difficulties of visibility inside the reactor,
- Blockage of sampling valves, etc.

For this purpose, an isochoric equilibrium cell which is a combination of precise and accurate measuring devices such as ROLSI and the visual observation of the gas hydrate formation and phase behaviour is used.

Table 26 presents the results of this measurement. It must be noted that all of the chromatography sampling were done at 272 K. Due to absence of characterization method, the composition of gases in the hydrate phase is not known, and therefore, formation of sII hydrate structure is not known. According to this table, the separation efficiency increases from 20% at 5.3 MPa to 45% at 8.4 MPa. Although an increase in the total pressure of the system may reveal the possibility of hydrogen enclathration, which has been discussed earlier in section 4.2.3., these results demonstrates that pressure increase is in favour of CO_2 separation. These results can be used for a further simulation of a CO_2/H_2 separation unit, in order to calculate the number of theoretical separation plates, and the number of separation units. For this purpose a more complete investigation of the $H_2 - CO_2 - H_2O$ system with variable initial H_2/CO_2 ratio and at variable equilibrium temperature would be required.

Table 26-Composition analysis of vapor phase in a mixture of CO_2 - H_2- H_2O

Dissociation pressure/ MPa	Initial composition / mol%	Final composition / mol%
5,29	50.4	40.1
5,54	54.2	43.3
6,48	50.4	34.9
6,23	51.0	41.6
8,22	51.2	31.0
8,41	50.4	27.6

Conclusions and perspectives

The main objective of this thesis was to carry out thermodynamic investigations on phase equilibria of hydrogen clathrate and semi clathrate hydrates with the final aim of H_2 storage and separation. In this regard, the following steps were proceeded and with the eventual subsequent conclusions:

1. A brief introduction on hydrogen and its properties were presented. Different production methods of hydrogen in industrial scale were introduced and different storage methods were explained. Hydrogen storage capacity & economy in conventional storage methods were compared with new innovative techniques.

2. A brief literature review on gas hydrates was done, including presentation of their physical and chemical properties, their different existing structures, effect of promoters on their stability and different features with the regard to hydrogen hydrates.

3. Two main experimental methods were applied for investigating phase equilibrium of clathrate and semi-clathrate hydrates and their storage capacity. These experimental methods are a combination of Differential Scanning Calorimeter (DSC) and p-v-T measurements. DSC is one of the most applied techniques in thermodynamic of phase behaviour. In this work, DSC was principally used for investigating the dissociation temperature of hydrates under different gas pressures. Its sensitivity and fastness, accompanied by its large range of temperature and pressure makes it a proper technique for investigating phase equilibrium of clathrate hydrates.

4. Determination of gas storage in the hydrates is of a great significance to design the H_2 storage systems. For this purpose p-v-T measurements were carried out by using a high pressure (40 MPa) isochoric reactor. p-v-T measurements are the basic of all experimental procedures in thermodynamic where three main thermodynamic

parameters *i.e.* Pressure, Volume and Temperature can be measured. In this work, p-v-T measurements were undertaken for investigating the hydrogen storage on semi-clathrate systems $TBPBH_4$ and TBAOH. Moreover, by coupling the isocbaric reactor with Gas Chromatograph (GC) molar composition of gas phase for the CO_2-H_2 system was investigated.

5. The phase behaviours in the system G-$TBPBH_4$-H_2O (G = H_2 or N_2) were studied. It was demonstrated, that $TBPBH_4$ can be used as a hybrid hydrogen storage material. The solutions of the new obtained $TBPBH_4$ by reacting of the $NaBH_4$ and TBPB were found to form hydrates at low temperature. Using the DSC measurements the dissociation (p, T) points of mixed hydrates at various salt concentrations were determined. The results show that the new additive has very efficient stabilizing effect on the hydrate structure, the dissociation temperatures ranging from 280 to 295 K, depending on the gas, in a pressure range of 0 to 40 MPa. The 1.26 wt. % of the chemically stored hydrogen was investigated using the volumetric analysis of the hydrogen, released by hydrolysis of the $TBPBH_4$ compound in the presence of acetic acid. The influence of the gas nature on the hydrate stability was investigated. The higher stabilization effect of nitrogen comparing to hydrogen was discovered.

6. The semi-clathrate system of hydrogen + tetra-n-butylammonium hydroxide + water was studied for the first time. The phase diagram of this system is presented in a concentration range of 0.83-3.23 wt% and temperature range of 273.15 K to 303.15 K. The phase equilibrium data collected using differential scanning calorimeter (DSC) show the capacity of hydrogen to stabilize one of the hydrate structures and therefore occupy the semi-clathrate cavities. By using a high pressure reactor cell and the help of atomic absorption analysis, hydrogen storage capacity of the system was measured to be 0.35 wt% at 10 MPa and 0.47 wt% at 20 MPa. This was compared with hydrogen storage capacity of some common hydrate structures. Although the storage capacity of the system is not high, however, considering the favourable thermodynamic conditions of formation and dissociation of TBAOH hydrates, and the absence of any volatile promoter, it may reveal to be a good replacement for conventional storage methods for in-place storage of hydrogen

7. Phase equilibrium of the system $C_3H_8+H_2O$ was investigated. The resulting equilibrium points obtained by DSC measurements are compared with literature data. Propane + H_2O have two quadruple points; a lower one, and a higher quadruple point which is due to its relatively high critical temperature. This second quadruple point presents the highest temperature for hydrate equilibrium above which no hydrate can be formed or exist.

8. The stabilizing effect of propane on hydrogen hydrate was studied by investigating H_2-C_3H_8-H_2O system, with three different gas mixtures compositions: 1 mol%, 3 mol% and 5 mol% propane. It was shown, at very low propane concentrations that hydrate dissociation temperature increases drastically. This is due to the enclathration of large hydrate cavities by propane molecules which results in hydrate stability. Moreover, it was seen that by increasing propane concentration in the system, hydrate stability continues to increase. Due to the low partial pressure of propane in the system, chromatographic peaks corresponding to propane did not have enough resolution and therefore further investigation on gas phase composition and hydrogen storage capacity, was unsuccessful.

9. CO_2-H_2-H_2O system was the last system studied. The stability effect of carbon dioxide was studied by comparison of equilibrium data of a CO_2-H_2 hydrate (50-50mol% gas composition) with pure carbon dioxide hydrate and pure hydrogen hydrate. These investigations were proceeded by gas molar composition analysis before and after hydrate formation. Due to the absence of information of gas composition in hydrate phase, investigation could not go further to analysis the performance of the system as separation unit.

Perspectives

1. Evolution of hydrogen storage investigation in clathrate hydrates, demonstrates that hydrogen storage capacity is limited to 5 wt% which is reachable only at very severe conditions. Although this storage capacity and these severe formation conditions are not proper for mobile application of hydrogen storage, they reveal potentials for in-place hydrogen storage technologies. In this field of application, still more economic studies are needed to evaluate the storage technology in industrial scale.

2. Application of hydrates in separation processes seems to have a more clear perspective in the future. In this respect, more profound experimental investigations on CO2-H2-H2O system, by analysing hydrate phase and aqueous phase would produce fruitful results. It should be noted these experimental investigations, accompanied by modelling of the system will give a useful perspective of the applicability of the system and prediction of its behaviour under a wider range of compositions and thermodynamic conditions.

References

1   PERRY's Chemical Engineers Handbook, 8th Edition, McGraw-Hill (2008)

2   Handbook of Hydrogen Storage, Edited by Michael Hircher, Wiley-VCH, ISBN 978-3-527-32273-2

3   Schlapbach, L., Züttel, A. "Hydrogen-storage materials for mobile applications", Nature Vol. 414 (2001) PAGES

4   Ramachandran, R., Menon, R. K. "An overview of industrial use of hydrogen", International Journal of Hydrogen Energy, Vol. 23, No.7 (1998) 593-598

5   Zhou, L. "Progress and problems in hydrogen storage methods", Renewable and Sustainable Energy Reviews, Vol. 9 (2005) 395-408

6   Di Profio P., Arca S., Rossi F., Filipponi M. "Comparison of hydrogen hydrates with existing hydrogen storage technologies: Energetic and economic evaluations", International Journal of Hydrogen Energy, Vol. 34 (2009) 9173-9180

7   Fierro, V., Szczurek, A., Zlotea, C., Mareche, J. F., Izquierdo, M. T., Albiniak, A., Latroche, M., Furdin, G., Celzard, A. "Experimental evidence of an upper limit for hydrogen storage at 77 K on activated carbons" Carbon, Vol.48 (2010) 1902-1911

8   Chahine, R., Bose, T. K. "Low-pressure adsorption storage of hydrogen", International Journal of Hydrogen Energy, Vol.19 (1994) 161-164

9   Panella, B., Hircher, M., Roth, S. "Hydrogen Adsorption in Different Carbon Nanostructures" Carbon, Vol.43 (2005) 2209-2214

10 Ye Y., Ahn C. C., Witham C., Fultza B., Colbert D., Smith K. A., Smalley R. E. "Hydrogen adsorption and cohesive energy of single-walled carbon nanotubes" Applied Physics Letters, Vol. 74 (1999) 2307-2309

11 Fitzgerald S. A., Yildirim T., Santodonato L. J., Neumann D. A., Copley J. R. D., Rush J. J., Trouw F., "Quantum dynamics of interstitial H_2 in solid C-60" Physical Review B, Vol.60 (1999) 6439-6451

12 Fitzgerald S. A., Forth S., Rinkoski M., "Induced infrared absorption of molecular hydrogen in solid C-60" Physical Review B Vol. 65, (2002), 140302 – 140304

13   Talyzin A. V., Klyamkin S., "Hydrogen adsorption in C60 at pressures up to 2000 atm" Chemical Physics Letters, Vol.397 (2004) 77-81

14   Talyzin A. V., Jacob A., "Hydrogen adsorption by ball milled C-60" Journal of Alloys and Compounds, Vol.395, (2005) 154-158

15   Weitkamp J., Fritz M., Ernst S. "Zeolites as media for hydrogen storage" International Journal of Hydrogen Energy, Vol. 20 (1995) 967-970

16   Langmi H.W., Book D., Walton A., Johnson S.R., Al-Mamouri M.M., Speight J.D., Edwards P.P., Harris I.R., Anderson P.A. "Hydrogen Storage in Ion-exchanged Zeolites" J. Alloys and Compounds, Vol. 404, (2005) p 637-642.

17   Furukawa H., Ko N., Go Y. B., Aratani N., Choi S. B., Choi E., Yazaydin A. O., Snurr R. Q., O'Keeffe M., Kim J., Yaghi O. M. "Ultrahigh Porosity in Metal-Organic Frameworks" Science, Vol. 329 (2010) 424-428

18   Rosi N. L., Eckert J., Eddaoudi M., Vodak D. T., Kim J., O'Keeffe M., Yaghi O. M. "Hydrogen Storage in Microporous Metal-Organic Frameworks" Science, Vol.300 (2003) 1127-1129

19   Dailly A., Vajo J. J., Ahn C. C. "Saturation of Hydrogen Sorption in Zn Benzenedicarboxylate and Zn Naphthalenedicarboxylate" Journal of Physical Chemistry B, Vol. 110 (2006) 1099–1101

20   Panella B., Hirscher M., Pütter H., Müller U. "Hydrogen Adsorption in Metal–Organic Frameworks: Cu-MOFs and Zn-MOFs Compared" Advanced functional Materials, Vol. 16, Issue 4, (2006) 520–524

21   Wong-Foy A. G., Matzger A. J., Yaghi O. M. "Exceptional H_2 Saturation Uptake in Microporous Metal−Organic Frameworks" Journal of the American Chemical Society, Vol.128 (2006) 3494–3495

22   Zaluska A., Zaluski L., Ström–Olsen J. O. "Nanocrystalline magnesium for hydrogen storage", Journal of Alloys and Compounds, Vol.288 (1999) 217-225

23   Grochala W., Edwards P. P. "Thermal Decomposition of the Non-Interstitial Hydrides for the Storage and Production of Hydrogen", Chemical Review, Vol. 104 (2004) 1283−1315

24 Züttel A., Wenger P., Rentsch S., Sudan P,. Mauron P. Emmenegger C. "LiBH$_4$ a new hydrogen storage material", Journal of Power Sources, Vol.118 (2003) 1–7

25 Urgnani J., Torres F.J., Palumbo M., Baricco M., "Hydrogen release from solid state NaBH$_4$" International Journal of Hydrogen Energy, Vol.33 (2008) 3111– 3115

26 Orimo S., Nakamori Y., Züttel A. "Material properties of MBH4 (M = Li, Na and K)" Materials Science and Engineering B, Vol.108 (2004) 51–53

27 Chłopek K., Frommen C., Léon A., Zabara O., Fichtner M. "Synthesis and properties of magnesium tetrahydroborate, Mg(BH$_4$)$_2$" Journal of Material Chemistry, Vol. 17 (2007) 3496-3503

28 Ronnebro E., Majzoub E.H. "Calcium borohydride for hydrogen storage: Catalysis and reversibility" Journal of Physical Chemistry B, ol.111 (2007) 12045-12047

29 Schlesinger H. I., Brown H. C., Hyde E. K. "New developments in the chemistry of diborane and the borohydrides. VII. The preparation of other borohydrides by metathetical reactions utilizing the alkali metal borohydrides" Journal of the American Chemical Society, Vol.75 (1953) 209-213.

30 Sloan E.D., Koh C.A. "Clathrate Hydrates of Natural Gases", Third Edition, 2008, CRC press.

31 Carrol J., "Natural Gas Hydrates A Guide for Engineers", Second Edition, 2009, Gulf Professional Publishing.

32 Jeffrey G. A. "Hydrate Inclusion Compounds" Journal of Inclusion Phenomena 1 (1984) 211-222

33 Strobel T. A., Koh C.A, Sloan, E.D. "Hydrogen storage properties of clathrate hydrate materials" Fluid Phase Equilibria, Vol. 261 (2007) 382-389

34 Strobel T. A., Hester K.C., Koh C.A., Sum K., Sloan E.D. "Properties of the clathrates of hydrogen and developments in their applicability for hydrogen storage" Chemical Physics Letters, Vol. 478 (2009) 97-109

35 Udachin K. "Double clathrate hydrates with helium and hydrogen" Supermolecular chemistry Vol. 3, Issue 3 (1994) 181-183

36 Dyadin Y.A., Lipkowski J., Tkacz M. "Clathrate hydrates of hydrogen and neon" Mendeleev Communications, Vol. 9, Issue 5 (1999) 209-210

37 Wendy L. Mao, Ho-kwang Mao, Alexander F. Goncharov, Viktor V. Struzhkin, Quanzhong Guo, Jingzhu Hu, Jinfu Shu, Russell J. Hemley, Maddury Somayazulu, Yusheng Zhao, "Hydrogen Clusters in Clathrate Hydrate" Science, Vol. 297 (2002) 2247-2249

38 Mao , W. Mao H.K. "Hydrogen storage in molecular compounds" Proceedings of the National Academy of Sciences, Vol. 101, Issue 3 (2003) 708-710.

39 Lokshin K., Zhao Y., "Fast synthesis method and phase diagram of hydrogen clathrate hydrate" Applied Physics Letters, Vol. 88 (2006) 131909-1 – 131909-3

40 Lokshin K., Zhao Y., He D., Mao W.L., Mao H.K., Hemley R. "Structure and Dynamics of Hydrogen Molecules in the Novel Clathrate Hydrate by High Pressure Neutron Diffraction" Physical Review Letters, Vol. 93, Issue 12 (2004) 15503(1-4)

41 Strobel T.A., Sloan E.D., Koh C.A. "Raman spectroscopic studies of hydrogen clathrate hydrates" Proceedings of the 6th International Conference on Gas Hydrates (ICGH 2008) Vancouver, British Colombia, CANADA, July 6-10, 2008

42 Florusse L. J., Peters C.J., Schooman J., Hester K.C., Koh C.A., Dec S.F., Marsh K.N., Sloan E.D. "Stable low-pressure hydrogen clusters stored in a binary clathrate hydrate" Science, Vol. 306 (2004) 469-471

43 Lee H., Lee J.W., Kim D.Y., Park J. Seo Y.T., Zeng H., Moudrakovski I.L., Ratcliffe C., Ripmeester J.A. "Tuning clathrate hydrates for hydrogen storage", Nature, Vol. 434 (2005) 743-746

44 Strobel T.A., Taylor C.J., Hester K.C. Dec S.F., Koh C.A., Miller K.T., Sloan E.D., "Molecular hydrogen storage in binary THF-H2 clathrate hydrates" Journal of Physical Chemistry B, Vol. 110 (2006) 17121-17125

45 Chapoy A., Anderson R., Tohidi B. "Effect of clathrate structure and promoter on the phase behavior of hydrogen clathrates", Proceedings of the 6th International Conference on Gas Hydrates (ICGH 2008) Vancouver, British Colombia, CANADA, July 6-10, 2008

46   Sugahara T., Haag J.C., Prasad S.R., Warntjes A.A., Sloan E.D., Sum A.K., Koh C.A., "Increasing hydrogen storage capacity using tetrahydrofouran", Journal of the American Chemical Society, Vol. 131, (2009) 14616-14617

47   Sugahara T., Haag J.C., Warntjes A.A., Prasad S.R., Sloan E.D., Koh C.A., Sem A.K. "Large occupancies of hydrogen in binary clathrate hydrates dependent on pressures and guest concentrations", Journal of Physical Chemistry C, Vol. 114 (2010) 15218-15222

48   Anderson R., Chapoy A., Tohidi B., "Phase relations and binary clathrate hydrate formation in the system H2-THF-H2O" Langmuir, Vol. 23 (2007) 3440-3444

49   Belosludov R.V., Mizuseki H., Kawazoe Y. "Accurate description of guest-guest and guest interactions in hydrogen clathrate: Role of help gas on stability of water hydrate framework", Proceedings of the 6th International Conference on Gas Hydrates (ICGH 2008) Vancouver, British Colombia, CANADA, July 6-10, 2008

50   Chapoy A., Anserdon R., Tohidi B. "Low-pressure molecular hydrogen storage in semi-clathrate hydrates of quaternary ammonium compounds" Journal of the American Chemical Society Vol. 129 (2007) 746-747

51   Deschamps J., Dalmazzone, D. "Hydrogen storage in semiclathrates of tetrabutyl ammonium chloride and tetrabutyl phosphonium bromide" Journal of Chemical & Engineering Data, Vol. 55, Issue 9 (2010) 3395-3399

52   Lipowski J., Komarov V.Y., Rodionova T.V., Dyadin Y.A., Aldako L.S. "The structure of tetrabutylammonium bromide hydrate, (C4H9)4NBr.2 1/3 H_2O" Journal of Supermolecular Chemistry, Vol. 2 (2002) 435-439

53   Shimada W., Shiro M., Kondo H., Takeya S., Oyama H., Ebinuma T., Narita H. "Tetra-n-butylammonium bromide water (1/38)", Acta Crystallographica C, Vol. 61 (2005) 065-066

54   Aladko L.S., Dyadin Y.A., "Clathrate hydrates of tetra-butylammonium and tetra-isoamyl-ammonium halides", Journal of Structural Chemistry, Vol. 43, Issue 6 (2002) 990-994

55   Shimada W., Ebinuma T., Oyama H., Kamata Y., Takeya S., Uchida T., Nagao J., Narita H. "Separation of gas molecule using tetra-n-butyl ammonium bromide semi-clathrate hydrate crystals" Japanese Journal of Applied Physics, Vol. 42 (2003) L 129-L 131

56   Kamata Y., Shimada W., Ebinuma T., Takeya S., Uchida T., Nagao J., Narita H., "Gas separation method using tetra-n-butyl ammonium bromide semi-clathrate hydrate", Japanese Journal of Applied Physics, Vol. 43, Issue 1 (2004), 362-365

57   Shimada W., Ebinuma T? Kamata Y., Oyama H., Narita H., "Free-growth forms and growth kinetics of tetra-n-butyl ammonium bromide semi-clathrate hydrate crystals" Journal of Crystal Growth, Vol. 274 (2005) 246-250

58   Oyama H., Shimada W., Ebinuma T., Kamata Y., Stoshi T., Tsutomu U., Jiro N., Narita H., "Phase diagram, latent heat and specific heat of TBAB semi-clathrate hydrate crystals" Fluid Phase Equilibria, Vol. 234 (2005) 131-135

59   Hashimoto S., Murayama S., Sugahara T., Sato H., Ohgaki K. "Thermodynamic and Raman spectroscopic studies on H_2+tetrahydrofuran + water and H_2 + tetra-n-butyl ammonium bromide+water mixtures containing gas hydrates", Chemical Engineering Science, Vol. 61 (2006) 7884-7888

60   Hashimoto S., Sugahara T., Moritiki M., Sato H., Ohgaki K. "Thermodynamic stability of hydrogen+tetra-n-butyl ammonium bromide mixed gas hydrates in nonstoichiometric aqueous solutions" Chemical Engineering Science, Vol. 63 (2008) 1092-1097

61   Chapoy A., Gholinezhad J., Tohidi B., "Experimental clathrate dissociation for hydrogen + water and hydrogen + tetrabutylammonium bromide+Water systems", Journal of Chemical & Engineering Data, Vol. 55 (2010) 5323-5327

62   Sakamoto J., "Thermodynamic and Raman spectroscopic studies on hydrogen+tetra-n-butyl ammonium fluoride semi-clathrate hydrates" Chemical Engineering Science, Vol. 63 (2008) 5789-5794

63   Shin K., Kim Y., Strobel T., Prasad P.S.R., Sugahara T., Lee H., Sloan E.D., Sum A.K., Koh C.A., "Tetra-n-butylammonium borohydride semiclathrate: A Hybrid

Material for Hydrogen Storage", Journal of Physical Chemistry A, Vol. 113 (2009) 6415-6418

64 Ogata K., Tsuda T., Amano S., Hashimoto S., Sugahara T., Ohgaki K., "Hydrogen storage in trimetylamine hydrate: Thermodynamic stability and hydrogen storage capacity of hydrogen +trimethylamine mixed semi-clathrate hydrates" Chemical Engineering Science, Vol. 65, (2009) 1616-1620

65 Differential Scanning Calorimetry, Edited by G.W.H. Höhne, W.F. Hemminger, H.-J. Flammersheim, Springer (2003) ISBN: 3-540-00467-X

66 Handbook of thermal analysis and Calorimetry, Edited by M. Brown (1998), Elsevier

67 Dalmazzone D., Dalmazzone C., Herzhaft B., "Differential Scanning Calorimetry: A New Technique to Characterize Hydrate Formation in drilling Muds", SPE 63962 (2000)

68 Kharrat M., Dalmazzone D., "Experimental determination of stabilityconditions of methane hydrate in aqueous calcium chloride solutions using high pressure differential scanning calorimetry" J. Chem. Thermodynamics Vol.35 (2003) 1489–1505

69 Grenet J., Legendre B., "Analyse calorimétrique différentielle à balayage (DSC) " Technique d'ingénieurs P 1 205

70 Mayoufi N. Thèse de doctorat : "Caractérisation de coulis d'hydrates contenant du CO_2 appliqué à des systèmes frigorifiques" ENSTA ParisTech, (2010)

71 Höhne G.W.H., Cammenga H.K., Eysel W., Thermochim. Acta, 160 (1990) 1-12

72 Guilbot, P., Valtz, A., Legendre, H., Richon, D. "Rapid on line sampler-injector: A reliable tool for HT-HP sampling and on line GC analysis" Analusis (2000), Vol.28, 426–431

73 Oyama H., Shimada W., Ebinuma T., Kamata Y., Takeya S., Uchida T., Nagao J., Narita H. "Phase diagram, latent heat and specific heat of TBAB semi-clathrate hydrate crystals." *Fluid Phase Equilib.* 2005, 234, 131-135

74 Hashimoto S., Murayama S., Sugahara T., Sato H., Ohgaki K. "Thermodynamic and raman spectroscopic studies on H_2 + tetrahydrofuran + water and H_2 + tetra-*n*-butyl

ammonium bromide + water mixtures containing gas hydrates" *Chem. Eng. Sci.* 2006, 61, 7884-7888.

75   Chapoy A., Anderson R., Tohidi B."Low-pressure molecular hydrogen storage in semi-clathrate hydrates of quaternary ammonium compounds" *J. Am. Chem. Soc.* 2007, 129, 746-747

76   Arjmandi M., Chapoy A., Tohidi B. "Equilibrium data of hydrogen, methane, nitrogen, carbon dioxide, and natural gas in semi-clathrate hydrates of tetrabutyl ammonium bromide" *J. Chem. Eng. Data.* 2007, 52, 2153-2158

77   Hashimoto S., Sugahara T., Moritoki M., Sato H., Ohgaki K. "Thermodynamic stability of hydrogen+tetra-*n*-butyl ammonium bromide mixed gas hydrate in nonstoichiometric aqueous solutions" *Chem. Eng. Sci.* 2008, 63, 1092-1097

78   Deschamps J., Dalmazzone D. "Hydrogen storage in semiclathrate hydrates of tetrabutyl ammonium chloride and tetrabutyl phosphonium bromide" *J. Chem. Eng. Data* published online on June 17th 2010, DOI: 10.1021/je100146b

79   Sakamoto J., Hashimoto S., Tsuda T., Sugahara T., Inoue Y., Ohgaki K. "Thermodynamic and raman spectroscopic studies on hydrogen+tetra-*n*-butyl ammonium fluoride semi-clathrate hydrates" *Chem. Eng. Sci.* 2008, 63, 5789-5794

80   Strobel T.A., Kim Y., Andrews G.S., Ferrell J.R., Koh C.A., Herring , Sloan E. D. "Chemical-Clathrate Hybrid Hydrogen Storage: Storage in Both Guest and Host" J. Am. Chem. Soc. *2008*, 130, 14975–14977

81   Shin K., Kim Yo., Strobel T.A., Prasad P. S. R., Sugahara T., Lee H., Sloan E. D., Sum A.K., Koh C.A. "Tetra-n-butylammonium Borohydride Semiclathrate: A Hybrid Material for Hydrogen Storage" Journal of Physical Chemistry Letters A, 2009, 113, 6415–6418

82   Demirci U.B., Akdim O., Miele P. "Ten-year efforts and a no-go recommendation for sodium borohydride for on-board automotive hydrogen storage" International journal of hydrogen energy 34, *2009*, 2638–2645

83   Ruman T., Kusnierz A., Jurkiewicz A., Les A., Rode W. "The synthesis, reactivity and ^{1}H NMR investigation of the hydroxyborohydride anion" *Inorg. Chem. Commun.* 2007, 10, 1074-1078

84   Dyadin Y.A. , Udachin K.A. "Clathrate formation in water-peralkylonium salts systems" J. Incl. Phenom. 2 (1984) 61-72

85   A. van Cleeff, G. A. M. Diepen "Gas hydrates of nit rogen and oxygen" Rew. Trav. Chim. 1960, 79, 582-586.

86   Seo Y.-T., Kang S.-P., Lee H. "Experimental determination and thermodynamic modeling of methane and nitrogen hydrates in the presence of THF, propylene oxide, 1,4-dioxane and acetone" Fluid Phase Equilib. 2001, 189, 99-110.

87   Deschamps J., Dalmazzone D., "Dissociation Enthalpies and Phase Equilibrium for TBAB semi-Clathrate Hydrates of N_2, CO_2, N_2 + CO_2 and CH_4 + CO_2" J. Therm. Anal. Calorim. 2009, 98, 113-118

88   Lokshin K. A., Zhao Y. , He D. , Mao W. L. , Mao H. K., Hemley R. J., Lobanov M. V., Greenblatt M. , Phys. Rev. Let. 93, 125503 (2004).

89   Huang H., Sandler S. I., Orbey H. "Vapor-Liquid equilibria of some hydrogen + hydrocarbon systems with the Wong – Sandler mixing rule" Fluid Phase Equilibria, Vol.96 (1994) 143-153

90   Ballard A.L., Sloan E.D. "Hydrate phase diagrams for methane + ethane + propane mixtures" Chemical Engineering Science, Vol.56 (2001) 6883-6895

91   Dyadin Yu. A., Larionov E. G., Aladko E. Ya., Zhurko F. V. "Clathrate Formation in Propane–Water and Methane–Propane–Water Systems under Pressures of up to 15 kbar" Physical Chemistry, Vol. 376 (2001) *pp*.497-500

92   M.M. Mooijer-van den Heuvel, Peters C.J., de Swaan Arons J. "Gas hydrate phase equilibria for propane in the presence of additive components", Fluid Phase Equilibria, Vol.193 (2002) *pp*.245–259

93   Gaudette J. , Servio P. "Measurement of Dissolved Propane in Water in the Presence of Gas Hydrate" J. Chem. Eng. Data Vol. 52 (2007) *pp*. 1449-1451

94   Lars Jensen, Kaj Thomsen, Nicolas von Solms "Propane hydrate nucleation: Experimental investigation and correlation" Chemical Engineering Science Vol. 63 (2008) *pp*.3069 – 3080

95   Reamer H.H. et al., (1952), "Some properties of mixed paraffinic & other olefinic hydrate", *Trans.Am.Inst.Min., Metall. Pet.Eng. 195-197-202*

96   Makagon Y. F. "Liquid Propane+Water Phase Equilibruia at Hydrate Conditions" Journal of Chemical Engineering Data Vol. 48 (2003) 347-350

97   Miller B., Strong E.R., Am. Gas Assoc. Monthly, 28, 63 (1946)

98   Deaton W.M., Frost E.M.Jr., "Gas Hydrates and Their Relation to the Operation of Natural-Gas Pipe Lines" U.S. Bureau of Mines Monograph, 8 (1946) 101.

99   Verma Y. K., Hand J.H., Katz D.L. [Donald L.], "Gas hydrates from liquid hydrocarbons methane-propane-water system" GVC/AIChE Joint Meeting, Munich, 1975, 10

100   Kubota H., Shimizu K., Tanaka Y., Makita T., J. Chem. Eng. Japan, 17 (1984) 423

101   Robinson D.B., Mehta B.R., J. Can. Pet. Tech., 10 (1971) 33

102   Thakore J.L., Holder G.D., Ind. Eng Chem. Res., 26 (1987) 462

103   M.M. Mooijer-van den Heuvel., "Phase Behaviour and Structural Aspects of Ternary Clathrate Hydrate Systems : The Role of Additives" Chemical Engineering Thesis, Delft University of Technology (2004)

104   Wilcox W.I., Carson D.B., Katz D.L., Ind. Eng. Chem., 33 (1941) 662

105   Sugahara T. et al., (2008), "Cage occupancy of hydrogen in carbon dioxide, ethane, cyclopropane, and propane hydrates", *The Open Thermodynamics Journal, 2008, 2, 1-6*

106   Skiba S. et al., (2009), "Double clathrate hydrate of propane and hydrogen", *J Incl Phenom Macrocycl Chem (2009) 63:383–386*

107   Zhang Sh., et al., (2000), "Hydrate Formation of Hydrogen + Hydrocarbon Gas Mixtures", *J. Chem. Eng. Data 2000, 45, 908-911*

108 Xiao-Sen Li, Zhi-Ming Xia, Zhao-Yang Chen, Ke-Feng Yan, Gang Li, Hui-Jie Wu "Equilibrium Hydrate Formation Conditions for the Mixtures of CO_2 + H_2 + Tetrabutyl Ammonium Bromide", *J. Chem. Eng. Data* Vol. 55 (2010) pp 2180–2184

109 Rajnish Kumar, Hui-jie Wu, Peter Englezos "Incipient hydrate phase equilibrium for gas mixtures containing hydrogen, carbon dioxide and propane" Fluid Phase Equilibria Vol.244 (2006) 167–171

110 Barchas, R., and Davis, R. (1992), "The Kerr-McGee/ABB Lummus Crest Technology for the Recovery of CO_2 from Stack Gases", Energy Convers. Mgmt., Vol. 33, (1992) pp 333-340

111 Audus, H., Olav, K., & Geoff, S. (1998). Proceedings of the 4th International Conference on Greenhouse Gas Control Technologies, (S. 557-562). Interlaken, Switzerland.

112 Deaton, W.M., Frost, E.M., Jr., "Gas Hydrates and Their Relation to the Operation of Natural-Gas Pipe Lines" U.S. Bureau of Mines Monograph (1946) Vol.8, 101

113 Unruh, C.H., Katz, D.L., (Gas hydrates of carbon dioxide-methane mixtures) Trans. AIME, (1949) Vol.186, 83

114 Larson, S.D., "Phase Studies of the Two-Component Carbon Dioxide-Water System, Involving the Carbon Dioxide Hydrate", University of Illinois, Urbana, IL (1955)

115 Takenouchi S., Kennedy G.C., "Dissociation pressures of the phase $CO_2 \cdot 5 \frac{3}{4}$ H_2O"Journal of Geology, (1965) Vol.73, 383

116 Miller, S.L., Smythe,W.D., "Carbon dioxide clathrate in the Martian polar cap" Science (1970) Vol.170, 531

117 Robinson, D.B., Mehta, B.R., "Hydrates in the propane-carbon dioxide-water system"J. Can. Pet. Tech. (1971) Vol.10, 33-35

118 Ng, H.-J., Robinson, D.B., "Hydrate formation in the CO_2-H_2O binary system"Fluid Phase Equilib. (1985) Vol.21, 145

119 Vlahakis, J.G., Chen, H.-S., Suwandi, M.S., Barduhn,A.J., "The Growth Rate of Ice Crystals: Properties of Carbon dioxide Hydrates, A Review of Properties of 51 Gas Hydrates, Syracuse U" Research and Development Report 830, prepared for US Department of the Interior, November (1972)

120 Falabella, B.J., "A Study of Natural Gas Hydrates" Ph.D. Thesis, University of Massachusetts, University Microfilms, No. 76-5849, Ann Arbor, MI (1975)

121 Song, K.Y., Kobayashi, R., "Water Content of CO_2 in Equilibrium with Liquid Water and/or Hydrates" SPE Formation Evaluation, (1987) 500-508

122 Adisasmito, S., Frank, R.J., Sloan, E.D., "Hydrates of carbon dioxide and methane mixtures"J. Chem. Eng. Data (1991) 36, 68-71

123 Ohgaki, K., Makihara, Y., Takano, K., "Formation of CO2 Hydrate in Pure and Sea Waters"J. Chem. Eng. Jpn., (1993) 26, 558-564 (1993)

124 Nakano, S., Moritoki, M., Ohgaki, K., J. "High-pressure phase equilibrium and Raman microprobe spectroscopic studies on the CO_2 hydrate system" Chem. Eng. Data, 43, 807-810 (1998b)

125 Fan, S.-S., Guo, T.-M., "Hydrate Formation of CO_2-Rich Binary and Quaternary Gas Mixtures in Aqueous Sodium Chloride Solutions" J. Chem. Eng. Data, (1999) Vol. 44, 829-832

126 Fan, S.-S., Chen, G.-J., Ma, Q.-L., Guo, T.-M., (2000) Chem. Eng. J., 3595, 1

127 Mooijer-van den Heuvel, M.M., Witteman, R., Peters, C.J., " Phase behaviour of gas hydrates of carbon dioxide in the presence of tetrahydropyran, cyclobutanone, cyclohexane and methylcyclohexane" Fluid Phase Equilib., (2001) Vol.182, 97-110

128 Zhang, Y., "Formation of Hydrate from Single-Phase Aqueous Solutions" M.S. Thesis, University of Pittsburgh, PA (2003)

129 Mohammadi, A.H., Anderson, R., Tohidi, B., "Carbon monoxide clathrate hydrates: Equilibrium data and thermodynamic modeling" AIChE J., (2005) Vol.51, 2825-2823

130 Wassila Bouchafaa, P.h.D Thesis "Mesure et modélisation des conditions de dissociation d'hydrates de gaz stabilisés en vue de l'application au captage du CO_2" ENSTA ParisTech, November 2011